Spring 2-2-2021

# Autophagic Reprogramming of Bone Marrow-Derived Macrophages

Mayada Mahmoud Zaki Mohamed Mazher
*The American University in Cairo AUC*, mayada_mazher1991@aucegypt.edu

THE AMERICAN UNIVERSITY IN CAIRO

الجامعة الأمريكية بالقاهرة

**School of Science and Engineering**

# Autophagic Reprogramming of Bone Marrow-Derived Macrophages

A Thesis Submitted to

**The Biotechnology Graduate Program**

in partial fulfillment of the requirements for

the degree of Master of Science

**by**

**Mayada Mahmoud Zaki Mohamed Mazher**

Under the supervision of

**Dr. Ahmed Abdellatif**

Assistant Professor Department of Biology

Spring February 2021

The American University in Cairo

School of Sciences and Engineering (SSE)

# Autophagic Reprogramming of Bone Marrow-Derived Macrophages

A Thesis Submitted by

**Mayada Mahmoud Zaki Mohamed Mazher**

Submitted to the Biotechnology Master's Program

In partial fulfillment of the requirements for the degree of

Master of Science in Biotechnology

Has been approved by

Thesis Committee Supervisor/Chair _____

Affiliation _____

Thesis Committee Co-advisor _____

Affiliation _____

Thesis Committee Reader/Examiner _____

Affiliation _____

Thesis Committee Reader/Examiner _____

Affiliation _____

Thesis Committee Reader/External Examiner _____

Affiliation _____

_____ _____ _____

Dept. Chair/Director Date Dean Date

***Acknowledgment***

*All praises to God, thank you for sciences blessing. From the bottom of my heart, I want to thank my great and beloved family, Mom, Dad, and my two Brothers Mostafa and Mohanad, for giving me support in my entire life. I want to give millions of thanks to my advisors, Dr. Ahmed Abdellatif and Dr. Ahmed Moustafa, for their endless support. Special thanks to Dr. Asma Amleh and Dr. Walid Fouad.*

*At children's cancer Hospital Egypt 57357 I want to thank Dr. Ahmed El-Sayed for giving me the chance to work in the immunology unit at basic research. Also, I want thank Dr. Mona Zidan and Dr. Nehal Kamal for their help in troubleshooting of flow cytometry experiments.*

*My special thanks to Laboratory Fellowship for covering my Tuition and Fees during my Biotechnology Master Degree and Graduate Research Grant from American University in Cairo.*

*My Thanks to the International Max Planck Research School for Cell Developmental and Systems Biology (IMPRS) for their Travel grant to attend Dresden Systems Biology Internship (2018 Dresden, Germany). My sincere thanks to Dr. Ivo Sabalzerin and his Lab members.*

*Also, my thanks to European Molecular Biology Laboratories EMBL for funding my application to participate in the following conferences; August 2019 EMBO Workshop Autophagy: From molecular principles to human diseases (Edinburgh, Scotland). And December 2020 EMBO Workshop: In situ Structural Biology: From Cryo-EM to Integrative Modelling (Virtual).*

*My Sincere Appreciation for Dr. Vojo Deretic, Head of Inflammation, Metabolism AIM Centre NIH, for supporting my application for participation in the conference October 2020 Early Career investigators in Autophagy by AIM center NIH.Also, to his valuable feedback on Autophagy laser confocal microscopy results.*

*I want to thank my AUC department of biology family and clinical pharmacy family at Children's Cancer Hospital (CCHE). I want to thank: Marwa Zahra, Eman Rabee, Alaa Hamed, Marina, Shimaa, Omnia Raheem, Naela Saleh, and Jihad Mahmood*

*My warmest appreciation to Diana George, Nehal Ghoniem, Nahla Osama, Nada Ezz El-Arab, and all Dr. Ahmed Abdellatif's team. My special thanks to my beautiful friend Yomna Adel Moqidem for being the perfect lab partner.*

*I want to thank the lab aids and administrators at the department of biology; Mr. Osama, Mr. Khaled, Mr. Mohamed, Mr. Zein, Mr. Amjad Aouf, Mr. Ahmed El-Hossiney*

*In CCHE, I want to thank Dr. Mohamed Kamal, Dr. Mohamed Nagy, Dr. Sara Mohamed, Dr. Hind Gouda, Dr. Mona El-harmeel, Dr. Nada Rizk, Dr. Louay El-Deep, Dr. Mohamed Yasser, and Mr. Ashraf Adel. And special thanks to my friend Dr. Fatima El-senosy*

*My sincere and warmest love and appreciation to my lifetime friends: Weam Mohamed, Marwa Atwan, Yara Essam and Hadeel Abdelgawad, Maha Medhat, Eman Reda, and Fatma Abdel Hameed.*

## Table of contents

## Table of Figures

# Autophagic Reprogramming of Bone Marrow-Derived Macrophages


## ABSTRACT

**Background:** Macroautophagy is a highly conserved catabolic process among eukaryotes. Autophagosome is a piece of double-membrane machinery that fuses with lysosomes during macroautophagy to form autolysosomes. Autolysosome degrades organelles and organizes the pathogen engulfment during phagocytosis in innate immunity. Macrophages are highly dynamic immune cells that orchestrate the host-pathogen interaction. Interestingly, autophagy is implicated in disease pathophysiologies such as Crohn's disease, cancer, and neurodegenerative diseases. Therefore, we studied the interplay between autophagy and macrophage polarization (activation) through two approaches:

1- Systems biology approach to construct the genetic regulatory network and pathway analysis. And to predict the target proteins that mediate the interplay between autophagy and macrophage activation(polarization).

2- In vitro experimental validation of target proteins using immune co-localization studies, flow cytometry studies, laser confocal microscopy studies, and gene expression analysis.

**Methods.** A systems biology approach was performed to find the interplay between Autophagy related genes (Atgs) & Differentially expressed genes of Macrophage Polarization M1-M2 (DEGs), followed by common pathway enrichment and construction of transcription factors and mi-RNAs regulatory networks. The Atgs and DEGs targets that mediate the interplay between autophagy and macrophage polarization were defined, and experimental validation for targets took place. Bone marrow-derived monocytes were isolated from the femur and tibia of female mice. After differentiation of monocytes to M0, M1, and M2a, the lineage phenotypes were characterized using flow cytometry. Afterward, we validated the targets of Smad1, LC3A&B, Atg16L1, Atg7, IL6, CD68, Arg-1, and Vamp7. Finally, we investigated the impact of autophagy inhibition on all immune lineages using autophagy inhibitor Bafilomycin-A.

**Results**: Immune phenotyping by flow cytometry revealed three macrophage phenotypes: (IL6+/CD68+) M0 φ, (IL6+/CD68+/Arg-1 +) M1 φ and (CD68+/Arg-1) M2a φ lineages. And 3D

reconstruction of laser confocal microscopy Z-stalk images revealed an increase of autophagy activity in both M1 and M2a lineages. In addition, a significant increase was also observed in pre autophagosome size and number of Atg-7, Atg-16L1 in interleukin -4 activated M2a cells compared to control M 0 naïve cells. The size of LC 3 A& B auto phagosomal aggregates showed an increase in M2a cells. RT qPCR supported these findings and showed the high gene expression profile of Atg 16 L 1- 3, smad1, and Vamp 7 in M2a lineage. Bafilomycin –A, an autophagy inhibitor, induced increased expression of CD68 and Arg-1 in all cell lineages. Phagocytosis assay with Heat killed E Coli bacteria showed decreased phagocytosis activity in IL-4 activated M2a cells but not M1 cells.

**Conclusion**: This study suggests that autophagy reprograms macrophages through CD68 and Arginase-1 phagocytosis markers and Atg 16 L 1 -3 dependent manner.

## INTRODUCTION

Macrophages are major key players in the immune system and contribute to host-pathogen defense mechanisms **(Silva (2011).** Phagocytosis is one of the tools that immune cells use in host-pathogen interaction **(Richards and Endres 2014).** The activation of macrophages affects the quality of the phagocytosis process **(Cassetta, Cassol et al. (2011).** Autophagy is a highly conserved catabolic process; it is essential for cellular recycling. Autophagy is implicated in the pathogenesis of several diseases such as cancer, neurodegenerative disease, innate immune response-related diseases Levine and Kroemer (2008). Autophagy regulates phagocytosis in macrophages by modulating surface scavenger receptors (Bonilla, Bhattacharya et al. (2013).

Here we investigate how autophagy reprograms macrophage polarization in phagocytosis, as the interplay between autophagy and macrophage polarization is poorly understood. Finding the targeted proteins that mediate the interplay between autophagy and macrophage polarization among a pool of autophagy-related proteins and hundreds of growth factors and proteins that regulate macrophage polarization is quite challenging. Therefore, we implemented a systems biology approach to narrow down the protein targets that mediate the interplay between the two processes. These target proteins were validated in vitro using bone marrow isolated macrophages.

# I- LITERATURE REVIEW

## AUTOPHAGY

Autophagy is a highly conserved cellular process among prokaryotes and eukaryotes **Mizushima and Levine (2010)**, associated with cellular growth and differentiation **King (2012).** It is composed of the following steps: vesicle or phagophore formation and elongation, autophagosome formation and lysosomal fusion, and finally auto lysosomal degradation **(Dikic and Elazar (2018).** Autophagy is involved in the pathophysiology of many diseases such as neurodegenerative disorders **Nixon (2013),** tumorigenesis Parkhitko, Favorova et al. (2013)**,** the immune response to infections **Pan, Chen et al. (2016),** and diabetes **Quan, Lim et al. (2012).**

There are several types of autophagy: Selective (micro and macro) autophagy, which degrade particular cell organelles such as; damaged mitochondria, and peroxisomes**.** In contrast, non-selective autophagy targets cytoplasmic bulk turnover **(Sharma, Verma et al. (2018)(Parzych and Klionsky (2014)**

## AUTOPHAGY RELATED PROTEINS

Autophagy-related proteins are highly conserved and contain several membrane proteins that regulate autophagy processes **Shibutani, Saitoh et al. (2015).**

Selective autophagy is initiated in response to starvation or amino acid depletion via the inhibition of the nutrient-sensing kinase mammalian target of rapamycin complex one (mTORC1) and the activation of the AMPK kinase pathway, which activates mammalian Atg1/ULK1 kinase **Shang and Wang (2011).** ULK1 mediates the interaction between Atg13, Atg16L1 **Gammoh, Florey et al. (2013), Zachari and Ganley (2017).** Atg16L1 is a component of the phagophore elongation complex (Atg5-Atg12-Atg16L1**) Matsushita, Suzuki et al. (2006).** The Atg13-FIP200-Atg101

complex activates phosphatidylinositol 3 - kinase (PIK3C3), which forms a complex with the Beclin1 gene, causing autophagy initiation **Mercer, Gubas et al. (2018).** After the recruitment of the (Atg5-Atg12-Atg16L1) complex, an autophagosome is formed **Zavodszky, Vicinanza et al. (2013).** The Atg16L1 and Atg9 regulate autophagosome formation by enhancing the conjugation of PE (phosphatidylethanolamine) with LC3 (Atg8-like) to form LC3-II (MAP1LC3A, MAP1LC3B, and MAP1LC3C) **Xie, Kang et al. (2015) & Yoshii and Mizushima (2017).** LC3 is critical for autophagosome – lysosomal fusion **Deretic (2008).**

**Autophagy-related protein Atg7** is a ubiquitin-activating enzyme. It helps the conjugation of Atg12 with its substrate Atg5, through conjugation with Atg12 and facilitation of binding of Atg10 to Atg12 **Geng and Klionsky (2008).** Atg7 enhances the binding of Atg3 to the Atg8 like protein LC3 and regulates LC3-PE conjugation **Kaiser, Qiu et al. (2013).** Therefore, Atg7 is considered a crucial regulator of nascent autophagosome formation and autophagosome-lysosome fusion **Arakawa, Honda et al. (2017).** It also acts as an autophagosome marker **Kuma, Komatsu et al. (2017),** and plays an essential role in bladder cancer tumorigenesis **Zhu, Li et al. (2017)**, and regulates brain angiogenesis. Knocking out Atg7 in endothelial cells decreased the expression of IL-6 **Zhuang, Liu et al. (2017).**

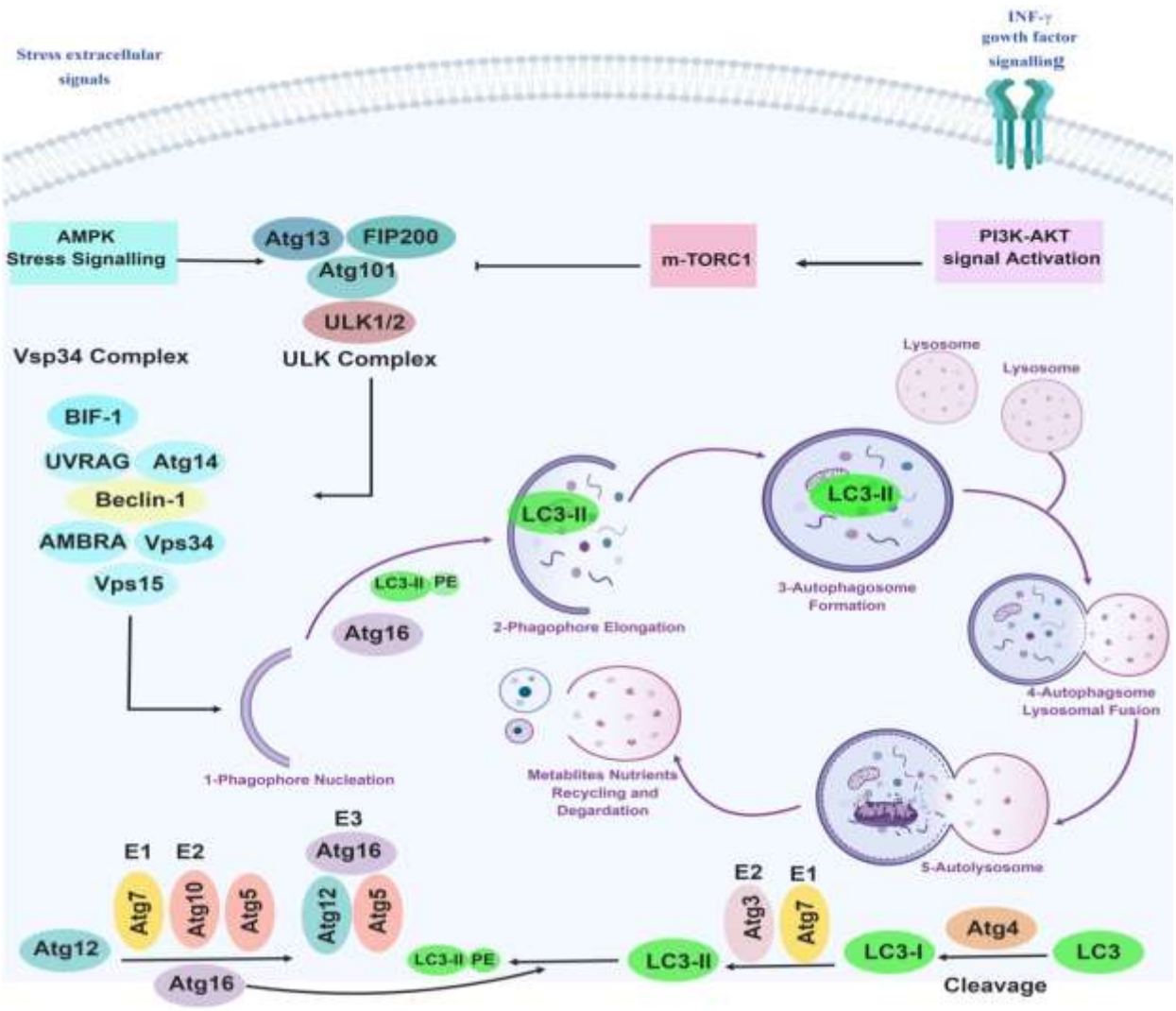


**FIGURE 1. MAMMALIAN TARGET OF RAPAMYCIN (MTORC1) AND AMPK INDUCED AUTOPHAGY.**

Activation of PI3K/AKT signaling activates m-TORC1, which is a nutrient-sensing kinase. Upon nutrient or amino acids depletion, activation of AMPK signaling inhibits m-TORC1 and phosphorylates the ULK complex. The Atg101-FIP200-Atg13 complex is phosphorylated by ULK1/2 kinase and activates the binding Beclin1, Atg14 to initiate autophagy. ULK1/2 and Atg7 ubiquitin regulate the conjugation of the Atg16 to Atg12-Atg5 complex. Atg7 regulates the interaction between Atg16 and LC3 in the presence of Atg3. **(Designed by Authors using Biorender.com).**

**Autophagy-related protein Atg 16L1** interacts with the Atg5-Atg12 conjugation system that mediates the conjugation of phosphatidylethanolamine (PE) to LC3-I to produce LC3-II **Gammoh (2020) (Figure 2).** Atg16L1 helps in pre-auto phagosome elongation and Autophagosome formation.

Atg16L1 protein has different isoforms. The most clinically significant is Atg16l-1 or Alpha, then Atg16L1-2 and Atg16L1-3 **Jiang, Qin et al. (2013).** Atg16L1 appears on the surface of Pre-auto phagosomes inside the cell. Therefore, it can be used to quantify autophagosomes using fluorescence microscopy **du Toit, Hofmeyr et al. (2018).** Other variants of Atg16l1 (ATG16L1 rs4663402) are used as a prognostic marker for hepatocellular carcinoma (HCC) **Shen and Lin (2019).**

**Autophagy-related protein Mitochondrial activated light chain LC3 A & B Protein Complex** appears on the surface of mature autophagosomes, under starvation and nutrient depletion. Mature autophagosomes **Kimura, Noda et al. (2008)** fuses with lysosomes to degrade autophagosomal contents. The lysosomal proteins VAMP7 is required for optimal phagocytosis of opsonized particles by RAW264.7 macrophages cell line **Braun, Fraisier et al. (2004) &Huynh, Kay et al. (2007).** Interestingly, Vamp7 mediates the cytotoxic granule release from human cytotoxic T cells. Knocking down VAMP7 significantly inhibited T cells' killing efficiency **Chitirala, Ravichandran et al. (2019)**

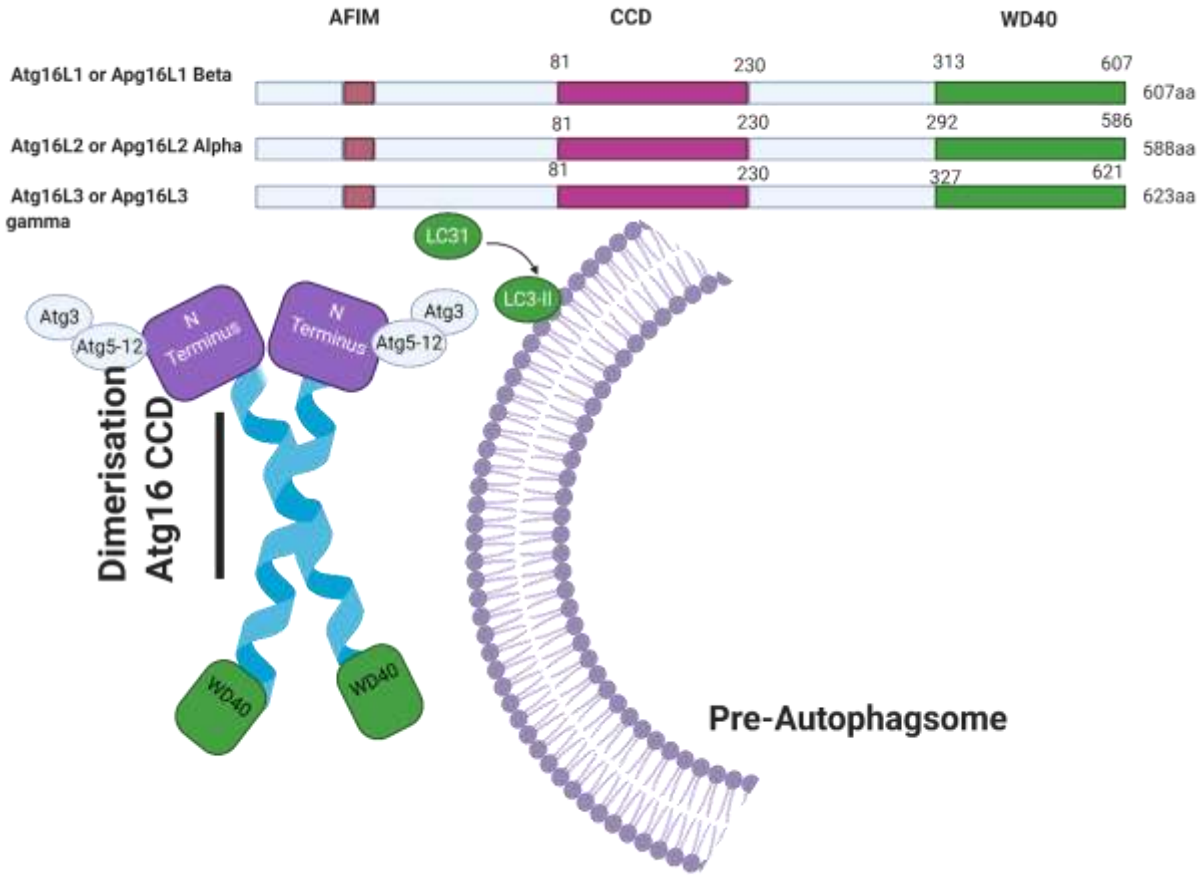


**FIGURE 2. GRAPHICAL ILLUSTRATION FOR THE DIFFERENT ISOFORMS OF ATG16L1.**

N-terminal of wd40 domain is important for interaction with atg5-atg12 complex. **(Designed by Authors using Biorender.com).**

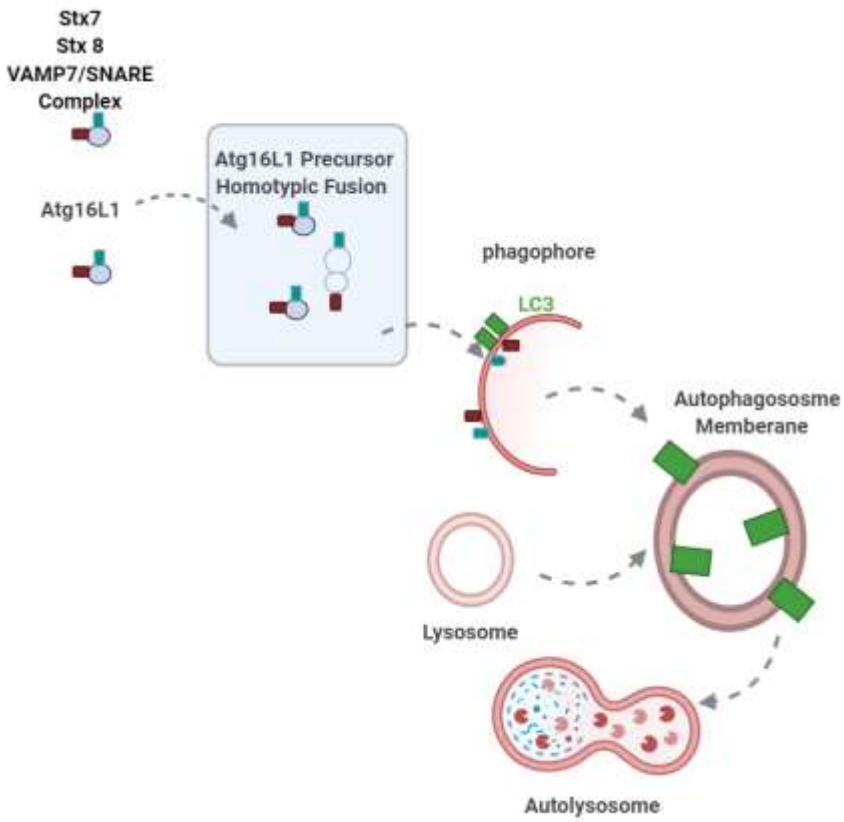


**FIGURE 3. REPRESENTATION OF FUSION OF LYSOSOMAL VAMP7 / SNARE PROTEINS WITH ATG16L1 PRECURSOR.**

Moving towards the phagophore (pre-auto phagosome) formation and Lc3 autophagosome maturation. Finally, the fusion of lysosome with autophagosome to form the proteolytic autolysosome vesicle**. (Designed by Authors using Biorender.com).**

## AUTOPHAGY IN INFLAMMATION:

Autophagy and inflammation are interdependent pathways. Autophagy regulates pro-inflammatory cytokines and chemokines. Atg16L1 is a target for Mir223, and it increased in Mir223 deficient mice **Li, Zhou et al. (2019).** The development of Crohn's disease is associated

with a polymorphism in numerous autophagy-related genes such as; ULK1, Immunity-Related GTPase M (IRGM), Atg2a, Atg4a, and Atg4d **Harris (2013).**

Autophagy regulates the secretion of pro-inflammatory cytokines, IL-1β **Iula, Keitelman et al. (2018)** and also regulates IL-23 **Peral de Castro, Jones et al. (2012).** It also acts as an inflammasome modulator for IL-18, IL-6, and IL-1α **Harris (2013).** Mice lacking the autophagy protein Atg5 in myeloid cells secrete higher levels of IL-1α, IL-12p70, CXCL1, and IL-17 in response to infection with *Mycobacterium tuberculosis* **Peral de Castro, Jones et al. (2012).**

Cytokines like Type-II interferon-gamma INF-γ play a dual role as a pro-inflammatory and inflammatory cytokine **Mühl and Pfeilschifter (2003).** INF-γ is an important immune modulator and macrophages stimulator, increasing the expression of IL-6 in monocytes **Biondillo, Konicek et al. (1994)**. In human hepatocellular carcinoma cell lines, INF- γ induced autophagy via increasing the autophagosome formation and the turnover of LC3-II protein through IFR-1 (interferon regulatory factor -1) signaling pathway **Li, Du et al. (2012).** INF- γ also mediates the up-regulation of STAT1, STAT2 in human peripheral blood mononuclear cells and macrophages **Lehtonen, Matikainen et al. (1997).**

## MACROPHAGE (M1 & M2) POLARIZATION

Macrophages are several families of immuno-inflammatory hematopoietic cells that mediate phagocytosis and are activated by inflammatory processes **Perdiguero and Geissmann (2016).** According to their polarization state, inflammatory macrophages are classified into pro-inflammatory M1 macrophages and inflammatory M2 macrophages **Italiani and Boraschi (2014).** Polarization is the process that enables macrophages to adapt to different signaling and different functions, e.g., innate immunity, tissue repair, and embryonic development **Shapouri-Moghaddam, Mohammadian et al. (2018).**

In vitro, murine derived bone marrow monocytes and dendritic cells were polarized into M1 macrophage via LPS, INF-γ, and MCSF. M1 phenotype express CD68 cell surface marker and produces cytokines such as; tumor necrosis factor TNF, IL-12, IL-18, IL-23, IL-1β, and IL-6 **Martinez and Gordon (2014) & Bogdan (2015).** Macrophages M2 polarization is initiated by infection and growth factor signaling such as; IL-4, IL-13, IL-10, TGF-β **Martinez and Gordon (2014).** M2 phenotype shows increased secretion of cytokines; IL6, IL-10, TGF-beta according to the M2 subset **(*Table 1*).**

IL-6 receptor protein complex is a pro-inflammatory cytokine produced by fibroblasts, T cells, endothelial cells, Keratinocytes, lymphocytes, and macrophages. It is encoded by the IL6 gene and consists of IL-6 receptor subunit (IL-6R) and IL-6 signal transducer glycoprotein 130 (gp130). Signal transducer and activator of transcription 3 (STAT3) is one of the critical components for IL-6 receptor signaling. IL-6 induces the production of C-reactive protein, which can induce an inflammatory M1 phenotype in macrophages **Del Giudice and Gangestad (2018).**

Previous studies reported in vitro polarization of macrophages with lipopolysaccharide and IL4 and showed high levels of IL6 in the M2 phase only **Yin, Ma et al. (2018).** The inhibition of the IL6/STAT3 pathway with Anti –IL6 treatment caused M2 to change into M1 type.

| Phenotype | M1 | M2a | M2b | M2c | M2d |
|---|---|---|---|---|---|
| Stimulation & Activation | IFN-gamma<br>LPS<br>GM-CSF | IL-4<br>IL-13<br>Fungal and Helminthes infection | ICs<br>IL-1R | IL-10<br>TGF-beta<br>GCs | IL-6<br>LIF<br>Adenosine |
| Marker Expression | CD86<br>CD80<br>CD68<br>MHC II<br>IL-1R<br>TLR2<br>TLR4<br>iNOS<br>SOCS3 | CD163<br>MHC II<br>SR<br>MMR/CD206<br>CD200R<br>TGM2<br>DecoyR<br>IL-1R II<br>*Mouse only:*<br>*Ym1/2*<br>*Fizz1*<br>*Arg-1* | CD86<br>MHC II | CD163<br>TLR1<br>TLR8 | VEGF |
| Cytokine secretion | TNF<br>IL-1 beta<br>IL-6<br>IL-12<br>IL-23 | IL-10<br>TGF-beta<br>IL-1ra | IL-1<br>IL-6<br>IL-10<br>TNF-alpha | IL-10<br>TGF-beta | IL-10<br>IL-12<br>TNF-alpha<br>TGF-beta |
| Function | Pro-inflammatory Th1 response, tumor resistance | Anti-inflammatory process and tissue remodelling | Th2 activation, immune-regulation | Phagocytosis of apoptotic cells | Angiogenesis, tumor progression |

**Table 1. Macrophage M1 and M2 polarization and their subsets.**

Growth factors for stimulation, cytokine secretion, and cell surface markers expression in each subset. Also, their function, especially in tissue remodeling and inflammation process.

## THE IMPLICATION OF AUTOPHAGY IN MACROPHAGES POLARIZATION

M1 Macrophage polarization is induced by Interferon Gamma (IFN-γ) / lipopolysaccharide (LPS) to stimulate the secretion of pro-inflammatory cytokines. Conversely, M2 macrophage polarization is induced by IL4 and or IL-13. Stimulation of macrophages with IL-4 and IL-13 leads to activation of the transcription factor STAT6, which is crucial for M2 polarization. Mammalian target of rapamycin mTOR kinase is a master regulatory protein for autophagy, critical in

regulating monocyte polarization into tumor activated macrophages M1 and M2. In LPS-stimulated monocytes, inhibition of the mTOR pathway by rapamycin leads to polarization toward the M1 phenotype. In contrast, activation of this pathway by knockdown of the MTOR repressor TSC2 (tuberous sclerosis 2) exerts the opposite effect.

Several studies reported that IL6/STAT3 signaling pathway as a potent mTOR activator **Pinno, Bongartz et al. (2016) & Kim, Jhun et al. (2014).** siRNA knockdown of Atg7 -/- mice inhibited autophagy and resulted in ULK1 inhibition and the activation of colony-stimulating factor-1 (CSF -1 or MCSF), which is involved in macrophage polarization M1 –M2 **Jacquel, Obba et al. (2012).** MCSF triggered the phosphorylation of ULK1 in primary monocytes **Boulakirba, Pfeifer et al. (2018),** and activated ERK1/2 stimulation. MCSF was also found to regulate LC3 Autophagy marker **Mancino and Lawrence (2010)**

## II- HYPOTHESIS:

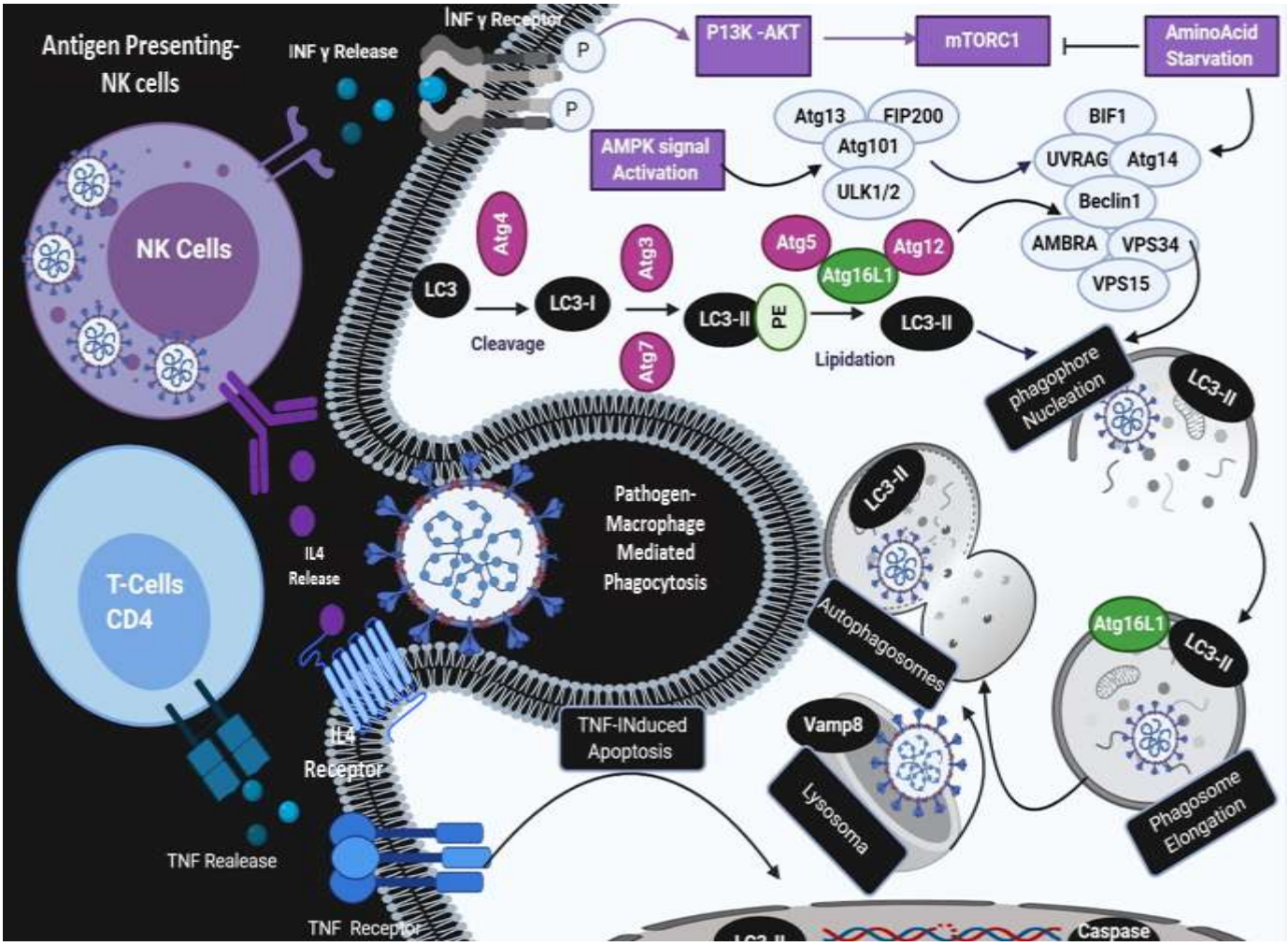


**FIGURE 4 OUR STUDY HYPOTHESIS; AUTOPHAGIC REPROGRAMMING OF MACROPHAGES POLARIZATION IN PHAGOCYTOSIS.**

**(DESIGNED BY AUTHORS USING BIORENDER.COM)**

Our Hypothesis is studying how autophagy reprograms the macrophages activation or polarization during phagocytosis.

## III- AIMS OF THE CURRENT STUDY:

1- Identification of the candidate proteins involved in the interplay between Autophagy and Macrophages polarization using a systems biology approach.

2- Isolation of Bone Marrow-Derived Macrophages from Female C57B/6J mice

3- Experimental validation the protein targets that mediate the interplay between Autophagy and Macrophages Polarization.

# METHODS:

## SYSTEMS BIOLOGY APPROACH (IN SILICO ANALYSIS) OF AUTOPHAGY-RELATED GENES

### AUTOPHAGY RELATED GENES

A total of 249 autophagy-related genes directly or indirectly involved in autophagy were obtained from the public Human Autophagy Database **(HADb)** and verified from the HCGN **Klionsky, Cregg et al. (2003).** A protein-protein interaction network was constructed using **STRING V11** online interface **Szklarczyk, Gable et al. (2019).** The produced protein Networks Data were integrated, verified, and visualized using **Cytoscape 3.8.2** software **Shannon, Markiel et al. (2003).** Moreover, the 249 Autophagy Associated proteins clustered using the "Molecular Complex Detection" **MCODE** algorithm a Cytoscape plugin **Bader and Hogue (2003).** MCODE clustering resulted in 7 clusters. Two clusters with the highest scores were picked to form a new hub gene of 75 genes list. Gene Ontology terms **(GO)** and pathway enrichment analyses were carried out for the 24 hub genes list using the Clue Go Cytoscape plugin **Bindea, Mlecnik et al. (2009).**

### MACROPHAGES DIFFERENTIALLY EXPRESSED GENES

Two raw Microarray datasets for screening differentially expressed genes **(DEGs)** associated with macrophages M1, M2 phase's polarization were obtained from the Gene expression omnibus database GEO of the National Center for Biotechnology Information under accession number **GSE81922 obtained from Jiang, Li et al. (2017)& GSE69607 obtained from Jablonski, Amici et al. (2015) .** Preprocessing and data quality control was performed using limma package 3.26.8. R studio **Ritchie, Phipson et al. (2015)** and Gene Expression Omnibus 2 Repository (GEO2R) open-source code. The data normalization and log -2 transformations were recalculated using limma package default parameters based on the threshold of fold-change > 2.0 and P-value < 0.05 for the raw data. Adjusted p-value was performed with the default parameter in the limma package using False discovery rate (FDR < 0.05) **Glickman, Rao et al. (2014).**

The top 250 highly expressed genes in M1 and M2 polarization were selected as the DEGs list for M1 and M2a polarization. Functional annotation and pathway enrichment analysis of the M1 & M2 DEGs list was performed using the Clue Go plugin Cytoscape 3.6. The enriched pathways appeared according to their significance p-value < 0.05 using Enrichment/depletion two-sided hypergeometric test **Rivals, Personnaz et al. (2007)**, using Bonferroni step down test to show the highest significance in the enrichment network**.**

The DEGs list of M1 and M2a curated from **GSE81922** and **GSE69607** Microarray Data were then used as protein input for STRING 11.V to construct a protein-protein interaction network. The parameters of prediction were set after removing the test mining to reduce the error in prediction. The confidence interval was set to high confidence (0.7). The top DEGs were clustered using the MCODE algorithm plugin on Cytoscape to extract the Hubs in the network. Clustering resulted in finding 18 Hub genes.

### COMMON TRANSCRIPTION FACTORS PREDICTION

In-silico prediction was performed to obtain the common regulon and transcription binding motifs that regulate both autophagy genes **(24 genes)** and M1, M2 polarization DEGs list (**18 genes). The I-regulon Janky, Verfaillie et al. (2014)** Cytoscape 3.8.2 plugin was used for this prediction, using the default parameters with a maximum false discovery rate (FDR) on motif similarity of 0.001. Prediction via I regulon resulted in 12 Gene regulatory transcriptional networks. Which then were manually verified using **TRANSFAC** and **JASPAR** databases.

### REGULATORY MIRNAS PREDICTION FOR GENE-TRANSCRIPTION

Three databases, Target scan Mouse 7.1 **Agarwal, Bell et al. (2015),** miRBase **Lewis, Shih et al. (2003)**, and Network Analyst **Zhou, Soufan et al. (2019),** were studied to predict the common regulating upstream miRNAs that link between autophagy and macrophage polarization. We found 8 predicted miRNAs to have a common link between Autophagy and Macrophages Polarization in the Phagocytosis process.

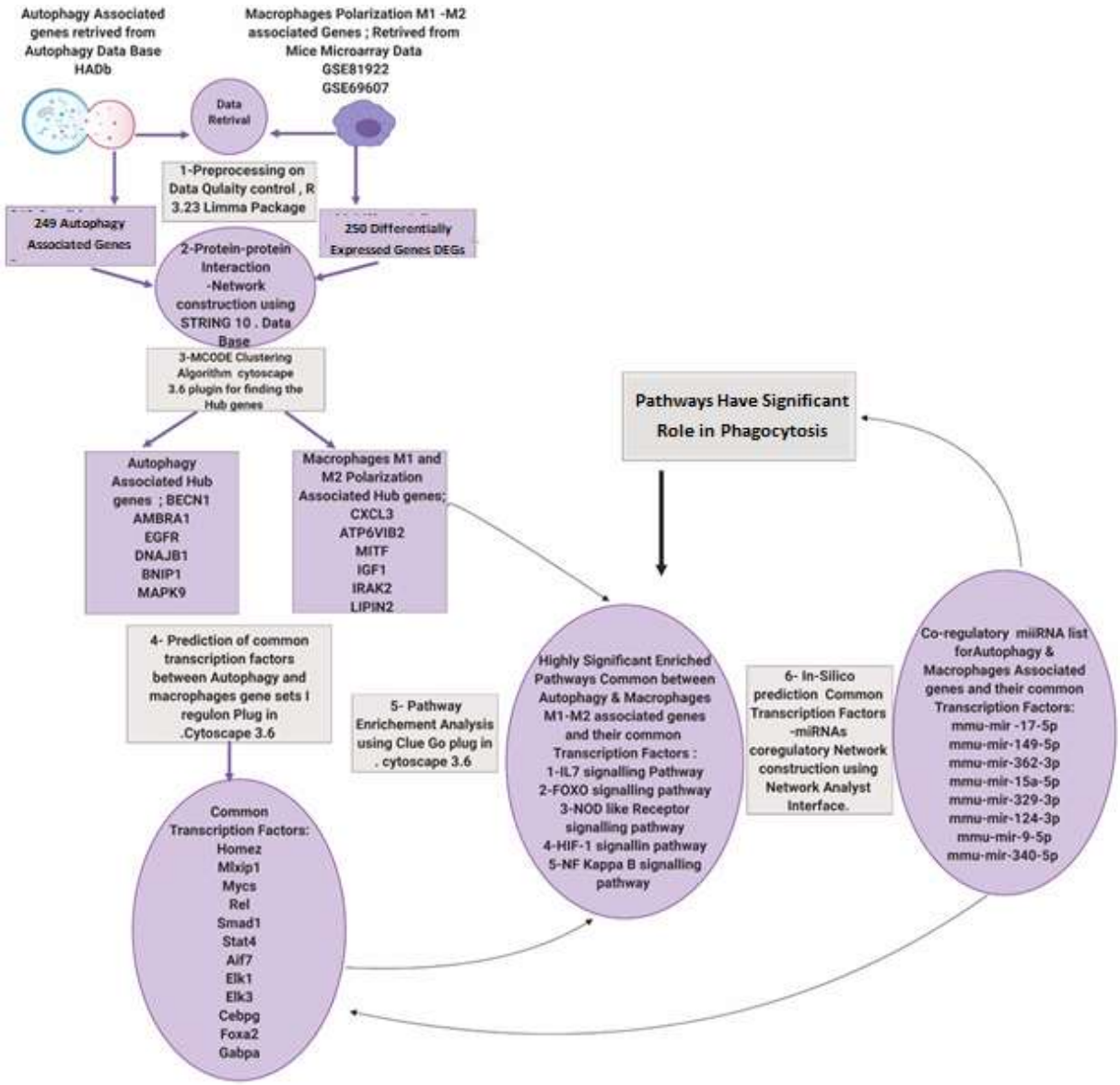


**FIGURE 5. REPRESENTATION OF SYSTEMS BIOLOGY APPROACH**

was performed on 249 autophagy-related genes (ATGs) retrieved from the public autophagy database HADb and gene expression data retrieved from Gene Expression Omnibus (GEO); GSE81922 & GSE69607 microarray data macrophages polarization 250 genes (DEGs). For both ATGs and DEGs gene sets; an integrated protein-protein interaction network was constructed, go terms pathway enrichment analysis was performed. Finally, common transcription factors and enriched miRNAs were predicted. (Designed by The Authors Using Biorender.Com).

# ISOLATION AND CHARACTERIZATION OF BONE MARROW-DERIVED MONOCYTES

## MONOCYTES ISOLATION

Female C57B/6J mice were obtained from Theodore Bilharz Research Institute (TBRI, Giza, Egypt). All experiments were performed in compliance with the national institute of health (NIH) guidelines for the Care and Use of Laboratory Animals. Mice were euthanized by an overdose of Ketamine Xylazine followed by cervical dislocation. The femur and tibia were removed and rinsed in ethanol 70% for 5 minutes, followed by Phosphate Buffered Saline (PBS) 1X, 6.7 mM PO4, without Calcium and Magnesium. The tibia and femur were then rinsed in Dulbecco's Modified Eagle Medium: F12, DMEM: F12 with HEPES (25mM), 1:1 mixture with 3.151 g/L glucose, with L-Glutamine (Lonza, Basil, Switzerland) for 10 minutes. The bones were flushed with 1x PBS over a 70 µm Cell Strainer (Greiner, Kremsmünster, Austria).

The cell suspension was lysed with Ammonium –Chloride- Potassium Lysing Buffer Saline 1x. (Lonza, Basil, Switzerland) for 5 minutes to eliminate Red Blood Cells and Thrombocytes contamination. Following the lysis, the cell suspension was centrifuged for 5 minutes at 500 g. The cells were re-suspended in lymphocyte separation medium (Lonza Basil, Switzerland) combined with DMEMF-12 Complete Medium (DMEMF-12+10% FBS+1% Penicillin and streptomycin) and centrifuged at 500 g for 10 minutes. The cell suspension was collected, counted, and seeded at a density of 300,000 cell/well in 12 well plates (Greiner, Kremsmünster, Austria), and incubated for 72 hr., at 37$^{o}$ C, 5% $CO_2$.

## M1-M2A LINEAGE POLARIZATION

Monocytes were maintained in complete DMEMF-12 medium (DMEMF-12 + 20% L929 Conditioned Medium + 10% FBS + 1% Penicillin, Streptomycin). Mouse skin Fibroblast Cell line L929 was used as a source for Monocyte Colony Stimulating Factor M-CSF for alternative activation of bone marrow-derived macrophages as previously reported by **Gordon and Martinez (2010).**

Five days after isolation, monocytes reached M0 or Naive Macrophage lineage. M0 were polarized to M1 by 1250 IU/ml Type II Interferon Gamma (INF γ, Stem Cell Technologies, Cambridge Research Park, United Kingdom), or M2a by 2500 IU/ml Interleukin - 4 (IL-4, Cambridge Research Park, United Kingdom) in combination with 10 ng/ml Lipopolysaccharide (LPS) from

*Escherichia coli (*Thermofisher Scientific, Waltham, Massachusetts, USA) for 48 hrs. as previously reported by **Zhang, Goncalves et al. (2008).** By day 7, cells were polarized to reach activated M1 or M2a lineage for further experimental use.

### AUTOPHAGY INHIBITION / INDUCTION IN POLARIZED MACROPHAGES

For autophagy inhibition, 200 n.M Bafilomycin A 1 (Cell signaling Technologies, Danvers, Massachusetts, USA) was added for M0 φ, M1 φ and M2a φ Lineages for 18 hrs. **Goeritzer, Vujic et al. (2015)**. To induce Autophagy, M0 φ were treated with Earle's Balanced Salt Medium (Lonza, Basil, Switzerland) for 16 hrs. **Min, Xu et al. (2013)**

### CELL VIABILITY AND CYTOTOXICITY ASSAY

Macrophages were seeded in 96 well plates (10000 cell /well). MTT tetrazolium reduction assay was performed as previously reported **Kumar, Nagarajan et al. (2018)**. In summary, following 3 hrs. incubation with MTT reagent, the media were removed, and DMSO was added to dissolve the formazan crystals. The cells were examined using an inverted microscope (Olympus 1X70, Tokyo, Japan), and absorbance was measured at 570 nm using a microplate reader (Ultrospec 3100 pro). Cell viability (%) was calculated based on the following equation:

$$Survival\ rate\ \% = (\text{Ab}\ sample - \text{Ab}\ blank) / (\text{Ab}\ control - \text{Ab}\ blank) \text{ X } 100$$

Where Ab sample is the sample absorbance, Ab blank is the absorbance of blank, and Ab control is the absorbance of the control.

### AUTOPHAGY ASSAY

At day 5, Macrophages M0 were seeded at 96 well plates at seeding density 10000 cell /well for 48 hrs. Autophagy assay was performed according to the manufacturer's instruction (MAK138 fluorometric assay kit, Sigma Aldrich, Saint Louis, Missouri, USA). The media was removed and autophagosome detection reagent was added and incubated in the dark for 1 hr. at 37$^{o}$C and 5% $CO_2$. Cells were washed gently by adding 100 ul washing buffer, and the fluorescence intensity was measured at (λex = 360/λ em = 520 nm).

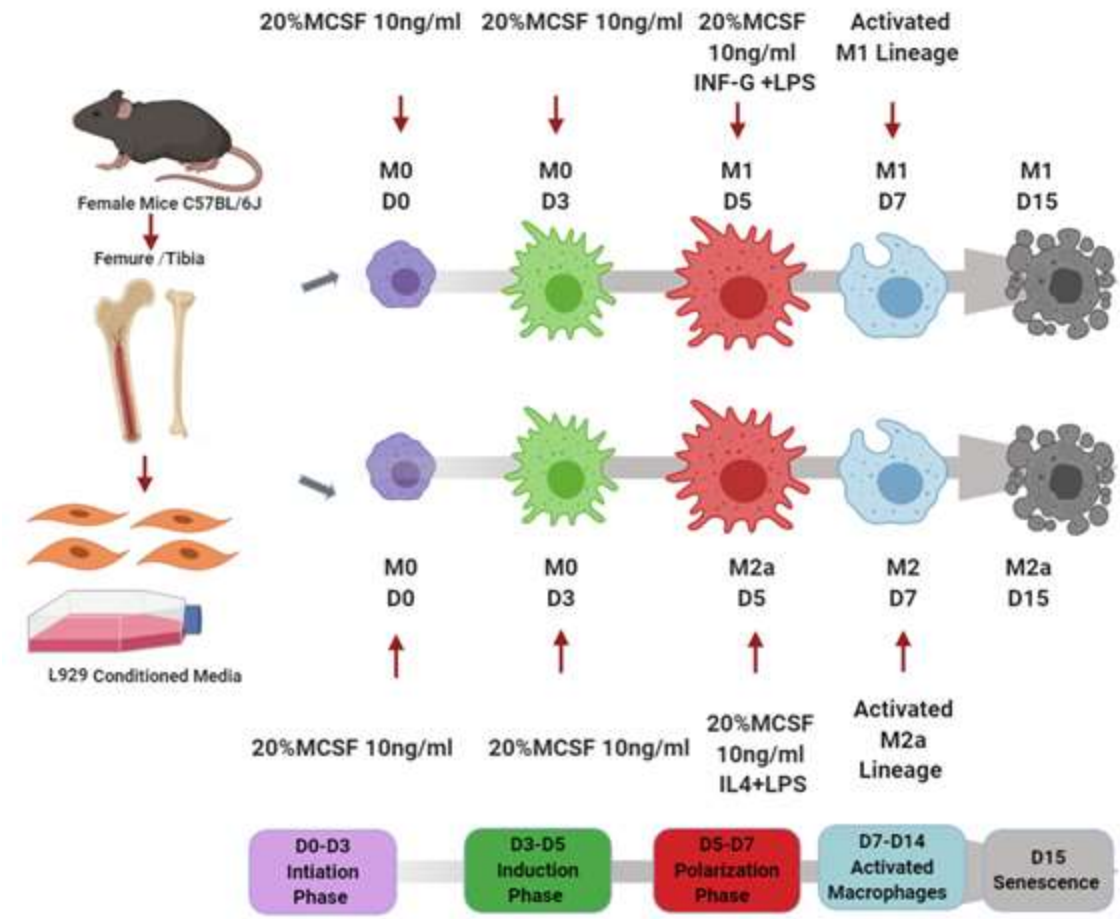


**FIGURE 6. ISOLATION PROTOCOL FOR MURINE BONE MARROW-DERIVED MACROPHAGES.**

Monocytes were collected from the femur and tibia of female mice C57B/6J. The initiation phase is from day 0 to day 3. Induction phase day 3 to day 5, to reach activated M0 macrophage. The polarization phase from day 5 to day 7 to reach either M1 or M2a lineage. Cell senescence usually starts by day 15. **(Designed by Authors using Biorender.com)**

### PHAGOCYTOSIS ASSAY

Macrophage M0 φ at day 5 were seeded at 96 well plate at seeding density 1000,0 cell /well to contain a final volume 100 ul /well primed for 48 hrs. to M1 φ and M2a φ lineage as previously mentioned. cells were stained with MAK 138 auto phagosome detection reagent as mentioned earlier. Escherichia Coli. Top ten strain was grown as previously mentioned. E. coli Top 10 bacteria were grown in LB broth liquid (Purchased (Thermofisher scientific, Waltham, Massachusetts, USA) were added to the cells. Cells were stained with 1 ug/ml (4',6-Diamidino-2-phenylindole·2HCl) DAPI stain ((Lonza, Basil, Switzerland)), and examined under fluorescent microscopy (Leica microsystem inverted fluorescent microscope, Germany). The number of phagocytic events were counted for each condition.

### EARLY APOPTOSIS DETECTION

Macrophages were primed to M1 and M2a as previously described. Neuroblastoma cell line SH-SY5Y were cultured in conditioned media from Macrophages M0, M1 and M2a for 24hrs. Cells were fixed with 4% PFA and permeabilized for 10 minutes with 0.3% triton 100x. Cells were washed and stained with DAPI, and mounted on slides. Cells were examined under the microscope (Leica microsystem inverted fluorescent microscope, Germany). Cells treated with cisplatin 20 ng/ml were used as a positive control.

### IMMUNE FLUORESCENT STAINING

Macrophages were fixed with 4% PFA for 10 minutes and washed with PBS. Cells were blocked and permeabilized with blocking buffer (5%BSA, 0.3% Triton 100X in PBS 1x) for 1 hr. Cells were incubated overnight at $4^{o}$ C in the dark with the following primary antibodies: Rabbit Mab LC3B (1:200), Rabbit Mab Atg16L1 (1:100), Rabbit Mab Smad1 (1:200), Rabbit Mab Atg7 (1:200), and Rabbit Mab IL6 (1:200) (Cell signaling Technologies, Danvers, Massachusetts, USA). Cells were later incubated with Anti-Rabbit Mab polyclonal secondary antibody for 2 hrs. (Alexa flour 488, 1:500), followed by washing and DAPI counterstaining for 10 minutes. Cells were examined under a fluorescence microscope (Leica microsystem fluorescent microscope, Germany). For confocal microscopy, a Leica Microsystems Laser confocal microscope was used. Images were deconvoluted using Carl Zeiss Zen blue 12 (Carl Zeiss, USA) software and Z-Stacks were 3D reconstructed. Using ICY software **de Chaumont, Dallongeville et al. (2012).**

To detect intracellular trafficking of Atg7, Atg16l1, and LC3B inside the cytoplasmic or nuclear compartment, an automated spot detector plugin SICE as described by Bayle, Platre et al. (2017). Images were taken by a fluorescent microscope (Leica microsystem, Germany) and imported to ImageJ software ®**.** A minimum of 8 images were counted for each condition.

### FLOW CYTOMETRY

Macrophages were collected and washed with 0.5% FBS in 1x PBS and centrifuged at 350g for 5 minutes. Cells were stained with mouse-specific antibody conjugate eflour660 CD68 and Alexa 488 conjugated Arginase- 1 (eBioscience, United States), for 30 minutes and washed with 1x PBS. Unstained samples M0, M1, M2a were used as a negative control. Samples were measured and gated on a flow cytometer (**CytoFlex, Beckman Coulter united states, at Immunology unit, Children's Cancer Hospital, Egypt 57357)** using two filters, for CD 68 at APC (660 nm) and for Arginase- 1 at FITC (488 nm).

### RNA EXTRACTION AND CDNA SYNTHESIS

M0, M1 and M2a cells were harvested at day 7 and day 14. RNA was isolated as described previously. using TRIZOL reagent (Invitrogen. United States). Isolated RNA yield was checked for integrity and purity (Multiplate Reader, Sigma Aldrich, Germany). A total of 0.5 µg/ul RNA was used for each sample and control to produce 0.5 µg/ul cDNA template using cDNA synthesis kit (Revert Aid First Strand cDNA, Thermofisher Scientific, United States)

### QUANTITATIVE REAL-TIME -PCR

The polymerase chain reaction was performed using (Real-Time quantitative PCR machine 7500, Applied Biosystems, United States). In summary, cDNA template was used at a concentration of 0.5 ug/ul and a total of 10 ul reaction volume by using a one-step qPCR Master Mix (HERA SYBR Green kit, Willow fort, United Kingdom). Each sample was normalized to GAPDH as endogenous housekeeping control, and M0 lineage was used as normal control. Quantification of the target mRNA was normalized according to the delta-delta Ct (ΔΔCt) method and the expression fold change (2-ΔΔCt) using GAPDH as reference. Table 2 shows the primers that were used in RT-qPCR.

**Table 2. Forward & Reverse Primers Used in This Study**

| Gene | F-primer 5'-3' | R-Primer 5'-3' | Reference |
|---|---|---|---|
| **Atg16L1 -*1*** | *TCTTCTGATGCTGC CAGGAGAC* | *TGCACTGCGTTGACC TCTC* | **Primer Plus Predicted** |
| **Atg16l1-3** | *TGCAGAAGCAGCAA AGGAACC* | *GACAGAGCGTCTCGT AGCTG* | **Primer Plus Predicted** |
| **SMAD1** | *GTGTATGAACTCAC CAAAATGTGC* | *TAACATCCTGCCGGT GGTATTC* | **Marks-Bluth, Khanna et al. (2015)** |
| **GAPDH** | *CTCCCACTCTTCCA CCTTCG* | *GCCTCTCTTGCTCAG TGTCC* | **Choi, Jeong et al. (2019)** |
| **VAMP7** | *TGGCTGCACAACTG AAGCAT* | *GCAATTCCAACCTTTC TCCACG* | **Primer Plus Predicted** |
| **Atg7** | *AGCAGTGATGACCG CATGAA* | *TCAGCAGCTTGGGTC TCTTG* | **Park, Ou et al. (2016)** |
| **Lc3A** | *TTGGTCAAGATCAT CCGGC* | *GCTCACCATGCTGTG CTGG* | **Scherz-Shouval, Weidberg et al. (2010)** |
| **Lc3B** | *CCCACCAAGATCCC AGTGAT* | *CCAGGAACTTGGTCT TGTCCA* | **Scherz-Shouval, Weidberg et al. (2010)** |

## CHAPTER III: RESULTS

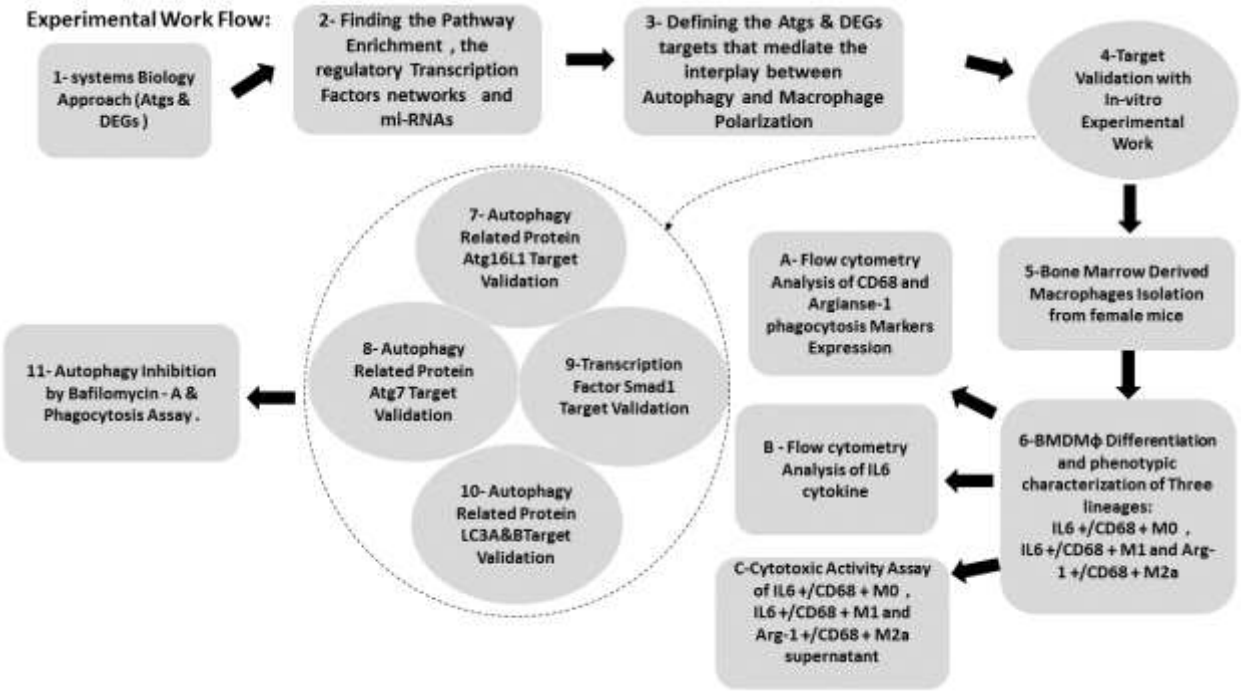


**Figure 7: The experimental workflow.**

A systems biology approach was performed to find the interplay between autophagy related genes (Atgs) & Differentially expressed genes of Macrophage Polarization M1-M2 (DEGs) (step 1), followed by common pathway enrichment and construction of transcription factors and mi-RNAs regulatory networks (step 2). The Atgs and DEGs targets that mediate the interplay between autophagy and macrophage polarization were defined ( step 3), and experimental validation for targets took place (step 4). Bone marrow-derived monocytes were isolated from the femur and tibia of female mice (step 5). After differentiation of monocytes to M0, M1, and M2a, the lineage phenotypes were characterized using flow cytometry (step). Afterward, we validated the targets of Smad1, LC3A&B, Atg16L1, Atg7, IL6, CD68, Arg-1, and Vamp7 (Steps 7, 8, 9, and 10). Finally, we investigated the impact of autophagy inhibition on all immune lineages using autophagy inhibitor Bafilomycin-A (step 11).

## 1- Systems Biology Approach

Autophagy and macrophage polarization are complex biological processes. We used a Network-based systems biology approach to model the interplay between these complex signaling pathways. The analysis of the different databases identified common significantly enriched pathways, common regulatory transcription factors, and upstream miRNAs that co-regulate both transcription factors and Atgs & M1-M2-DEGS.

**Genetic regulatory networks.**

The protein-protein interaction network of autophagy-related genes in mice was constructed by STRING **V11** online interface ***(Szklarczyk, Gable et al. (2019)).*** The number of nodes was 221, the number of edges was 638, the average node degree is 5.7, and the average local clustering coefficient was 0.42 with a protein-protein interaction enrichment p-value < 1.0 e-16 (**figure 8)**.

The network was visualized using the String plugin in **Cytoscape 3.8.2** software ***(Doncheva, Morris et al. (2019),*** and the network was clustered using the MCODE algorithm plugin to find the highly connected genes in this network**.** A total of 7 clusters **(figure 9)** ranked from the highest score to the least score. Networks with the highest two scores were selected for pathway enrichment with Clue Go. The highly significant pathways were; Cellular response to nitrogen starvation, Apelin signaling pathway, selective autophagy, and autophagosome assembly **(figure 10).**

**Protein-Protein Interaction Network Construction Autophagy Related Genes**

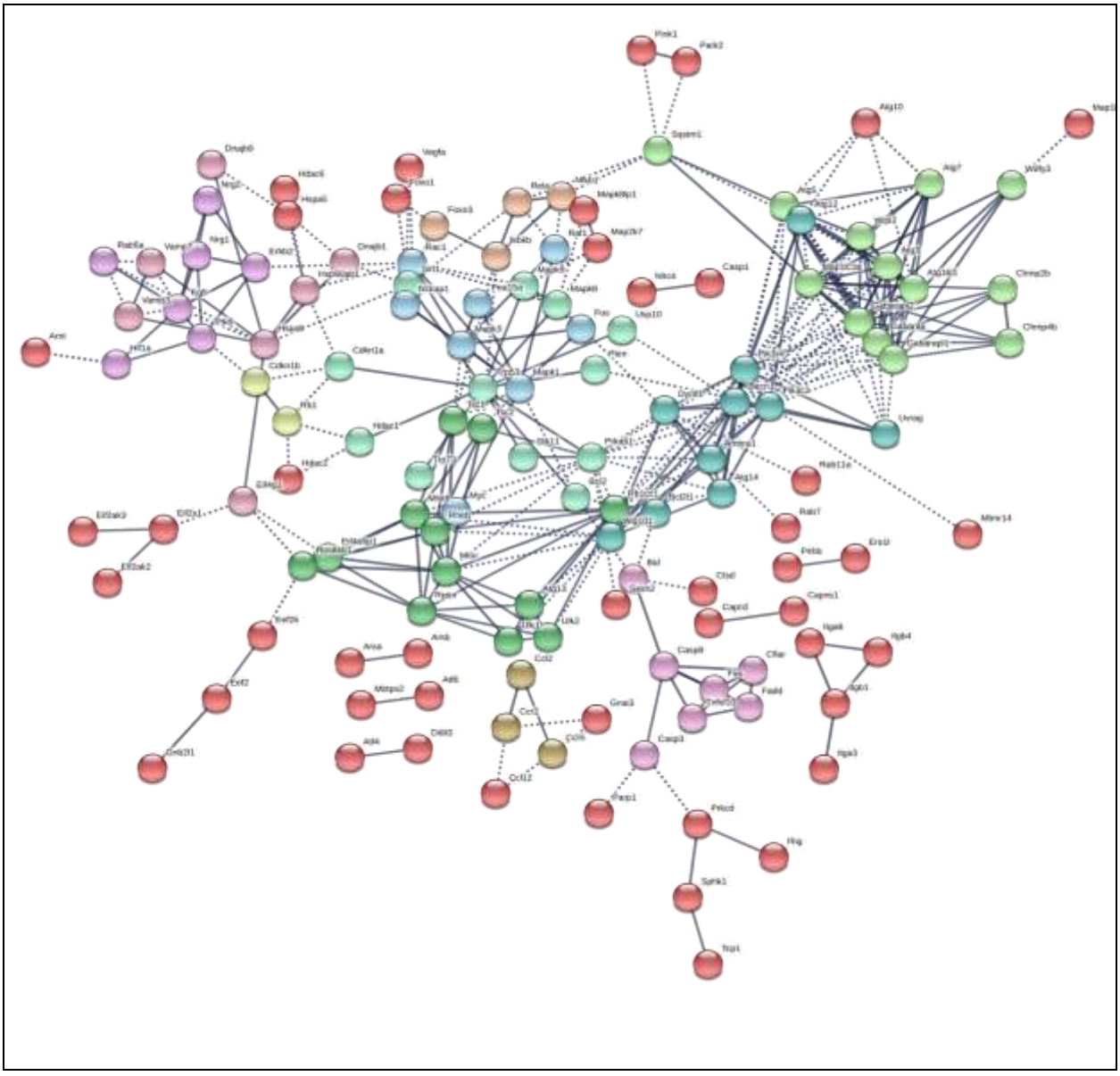

**Figure 8. Protein-Protein interaction**

Autophagy associated proteins were entered as protein list on STRINGVI software then. STRING predicted the interaction between these proteins forming a protein-protein interaction network where thick lines mean strong interactions. Red nodes query proteins and the first shell of interactors. The significance of this network is **(p-value < 1.0e-16).** Here significance means the confidence degree of interactions presented in the network.

## MCode Algorithm clustering for Hub Genes

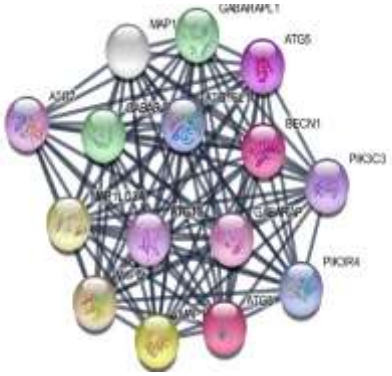


A

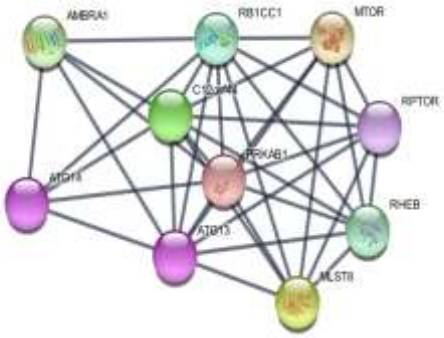


B

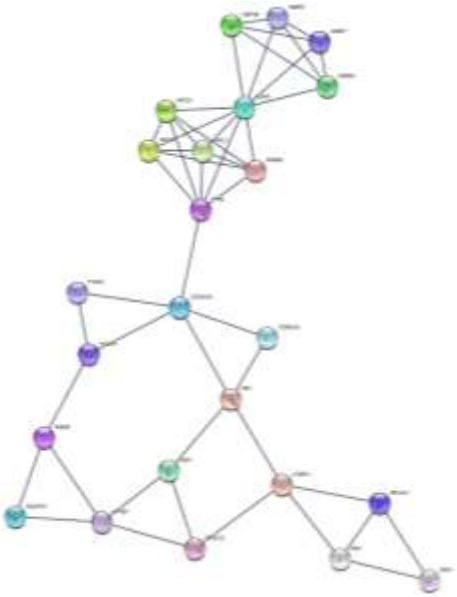

C

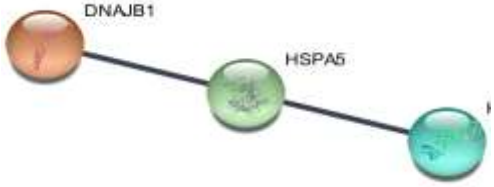


D

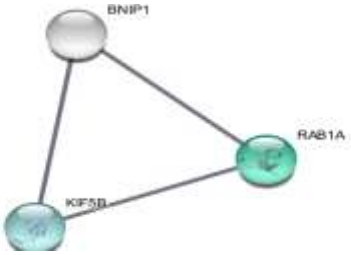


E

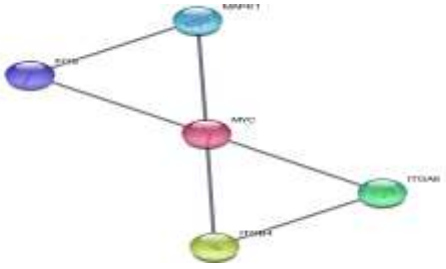

F


G

**Figure 9. Autophagy gene set & highly connected gene clusters.**

Using the MCODE algorithm clustering plugin, 7 clusters were generated. A) cluster 1 contained 15 genes with a score of 14.7 and BECN1 hub gene. B) Cluster 2 score of 8.22 and AMBRA1 hub gene. C) Cluster 3 score of 4.087 and EGFR hub gene. D) cluster 4 score 3 and RELA hub gene. E) Cluster 5 score of 3 and DNAJB1. F) Cluster 6 score of 3 and MYC hub gene) cluster 7, score 3, and MAPK 9 hub gene. The importance of clustering is sorting the hub proteins in the protein-protein interaction network. Hub proteins are the most proteins that have interactions (binding sites) for non -hub proteins.

**Biological Process GO terms Enrichment:**

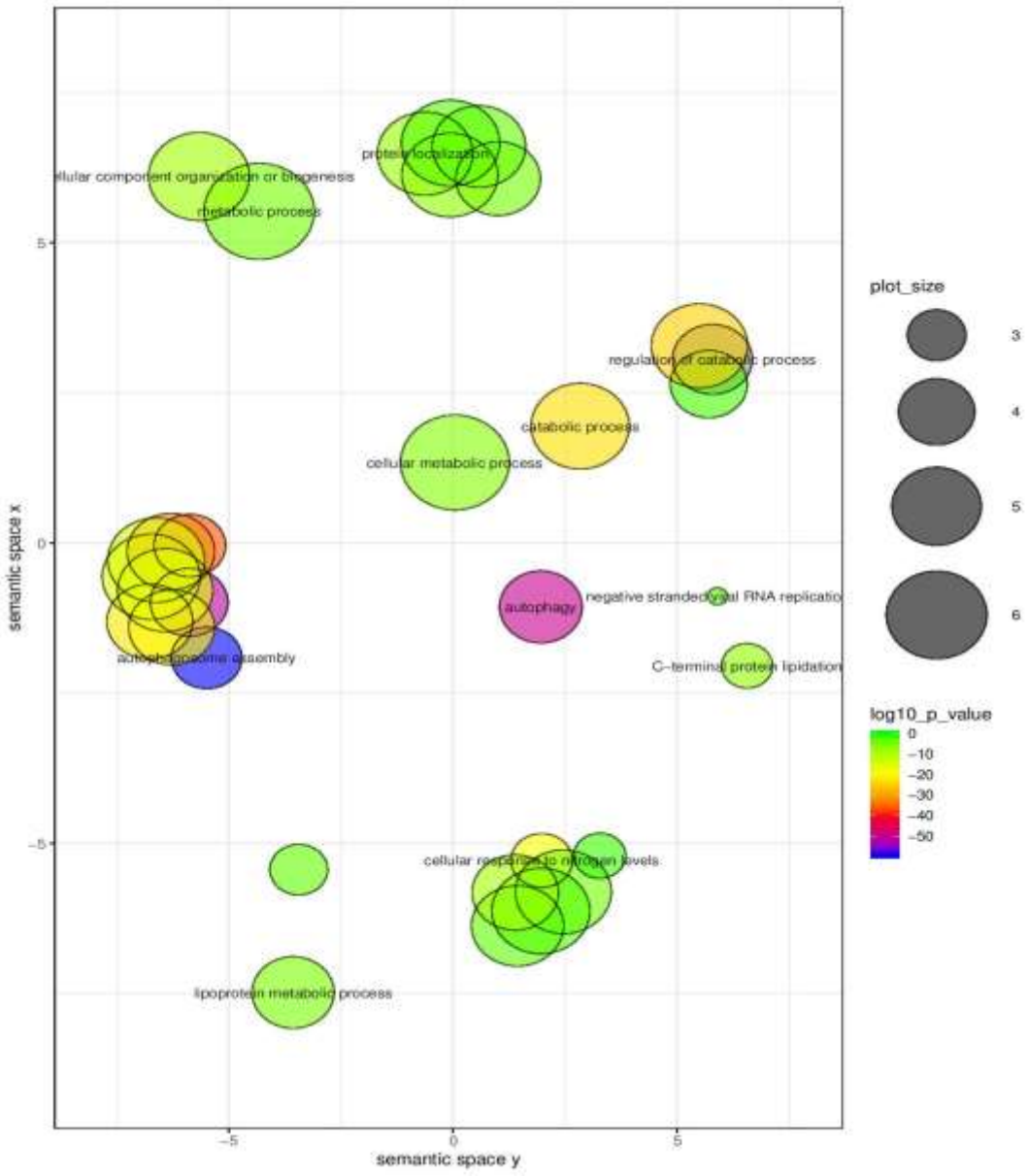


**Figure 10. Significantly enriched biological process in the autophagy-related proteins.**

Biological processes visualized the significance in terms of node size and log10 p-value as autophagy, lipoprotein metabolic process, cellular response to nitrogen levels, and autophagosome assembly are the highly significant biological process. The autophagosome assembly biological process significance indicates the importance of proteins responsible for autophagosome assembly such as; Atg16L1, LC3A&B, and Atg7 in this process.

**Pathway Enrichment Analysis**

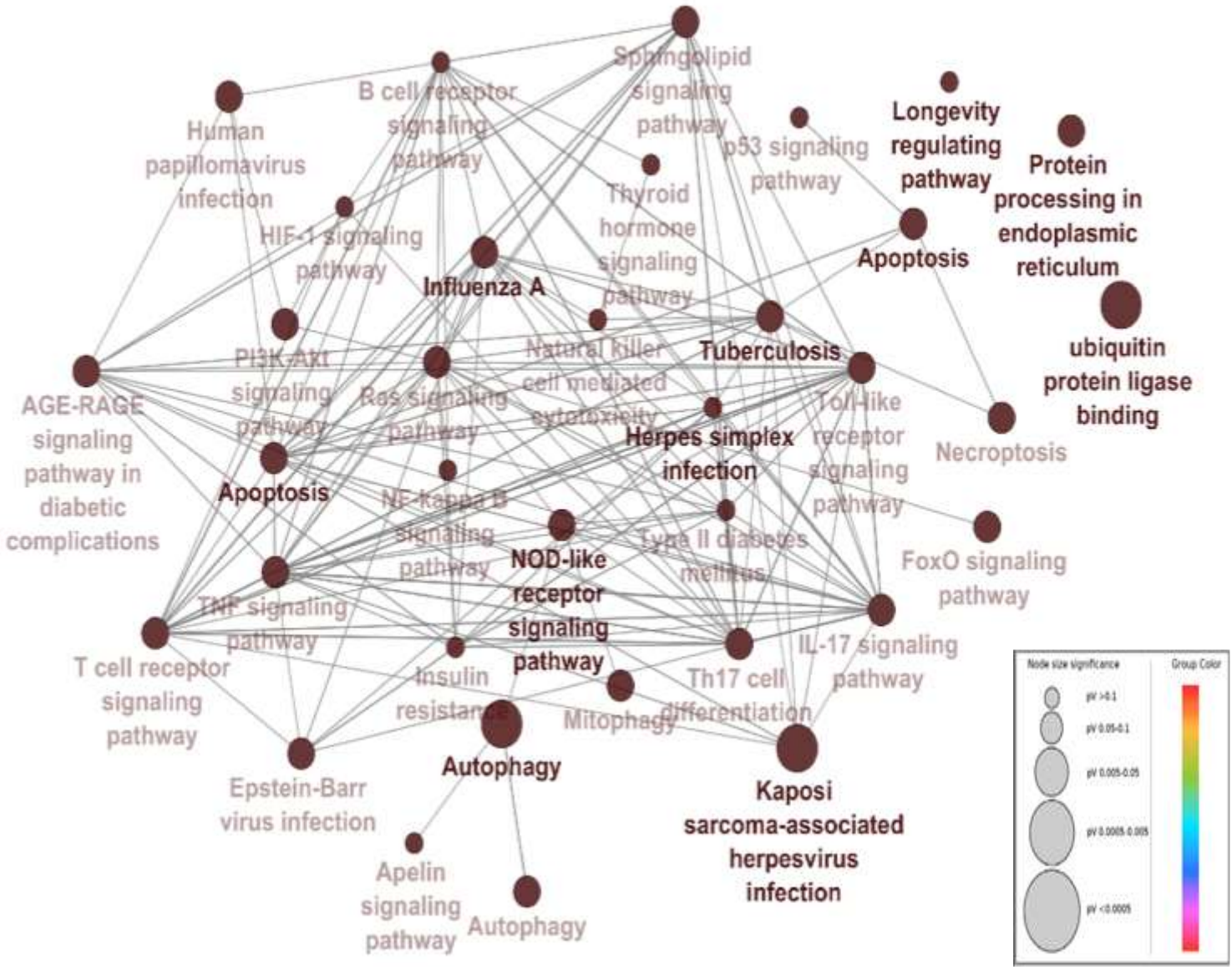


**Figure 11. Autophagy Related Proteins.**

The Cluego plot showed the significant functional go terms from KEGG pathways. Significance in terms of p-value < 0.05 and node size and nodes are linked according to their kappa score level (≥ 0.3). Autophagy, IL7 signaling pathway, FOXO signaling pathway, NOD-like receptor signaling pathway, HIF-1 signaling pathway, and NF-Kappa B signaling pathway.

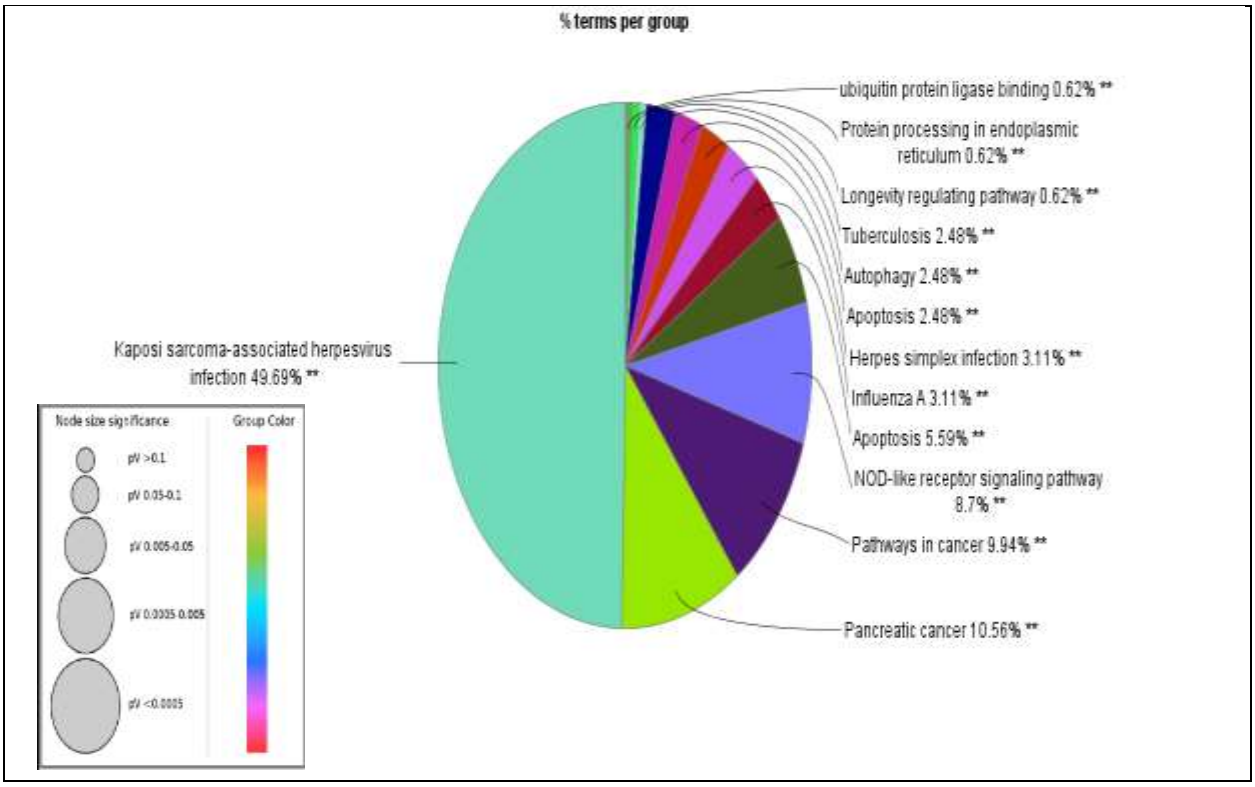


**Figure 12. Pie chart for functional groups in Clue-go enrichment.**

Pie chart showing the percentage of the most significant pathways in the autophagy proteins set. 8.7% of the proteins were enriched in the NOD-like receptor signaling pathway. This result refers to the interplay between autophagy-related proteins and NOD-like receptor pathway. The NOD-like receptor pathway is a key regulator for immune responses.

### M1-M2 Macrophages Polarization Networks

A protein-protein interaction network generated by string interface for the macrophages M1 –M2 gene set of 250 DEGs from GSE69607& GSE81922 the resulted network (**figure 13**). The number of nodes is 218, the number of edges is 160, and the average node degree is 1.47. The Average local clustering coefficient was 0.304, and PPI enrichment p-value: 1.03e-14.

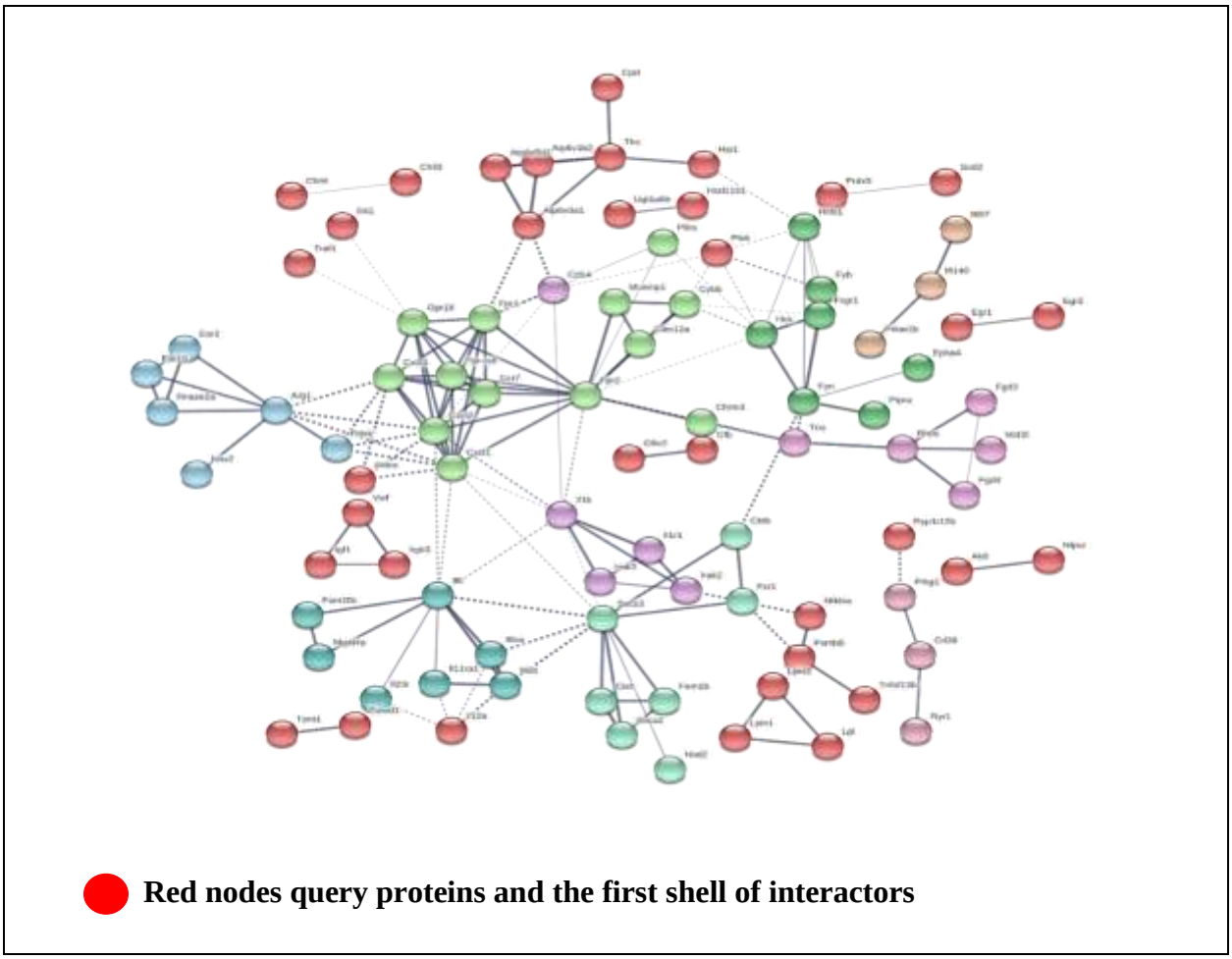


**Figure 13. String protein-protein interaction network of M1-M2 polarization.**

250 DEGs gene set, the thick lines between nodes based on their evidence of interaction and significant interaction. Number of nodes: 218, number of edges: 160, average node degree: 1.47, avg. local clustering coefficient: 0.304, significance in terms of protein-protein interaction enrichment p-value <0.01(1.03e-14) with confidence of 0.4. Here significance means the confidence degree of interactions presented in the network.

**GO terms Cellular process enrichment significance**

The 6 clusters generated from MCODE clustering were then analyzed for GO term pathway enrichment. The significant processes include tissue remodeling, response to interleukin -4, response to interleukin –1, positive regulation of NF-Kappa transcription factor activity, and aging (**figure 14).**

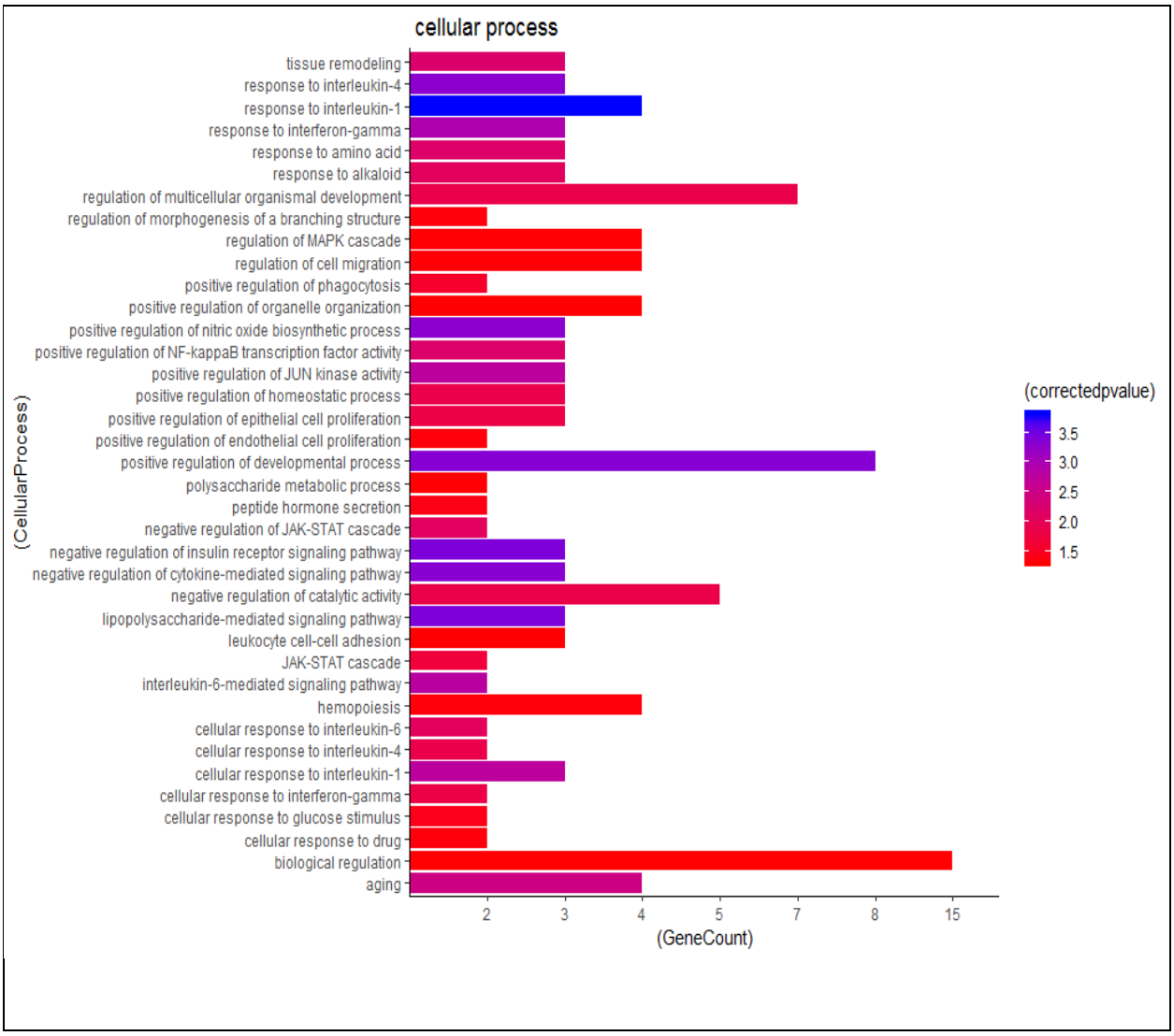


**Figure 14. Significant cellular process in M1 and M2 DEGs.**

The significance of corrected p-value includes tissue remodeling, response to interleukin -4, response to interleukin –1, positive regulation of NF-Kappa transcription factor activity, and aging.

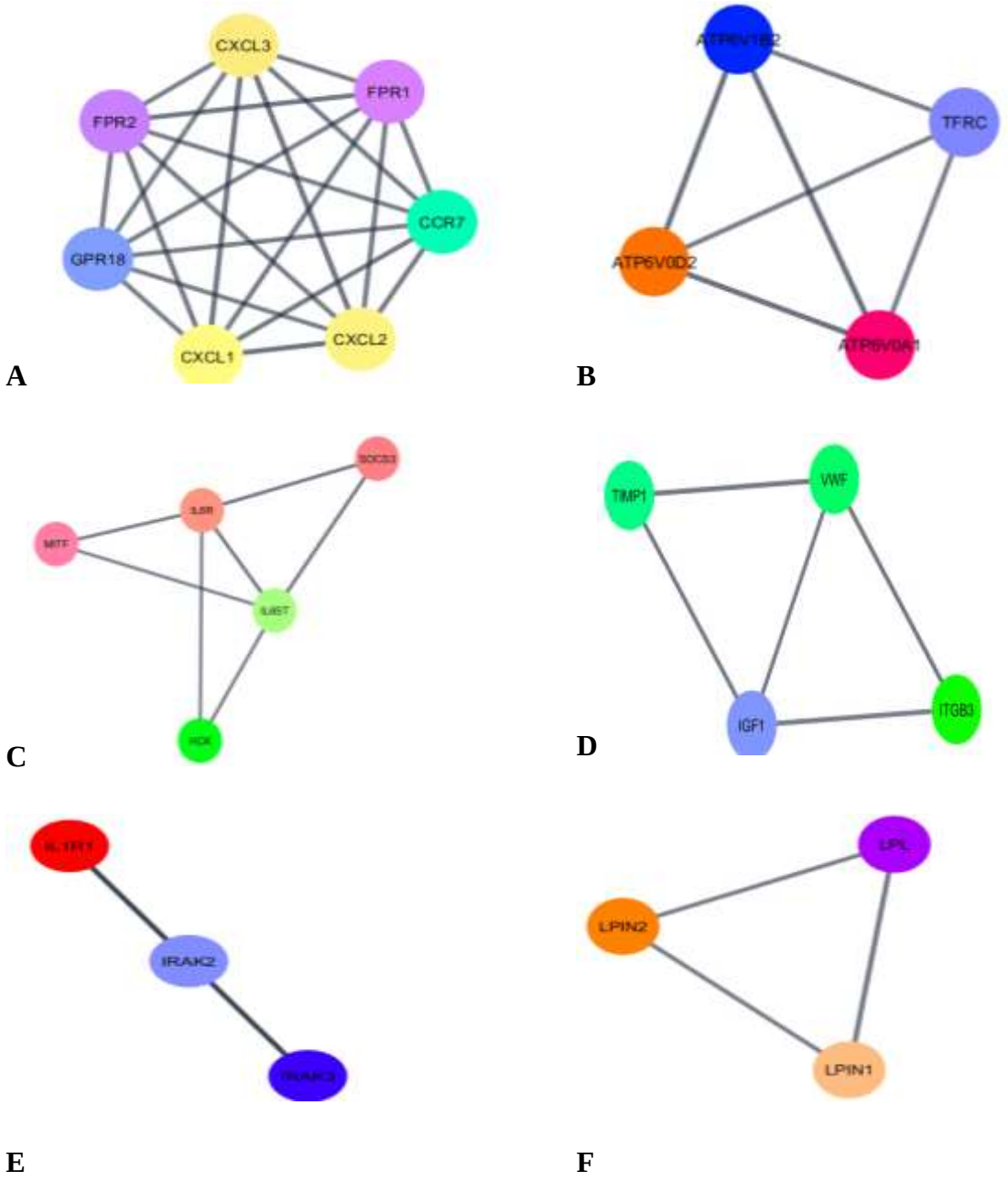


**Figure 15. MCODE clustering plot of M1 &M2 DEGs**

The highly connected genes clustered with MCODE algorithm plugin – Cytoscape. Six clusters with 6 hub genes were identified by the MCODE clustering algorithm as following; A) Cluster 1 with a score of 7 and CXCL3 hub gene. B) Cluster 2 with a score of 4 and ATP6V1B2 hub gene. C) Cluster 3 with a score of 3.5 and MITF hub gene. D) Cluster 4 with a score of 3.33, IFG1 is hub gene. E) Cluster 5 with a score of 3, and IRAK2 as a hub gene. F) Cluster 6 with a score of 3, and LPIN2 as a hub gene.

## MCODE Clustering Algorithm

The top 250 gene set of DEGs genes were Clustered by the MCODE Clustering algorithm to define the areas in the network that have the highest interaction. And also to define the gene hubs in the generated 6 clusters and 6 hub genes identified (**Figure 15).** Clusters were identified with CXCL3, ATP6V1B2, MITF, IFG1, IRAK2, and LPIN2 as hub genes. The importance of clustering is sorting the hub proteins in the protein-protein interaction network. Hub proteins are the most proteins that have interactions (binding sites) for non -hub proteins. Hub proteins such as CXCL3 and IRAK2 have a role in innate immunity in addition to their role in macrophage polarization.

## Pathway Enrichment Analysis

KEGG pathway enrichment (P-value is <0.05) involved pathways such as; regulation of wound healing, IL7 signaling pathway, TNF signaling pathway, keratinocyte migration, and FOXO signaling pathway.

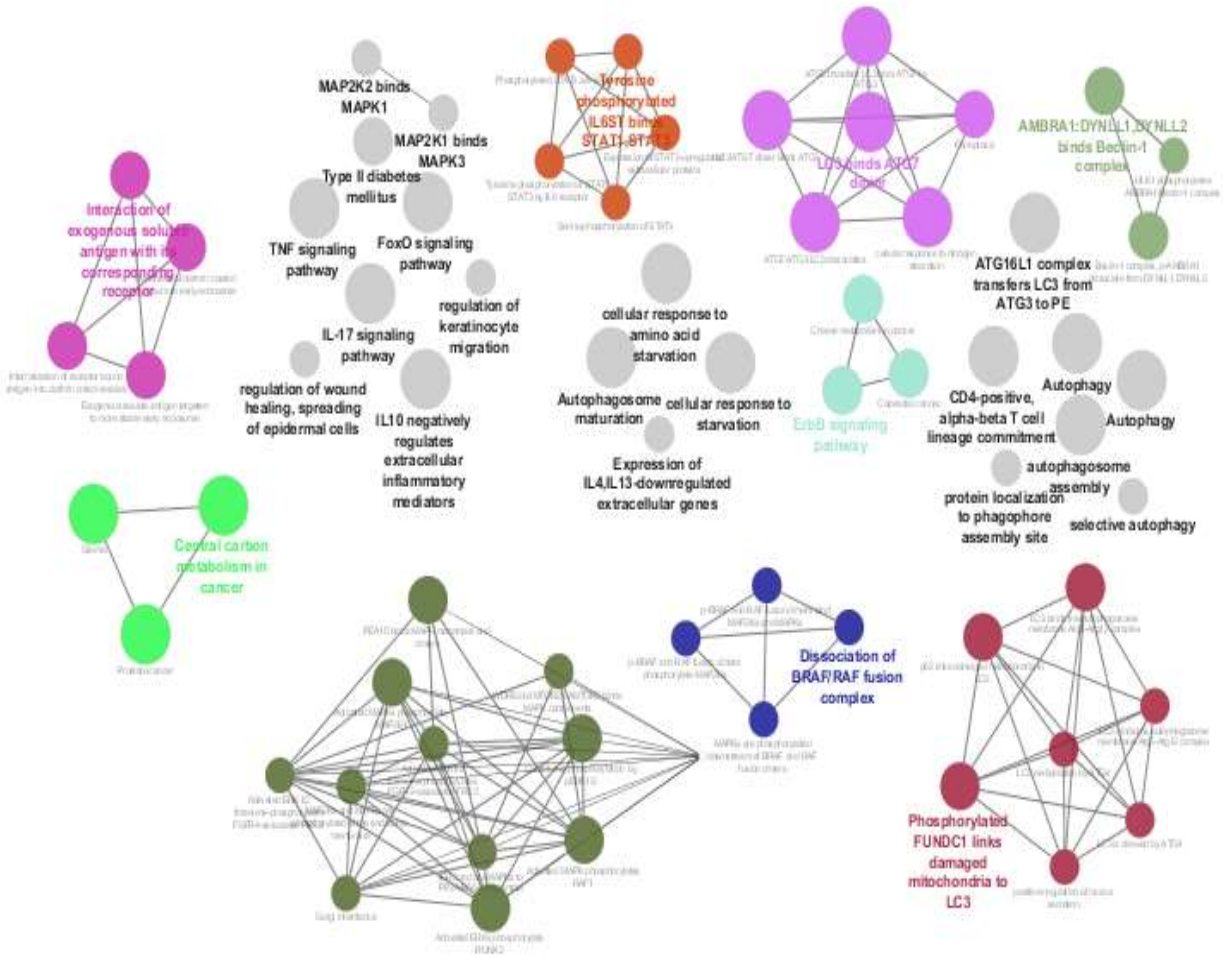


**Figure 16. Clue Go pathway enrichment graph.**

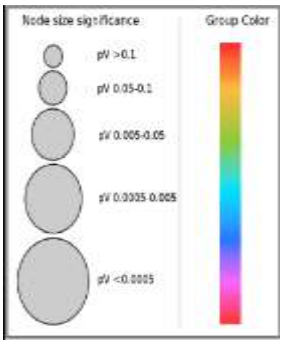


Highly enriched pathways in M1 & M2 Polarization. 6 Clusters were significant in terms of node size (brown nodes are highly significant). Also, KEGG pathway enrichment (P-value is <0.05) involved pathways such as; regulation of wound healing, IL7 signaling pathway, TNF signaling pathway, keratinocyte migration, and FOXO signaling pathway.

## 2- Transcription Binding Networks and pathways Enrichment Analysis.

### NF kappa, FOXO, HIF1, NOD-like receptor, and IL17 signaling pathways were significantly enriched , and common pathways between Atgs and DEGs:

Transcription binding motifs or Transcription factor (TF) regulatory networks aim for better mapping of complex biological processes such as the interplay between macroautophagy and M1 & M2 polarization. Our model shows that TF-miRNA mediated Atgs and DEGs gene regulation. It is also essential to identify the pathways enrichment for TF; consequently, upon looking for GO terms pathways enrichment analysis, we found common significantly enriched pathways among autophagy and M1-M2 Go terms. GO terms showed NF kappa, FOXO, HIF1, NOD-like receptor, and IL17 signaling pathways (**figure 14 & 16**).

LC3A & B and Atg7 proteins are autophagy-related proteins that are also enriched in autophagosome assembly (figure 9). Also, figure 16 showed enriched Atg16l1 related pathways and autophagosome assembly pathway. We previously mentioned that Atg16L1 is an autophagy-related protein and has a role in autophagosome assembly. Interestingly, we found a related pathway in the autophagy associated proteins enriched in Macrophages Polarization DEGs Set. This refers to the link between autophagy and macrophage polarization.

### IL6, MAP1LC3A, B, Atg16L1, and Atg7 represent potential candidate genes for macroautophagy induced Macrophage polarization

Our model revealed the interplay between two major complex biological processes such as; Autophagy and macrophage polarization. For instance, the Fork Head of box -1 FOXO 1 Transcription factor is a key regulator in the wound healing process and common regulator for IL6, MAP1LC3B, Atg16L1 (**figure (18).** In our model, the FOXO1 transcription factor signaling pathway showed high significance in terms of pathway enrichment (**figure 14**).

**Common Transcription Factors Regulatory Networks for both Autophagy Associated Gene and M1-M2 DEGs Clusters**

Figure **(18 & 19)** explained transcription binding motifs (MLXIPL, HOMEZ, RELA, SMAD1, and STAT4) predicted by I-regulon a Cytoscape plugin. We noted that Atg16L1, MAP1LC3A&B, IL6, and Atg7 were the most abundant genes in the 12 predicted transcriptional factor regulatory networks.

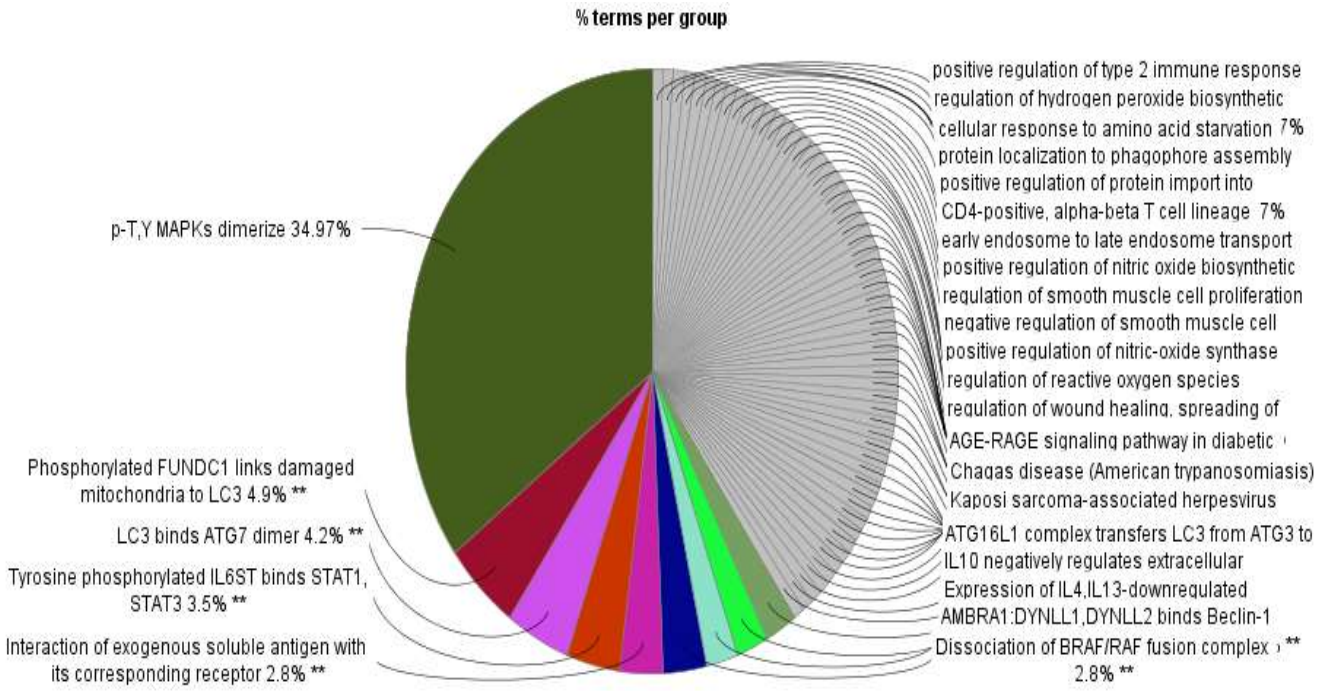


**Figure 17. Pie Chart of functional groups and their corresponding percentage.**

The figure **s**hows the most significantly enriched pathways as follows; 2.8%** Dissociation of BRAF/RAF fusion Complex, LC3 binds ATG7 dimer 4.2%**.

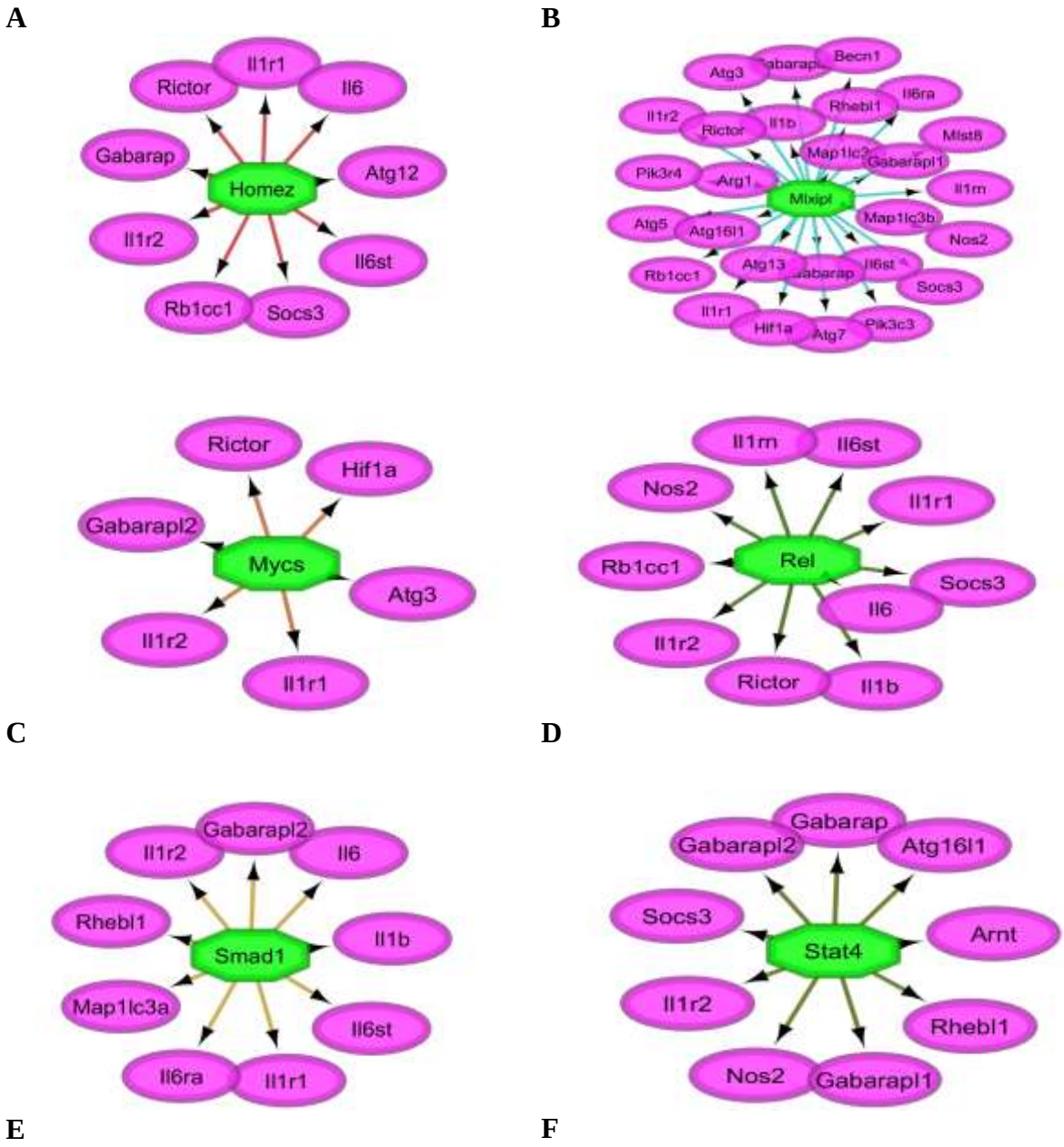


**Figure 18. I regulon plugin – Cytoscape predicted common transcription factors.**

Predicted common transcription factors that regulate both Autophagy genes clusters and M1 & M2 polarization genes 6 clusters. The transcription factors are shown in green, and downstream target genes are shown in pink. Homez (A), MLXipl (B), Mycs (C), Rel (D), Smad1 (E), and Stat4 (F) transcription factors are common transcription factors that regulate both autophagy and M1 & M2 polarization genes.

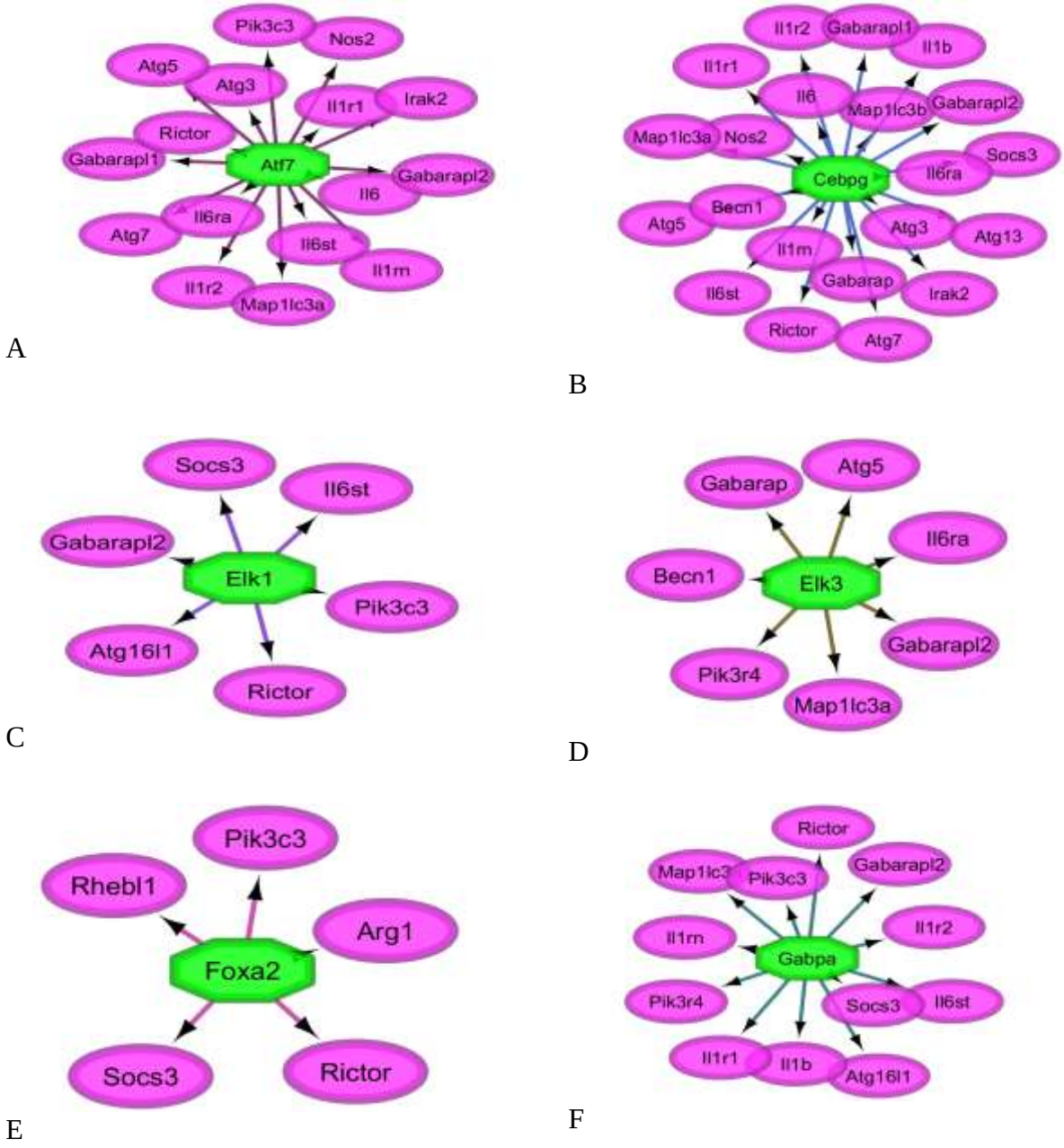


**Figure 19. I-regulon plugin – Cytoscape predicted common transcription factors.**

The transcription factors are shown in green, and downstream target genes are shown in pink. Atf7 (A), Cebpg (B), Elk1 (C), Elk3 (D), Foxa2 (E), and Gabpa (F) transcription factors regulate common transcription factors that regulate both autophagy and M1 & M2 polarization genes.

### 3- Predicted miRNAs and their Gene-Transcription Factor Networks

We predicted a new correlation between mmu-miRNAs and their downstream targets through transcriptional network construction, such as mir-149-5p and smad1 transcription factor **(Table 3)**. We also predicted a complete network for mmu-mir124-5p downstream targets of transcription factors; Atf7, Stat3, Rel and Elk3, and Mitf, Wipi2, Ulk2 Atgs & DEGs, respectively. Also, we predicted that mi-9-5p to regulate the downstream targets FOXO1 transcription factor and autophagy associated genes ULK and Atg14. mmu-mir-340-5p has predicted transcriptional network of Gabpa, Mycs, Rb1cc1, Map3k2, Hif1a, CXCL5, and Atp6voc. The network of mmu-mir-362-3p includes transcriptional factors MILXipI, ELK1 and CXCL5, Atg10, MAP1LC3B, and ATP6V1D. Finally, mmu-mir-329-3p transcriptional factors are MILXipI, ELK1and FOXO1, Atg10, CXCL5, and Hif3a. (**figure 20)**.

Finally, the systems biology approach revealed that Atg7, Atg16l1 serve as a center protein for several signaling pathways enriched in autophagy, polarization, and phagocytosis of macrophages. Also, during the inflammatory response, NOD-like receptor NOD1 and NOD2 (**figure 20**) might be potential targets in Macrophages polarization. Nevertheless, more experimental validation is needed regarding the candidate predicted targets; Atg16L1, Atg7, MAP1LC3A, MAP1LC3B, IL6, ARG1, CD68, SMAD1and VAMP7 (**figure 21, 22**).

**Table 3. Summary of both upstream and downstream mi-RNAs and their downstream targets.**

| Predicted miRNA | Down Stream Transcription Factor | Down Stream Autophagy and M1&M2 Genes |
|---|---|---|
| mmu-mir-26a-5p | Smad1, Cebpg | ULK1, ULK2, MAPK6 |
| mmu-mir-149-5p | Smad1 | New predicted Finding |
| mmu-mir-124-3p | Atf7, Rela, ELK3, Stat3 | Mitf, Wipi2, Ulk2 |
| mmu-mir-9-5p | Foxo1 | ULK2, Atg14 |
| mmu-mir-340-5p | Gabpa, Mycs | Rb1cc1, Map3k2, Atp6v0c, Hif1a, CXCL5 |
| mmu-mir-362-3p | MLXipl, ELK1 | CXCL5, Atg10, MAP1LC3B, ATP6V1D |
| mmu-mir-329-3p | MLXipl, Foxo1, Elk1 | Atg10, CXCL5, Hif3a, ATP6V1D, MAP1lc3b (LC3-B) |
| mmu-mir-17-p5 | ELK3 | Atg16L1, Rb1cc1, ULK1, MAPK4, Atg2b Hif1a, il6ra, Atg7 |

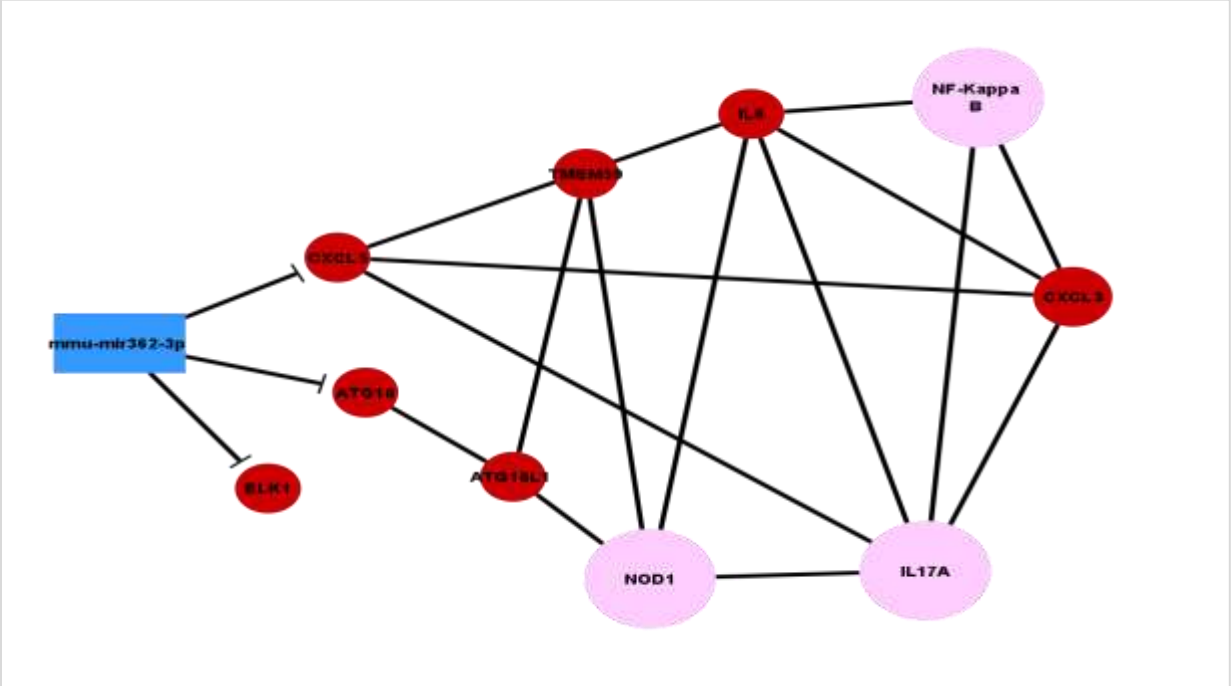


**Figure 20. NOD signaling pathway and IL17 signaling pathway**

Representation of the interaction between autophagy associated genes using Cytoscape 3.8. Atg16l1, Atg10, and Macrophages polarization Degs; IL6, CXCL5 through NOD signaling and IL17 signaling pathways. mmu-mir362-3p is a hub for negative regulation of Elk1 transcription factors Atg10 and CXCL5.

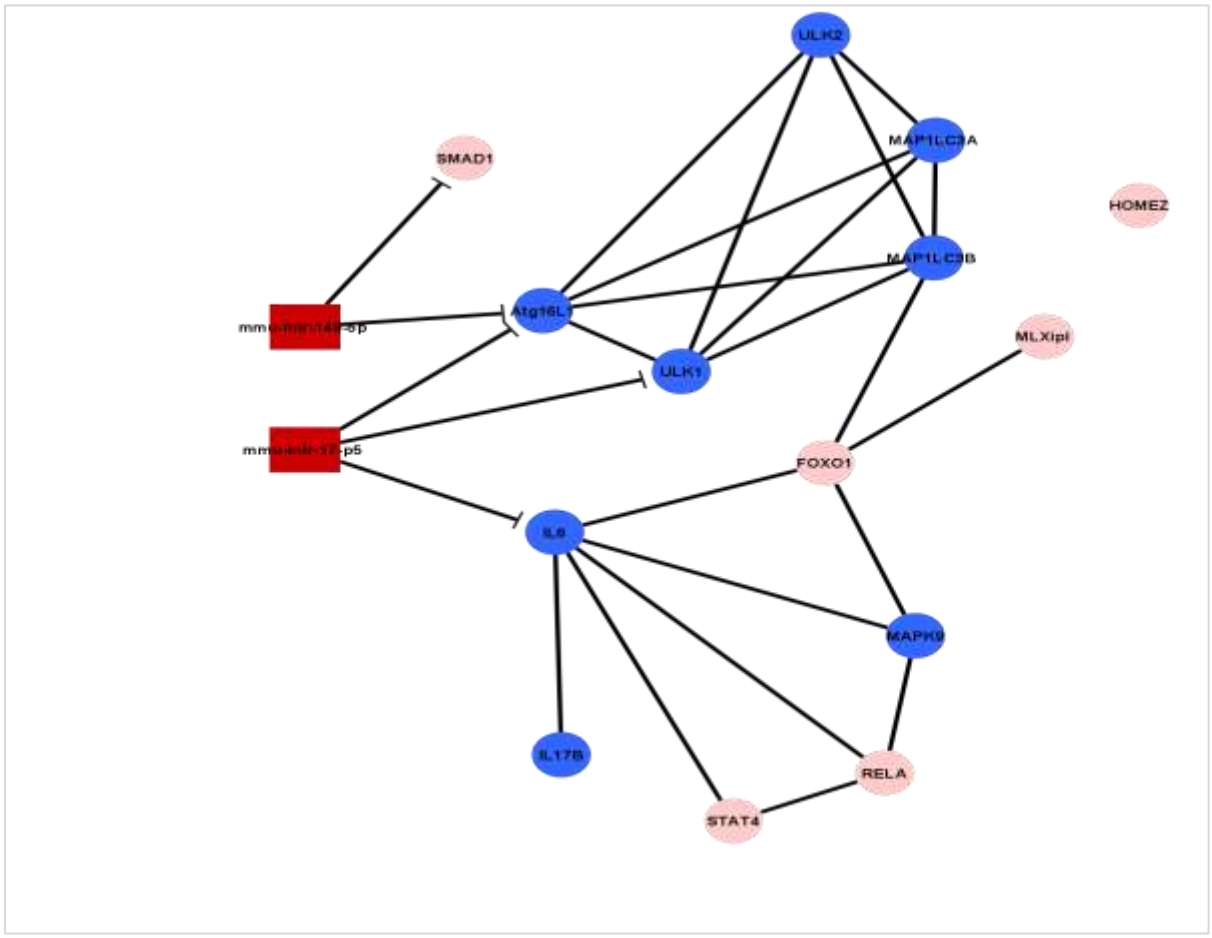


**Figure 21. FOXO signaling pathways and IL17 signaling pathway**

Cytoscape 3.8 representation for the interaction between autophagy associated genes Atg16l1, ULK1, ULK2, MA1LC3A, MA1LC3B, and Macrophages polarization DEGs; IL6 through FOXO signaling pathways and IL17 signaling pathway. mmu - mir-17-p5 is a hub for negative regulation of Atg16l1, ULK1, IL6. mmu-mi-149-5p is a hub for negative smad1 transcription factor and Atg16l1.

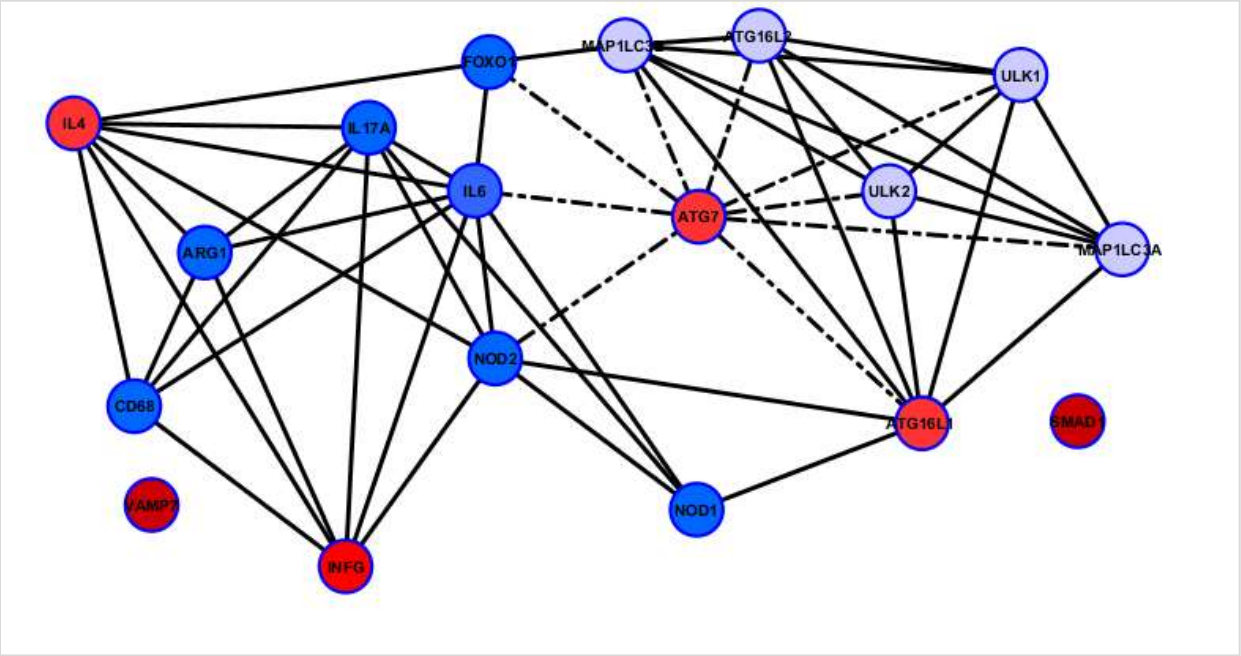


**Figure 22. Candidate predicted targets of ATGs.**

Cytoscape Network shows candidate predicted targets of systems biology approach for experimental validation. Atg7, Atg16L1 IL4, and INFG are hub proteins. Atg7 appeared the more likely to have interaction edges (dashed dot edges). The confidence score for this network is 0.4. we picked Atg16L1, Atg7, MAP1LC3A, MAP1LC3B, IL6, ARG1, CD68, SMAD1and VAMP7 for experimental validation.

**4- In vitro polarization of bone marrow macrophages**

Murine bone marrow monocytes were isolated from the femur and tibia of C57Bl6 female mice. Then the Monocytes were differentiated to M0 φ using (20%L929 condictiond media) . On day 5, type II interferon-γ was used (1250 IU/ml) combined with Lipopolysaccharide LPS (100 ng/ml) for 48 hours to activate the M0 φ into M1 φ lineage. For the M2a, Interleukin-4 (IL4) was used (2500 IU/ml) in combination with Lipopolysaccharide LPS (100 ng/ml) for 48 hrs. The resulting three lineages were characterized using flow cytometry with three markers, Interleukin -6, CD68, and Arginase -1. The resulting phenotypes were M0 φ (IL6+/CD68+), M1 φ (IL6+/CD68+/ Arg-1+), and M2a φ (CD68+/ Arg-1+) (**figures 23, & 24**).

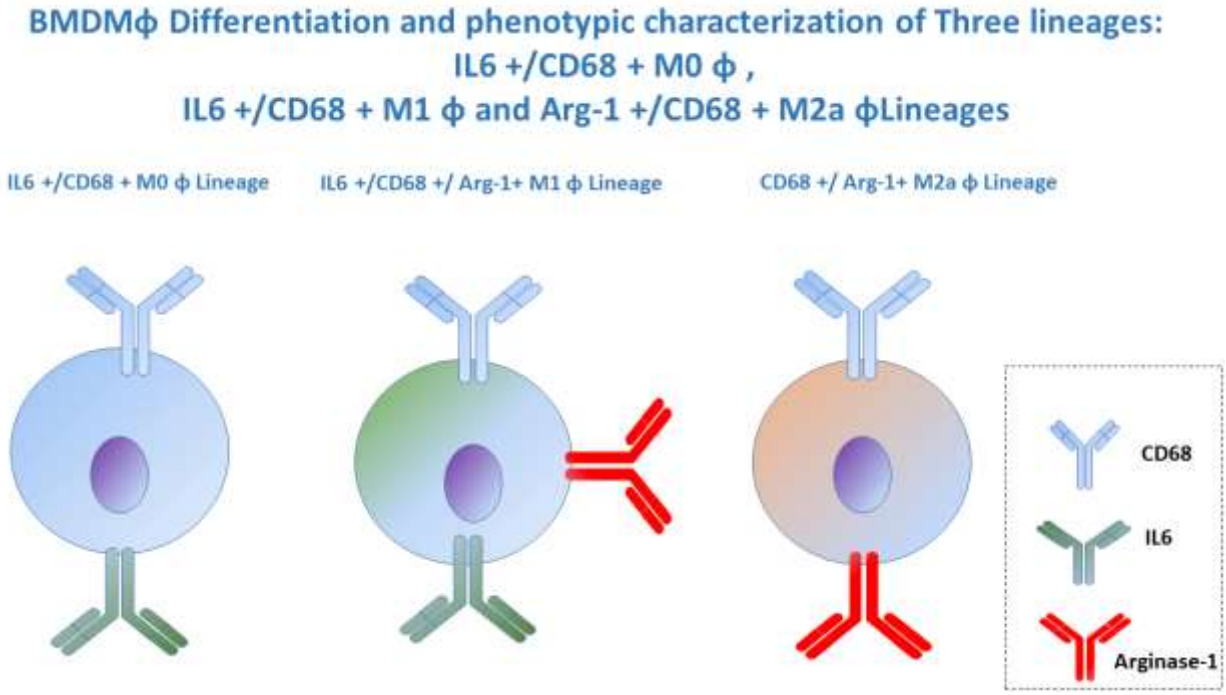


**Figure 23. Bone Marrow-Derived Macrophage Differentiation and Phenotypic Characterization.**

**A- M0 φ at Day 7 Isolation**

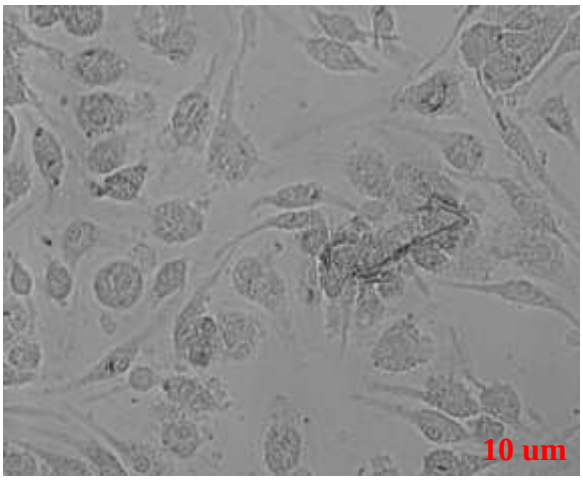


**B- M1 φ at Day 7 Polarization**

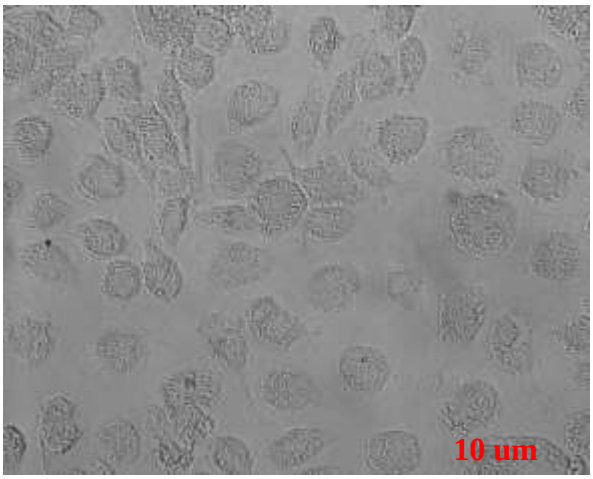


**C- M2a φ at Day 7 Polarization**

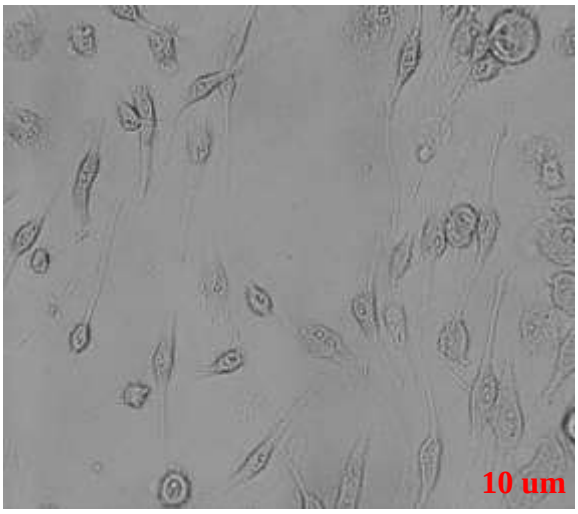


**Figure 24. -Microscopic Examination of Bone Marrow-Derived Macrophages.**

Morphological examination of bone marrow-derived macrophages. A) represents the fully differentiated M0 φ using L929 conditioned medium 20ng/ml at day 7. B) represents the fully differentiated M 1 φ activated by INFγ (1250 IU/ml) +LPS (100 ng/ml) for 48 hrs) at day 7 polarization. C) represents the fully differentiated M 2a φ activated by IL4 (2500 IU/ml) +LPS (100 ng/ml) for 48 hrs. at day 7 polarization.

**IL4 significantly promotes the expression of phagocytosis markers CD-68 and Arginase 1 in M2a lineage.**

We successfully verified the phenotypes of the isolated murine bone marrow-derived macrophages M1 and M2a lineage, as previously mentioned using M0 as a control (**figure 23**). CD68 and Arginase 1 were used as phagocytosis markers. It is noteworthy to mention is that CD 68 is a cell surface protein and is well defined as a phagocytosis and lysosomal marker **(Chistiakov, Killingsworth et al. (2017).** CD68 was expressed in all cell phenotypes, although M2a showed a significantly higher expression of 84%. Furthermore, Arginase 1 is a specific intracellular marker for mice M2a cells ***(Briken and Mosser (2011)***. Flow cytometry analysis showed a significant increase in total cell percentage expressing Arginase 1 in M2a phenotype more than M1 and was absent in the control M0 lineage (**figure 25)**.

**Flow cytometry Analysis for Bone Marrow-Derived Macrophages**

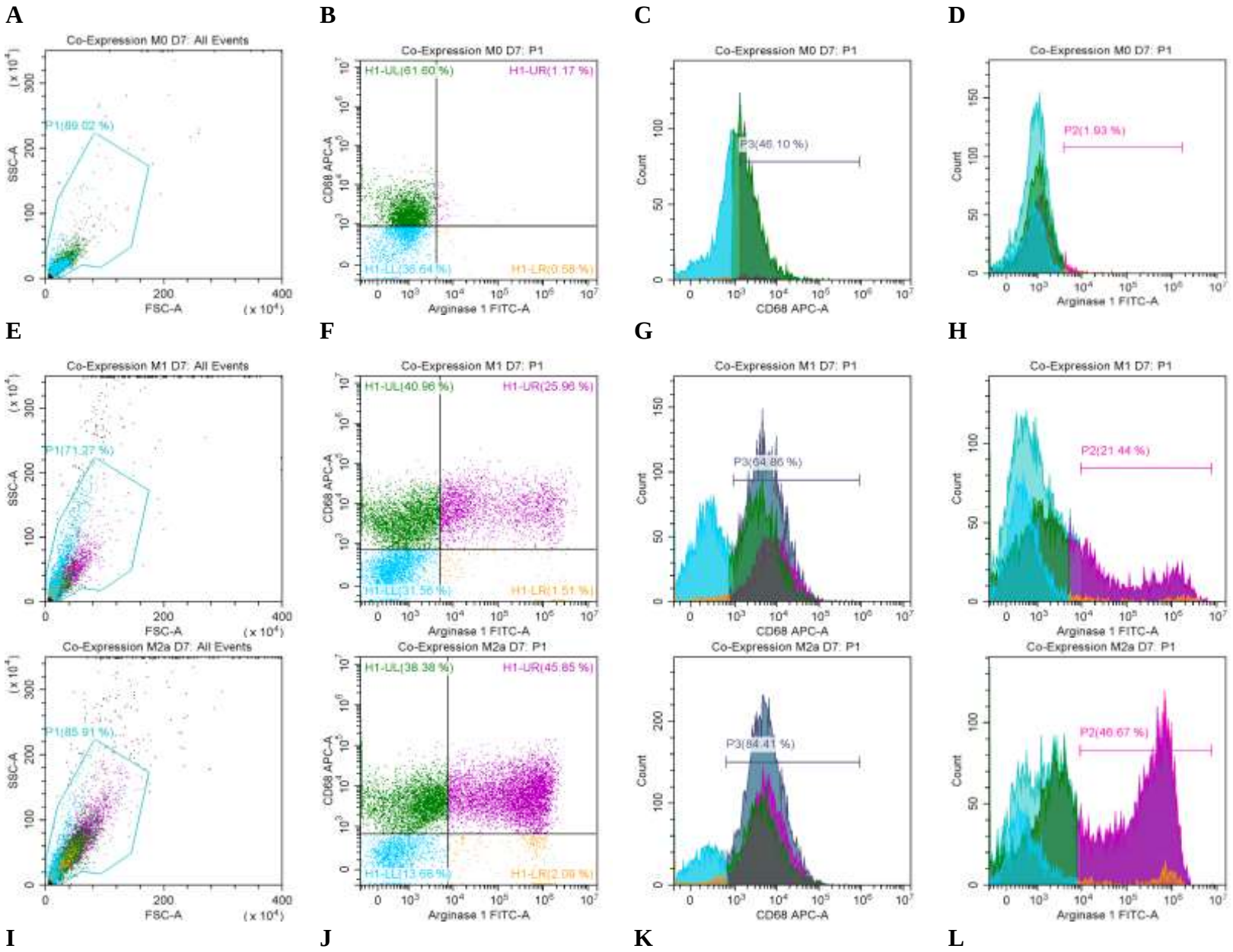

**Figure 25. Flow cytometry Analysis for Bone Marrow-Derived Macrophages**

Flow cytometry shows the co-expression of both Cd-68 and Arginase -1 in M1 and M2a. M0 macrophages were used as control. Samples were gated on 81%, and Cd-68 expression was assessed at APC - Filter, and Arginase-1 was read at FITC- Filter. where (A, E, and I) represent the gating for 5000 events (event= single cell) inside scatter plots (SSC-A) on X-axis and forwarded scatter plots (FSC-A) on Y-axis. (A, E, and I) for M0, M1, and M2a lineages, respectively. On the other hand, B, F, and J are quadrant plots M0, M1, and M2a, respectively. C, G, and K are fluorescence Peak signal plots for CD68 expression in M0, M1, and M2a cells, which indicates high expression of arginase-1 by M0, M1, and M2a lineages. D, H, and L are fluorescence Peak signal plot for Arginase-1 expression in M0, M1, and M2a, which indicate no expression for arginase-1 at M0 lineage (D). However, high expression of Arginase-1 at M1 and M2a lineages. (n=3).

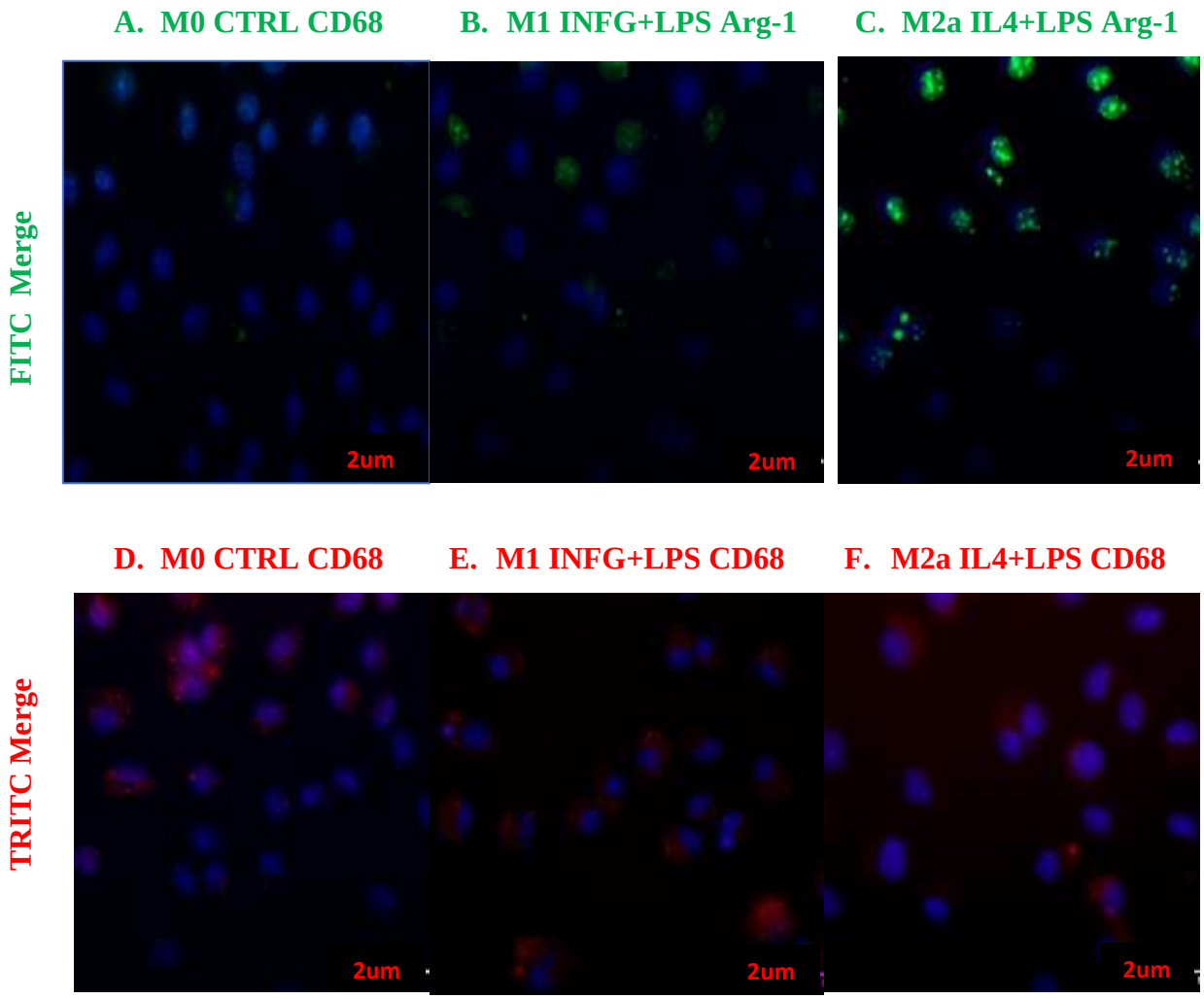


**Figure 26. Immune co-localization studies for Bone Marrow-Derived Macrophages.**
A, B, and C show M0, M1, and M2a cells respectively stained with Arginase -1 and counterstained with DAPI. Green dots indicate the expression of intracellular Arginase -1. D, E, and F show M0, M1, and M2a cells respectively stained with CD 68 marker and counterstained with DAPI. Red dots at (figures D, E, and F) indicate the expression of intracellular CD68. 2um scale bar.

**Immune co-localization studies for Bone Marrow-Derived Macrophages**

The expression of both phagocytosis markers CD68 (cell surface and intracellular) and Arg-1 (intracellular only) can be seen in figure 26. To quantify the immunostaining results, cell counting

for cells expressing Cd68 and Arg-1 in M0, M1, and M2a was performed using ImageJ ® (n=4). Statistical analysis for flow cytometry and immunostaining results are shown in figure 27.

**A- Arginase -1 Flow cytometry**

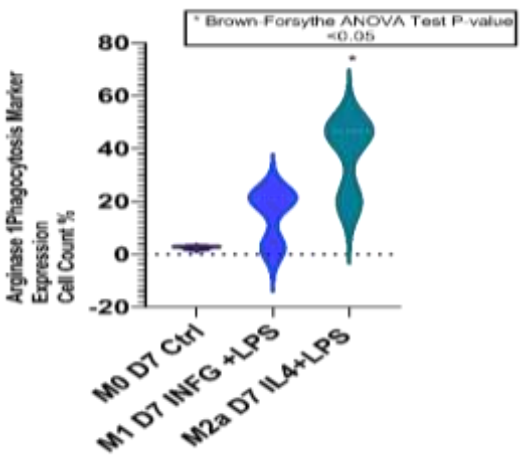


**B- CD 68 Flow cytometry**

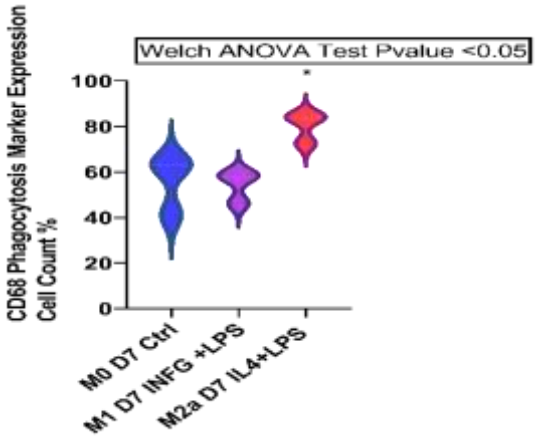


C- **Arginase -1 immune staining counting**

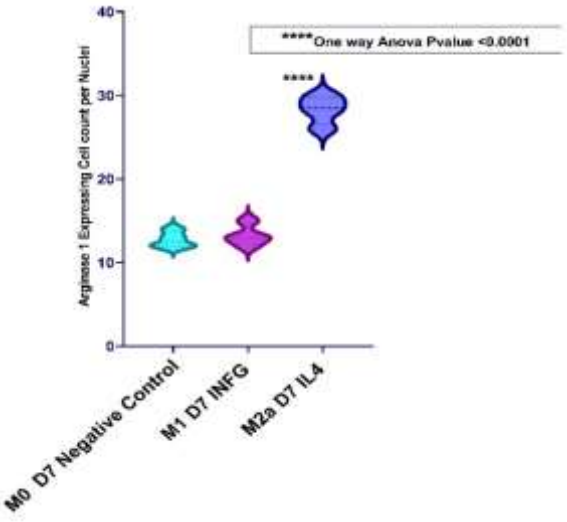


**D- CD68 immune staining counting**

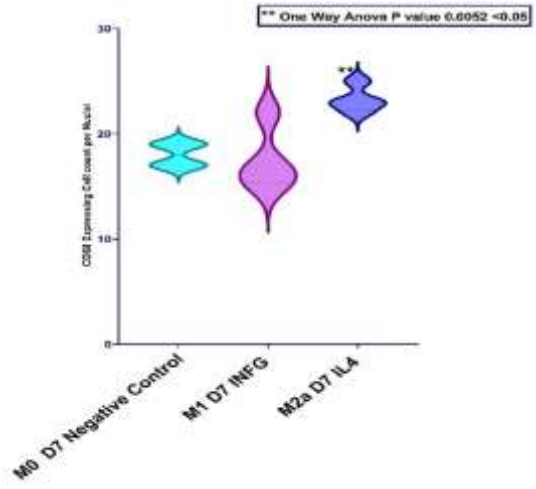


**Figure 27. Statistical analysis for the expression of CD 68 and Arginase-1 in Bone marrow-derived macrophages at D7.**

(A) a statistical significance for CD 68 total expression percentage with ordinary one-way ANOVA (number of replicates n=3) and (p-value 0.024<0.5 and R2 = 0.7) and M2a cells were

most significant. Data presented as mean and standard deviation (Mean= 55.9, 54.3 and 80.2, Standard deviation =± 10.5, ±5.7 and ±5.4 for M0, M1, and M2a respectively). (B) statistical representation of Arginase 1 total expression percentage, Brown –Forsythe ANOVA test was used (number of replicates n=3) and (p-value 0.04<0.5). M2a lineage significantly expressed both CD68 and Arginase 1. Also, for arginase 1 Mean and standard deviation were calculated using Excel (Mean=2.5, 15 and 37, Standard deviation =±0.44, ±8.9 and ±12.6 for M0, M1 and M2a respectively). On the other hand, (C) Violin Plot for statistical analysis of manually counted cells of M0, M1 and M2a expressed Arginase 1 (number of images for each condition n=4), where one-way ANOVA was performed (p-value <0.0001, R2= 0.9). Mean and the standard deviation were calculated using Excel (Mean= 13, 13.6 and 29, Standard deviation =± 0.81, ± 0.91 and ±0.86 for M0, M1 and M2a respectively). (D) for Cd68 ordinary one-way ANOVA was performed for all conditions (number of images for each condition n=4). Statistical significance was Performed using ordinary one-way ANOVA (p-value 0.0057<0.05, R2=0.68). Finally, Mean & standard deviation was calculated using Excel (Mean= 17.6, 16 and 23.6, Standard deviation =± 0.94, ± 0.81and ±0.94 for M0, M1 and M2a, respectively).

**Type II Interferon Gamma INF-γ promotes the expression of Interleukin -6 (IL6) in M1 lineage, while IL4 inhibits the IL6 expression in M2a lineage:**

Our systems Biology approach revealed that IL6 is one candidate for the interplay between autophagy and macrophage polarization (figure 22). IL6 is a cytokine secreted by T cells and Macrophages in response to infection and inflammation ***(Velazquez-Salinas, Verdugo-Rodriguez et al. (2019)***).

Our flow cytometry studies show that Interferon-gamma stimulated M1 lineage expressing IL6 significantly (56%) compared to M2a lineage (37%). However, IL6 expression was high at the control M0 lineage, indicating that IL4 decreased the IL6 expression in M2a cells. Also, the fluorescence intensity for IL6 protein showed that M1 lineage had the most significant increase in IL6 protein expression (**figure 28**).

## Flow Cytometry Analysis for IL6 expression in BMDM

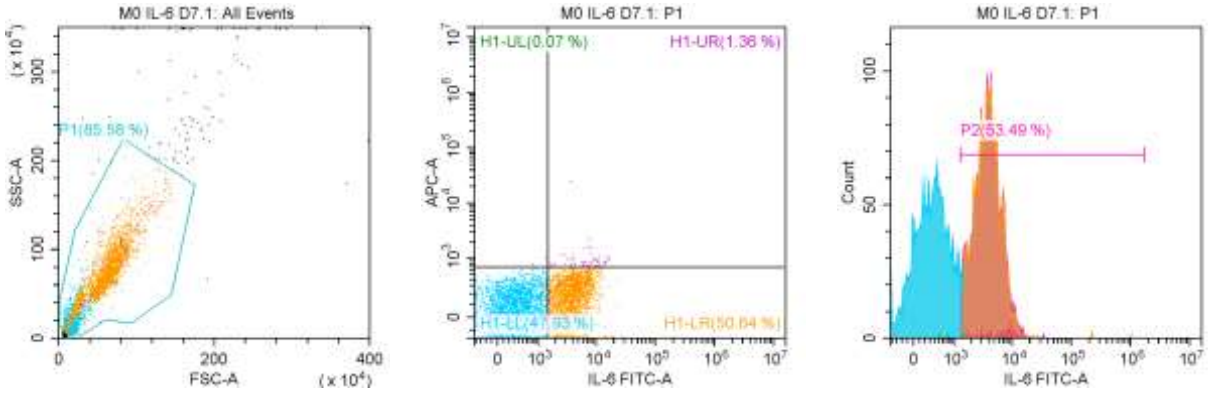


**A** **B** **C**

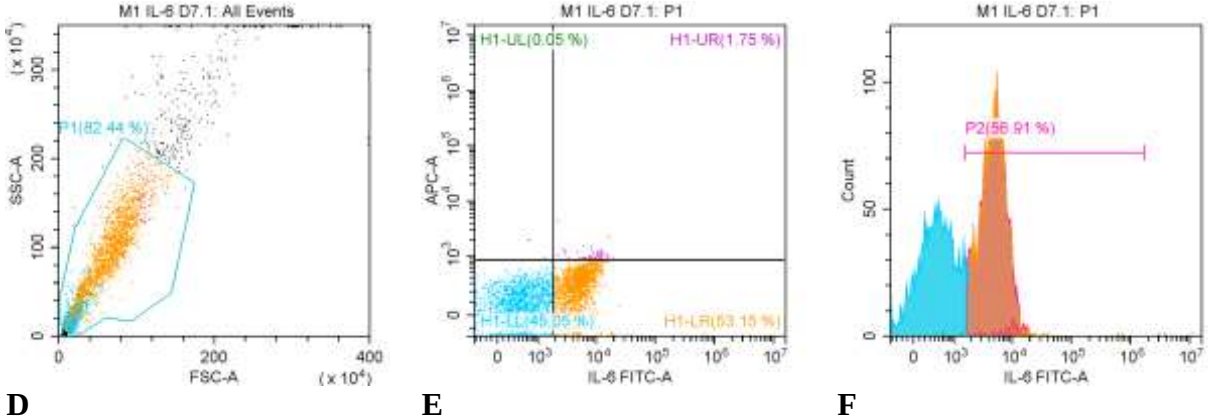


**D** **E** **F**

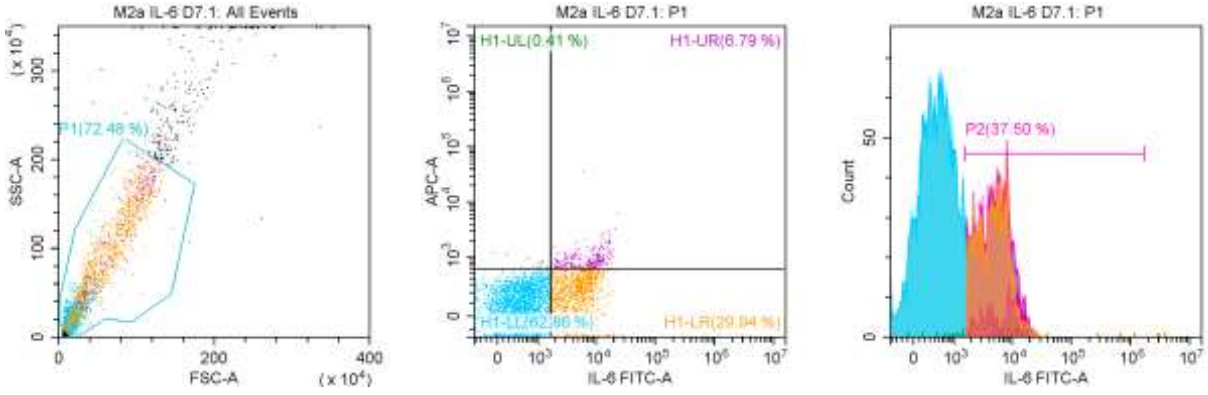


**G** **H** **I**

**Figure 28. Expression of IL6 by the flow cytometry**

Figures represent IL6 flow cytometry analysis for M1 and M2a. M0 macrophages were used as control. Samples were gated on 81%, and IL6 expression was read with FITC- Filter. A, D, and G represent the gating for 5000 events (event= single cell) inside scatter plots (SSC-A) on X-axis and forwarded scatter plots (FSC-A) on Y-axis. A, D, and G for M0, M1, and M2a lineages, respectively. On the other hand, B, E, and H are quadrant plots for M0, M1 and M2a respectively. C, F, and I are fluorescence Peak signal plots for IL6 percentage expression in M0, M1, and M2a cells, which indicates high expression of IL6 at M0 and M1. However, M2a lineages showed very low expression. (n=3).

**A- Statistical Analysis for Flow Cytometry IL6 Expression**

**B- Relative Fluorescence inetnsity for IL6 Expression**

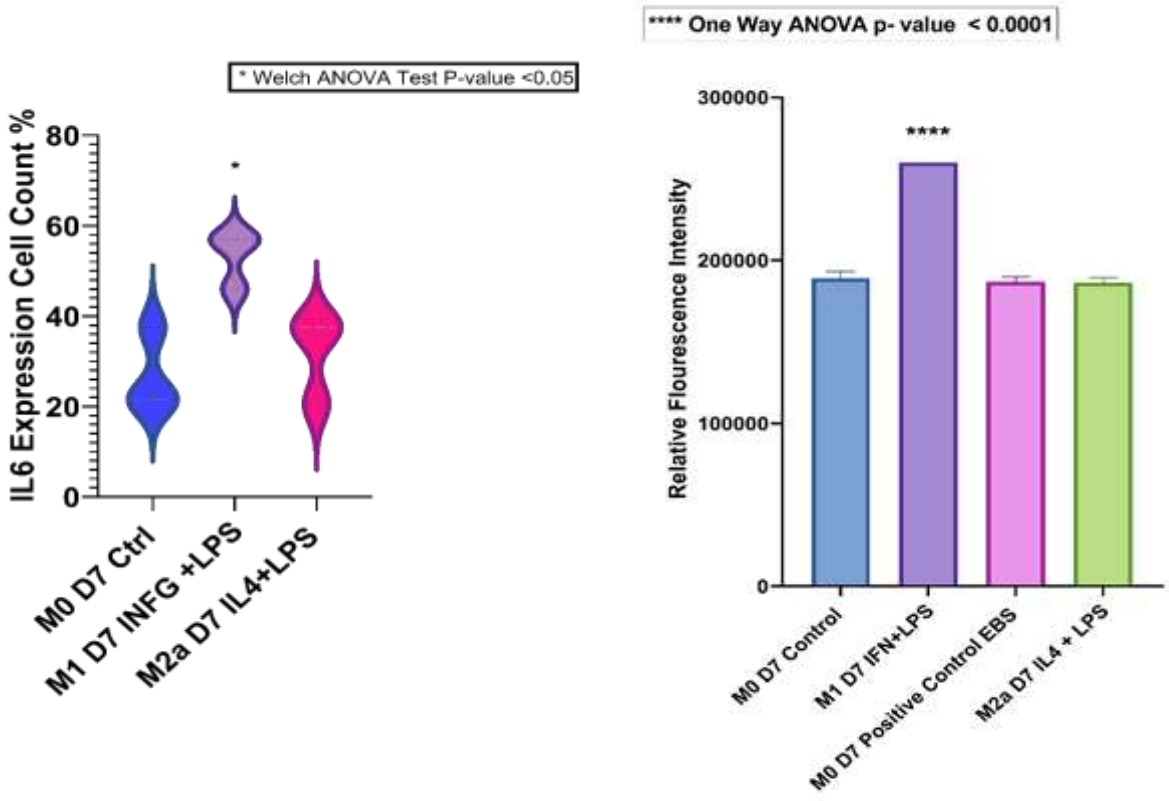


**Figure 29. Expression of phagocytosis Marker IL6.**

Figure (A) Violin plot shows statistical significance for IL6 total expression. M1 cells were significant (number of replicates n=3, p-value 0.036 < 0.05). B) bar plot showing the statistical representation of IL6 relative fluorescence intensity, with M0 D7 was used as a control, and M0 + Earle balanced salt used as positive autophagy control. One-way ANOVA test was performed (number of replicates n=3, p-value <0.0001, R2=1). M1 lineage significantly expressed IL6.

**M2a phenotypes express IL6, and their conditioned media has an anti-proliferative effect on SHSY5Y neuroblastoma cells**

Earlier, we mentioned that we found M1 significantly expresses IL6, which means they release IL6 in their conditioned medium. Interestingly, we found the conditioned media of M0, M1 to have proliferative effects and M2a to have a potential to anti-proliferative effect on neuroblastoma cell line SHSY5Y. MTT Cytotoxicity assay on SHY5Y neuroblastoma cells treated with conditioned media showed significant cell proliferation of SHSY5Y cells treated with M1 supernatant (1250IU INFG+100 ng LPS) for 24 hrs. However, cells treated with M2a supernatant (2500IU IL4) showed the least cell viability (less than 40%), which was also lower than cells treated with Cisplatin **(figure 30)**.

These results were supported by the early nuclear apoptosis assay. DAPI staining **(Figure 31)** and quantitative image analysis (mitotic partitioning) were used to quantify the relative DNA distribution in each nucleus. The amount of DNA in each nucleus was measured using image pixel intensities. The relative DNA distribution between progeny nuclei or the partition coefficient (PC) was then reported as the ratio of nuclear signal intensity (PC = I1/I2, where I1 and I2 are integrated pixel intensities of each of the progeny nuclei, i.e., total DNA amount per nucleus). This analysis was carried out in three steps: image deconvolution, determination of the pixel intensity threshold, and image binarization. First, image deconvolution was accomplished by an Unsharp mask algorithm. Pixel intensity for image thresholding was defined as the intra-nuclear pixel intensity level that maximizes the number of detectable foci. In our quantitative analysis, the image binarization is performed by assigning the value of 1 to pixels with grayscale values higher than the threshold; all other pixels are assigned the value of 0.

Quantification of nuclear foci from the binary image included determining the number (connected components), the size in pixels (1 pixel 0.028 m2), and the location of each of the foci (centroid image coordinates). The spatial organization of intranuclear foci is expressed as the coefficient of variation of nearest-neighbor distances. For this purpose, the Euclidean nearest-neighbor distance was determined for each focal point by using the centroid coordinates (**figure 31)**.

**A-MTT cytotoxicity assya for for SHSY5Y cultured in BMDM Conditioned media**

**B-cell viability precnetage for SHSY5Y cultured in BMDM Conditioned media**

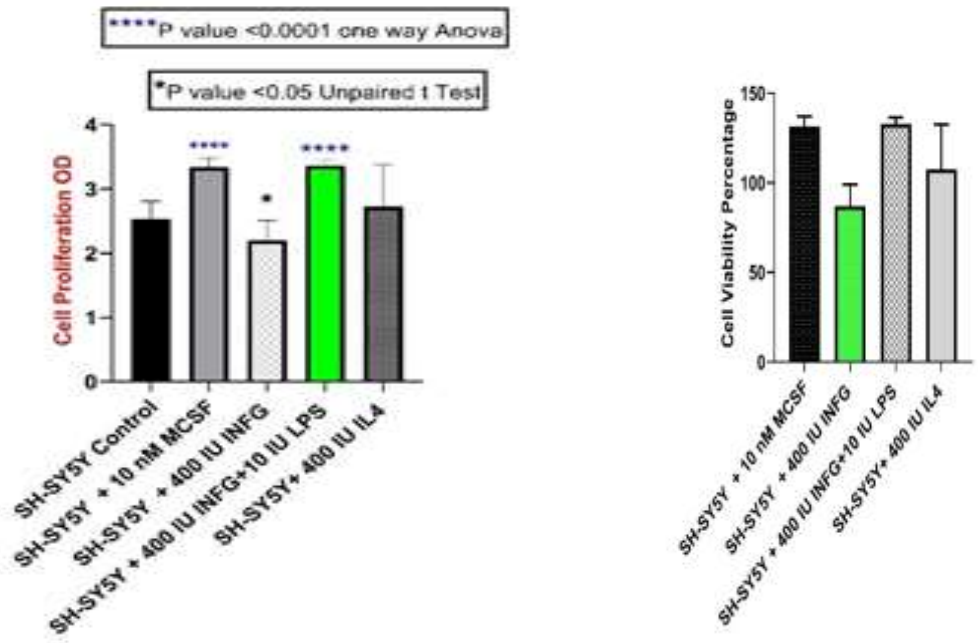


**C-MTT cytotoxicity assya for for SHSY5Y cultured in BMDM Conditioned media**

**D- Cell Viability Percentage for SHSY5Y cells in BMDM conditioned media**

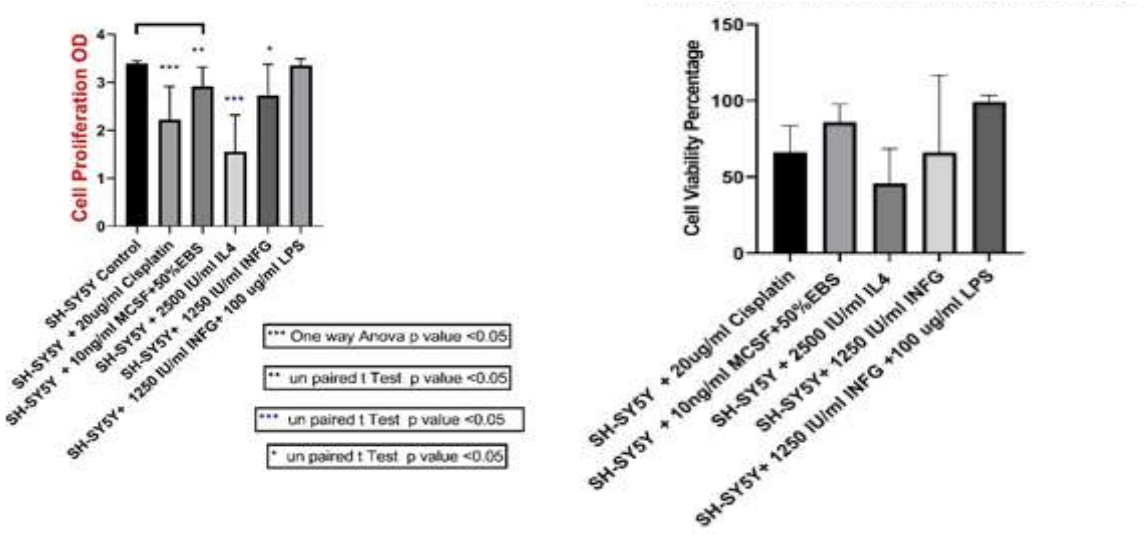


**Figure 30. Effect of bone marrow-derived macrophage conditioned media on SHSY5Y cells.**

MTT and cytotoxicity assay of neuroblastoma cells SHSY5Y treated with bone marrow-derived macrophage conditioned media. A) represents the statistical significance of cell proliferation, SHSY5Y cells treated with M0 condictioned media (10 ng MCSF) and SHSY5Y treated with M1

conditioned media (400 IU INFG +10 IU LPS) p-value <0.0001. However, cells shsy5y treated with M 1 conditioned media containing (400IU INFG) showed the least proliferation p-value <0.05. B)shows cell viability precnetage for SHSY5Y cultured in BMDM Conditioned media, where dose of (400IU) INFG decreased the cell viability. C) MTT cytotoxicity assay for for SHSY5Y cultured in BMDM Conditioned media. SHSY5Y cells were cultured in M2a conditioned media containing (2500 IU IL4 ) showed the most significant decrease in cell proliferation when compared to the negative control (p-value <0.05).shsy5y Cells treated with 20 ug/ml cisplatin were used as positive control and showed a decreased proliferation (p-value <0.05). (D) Cell Viability Percentage for SHSY5Y cells in BMDM conditioned media , shsy5y cells cultured in M2a conditioned media containing (2500IU IL4) showed the least viability.

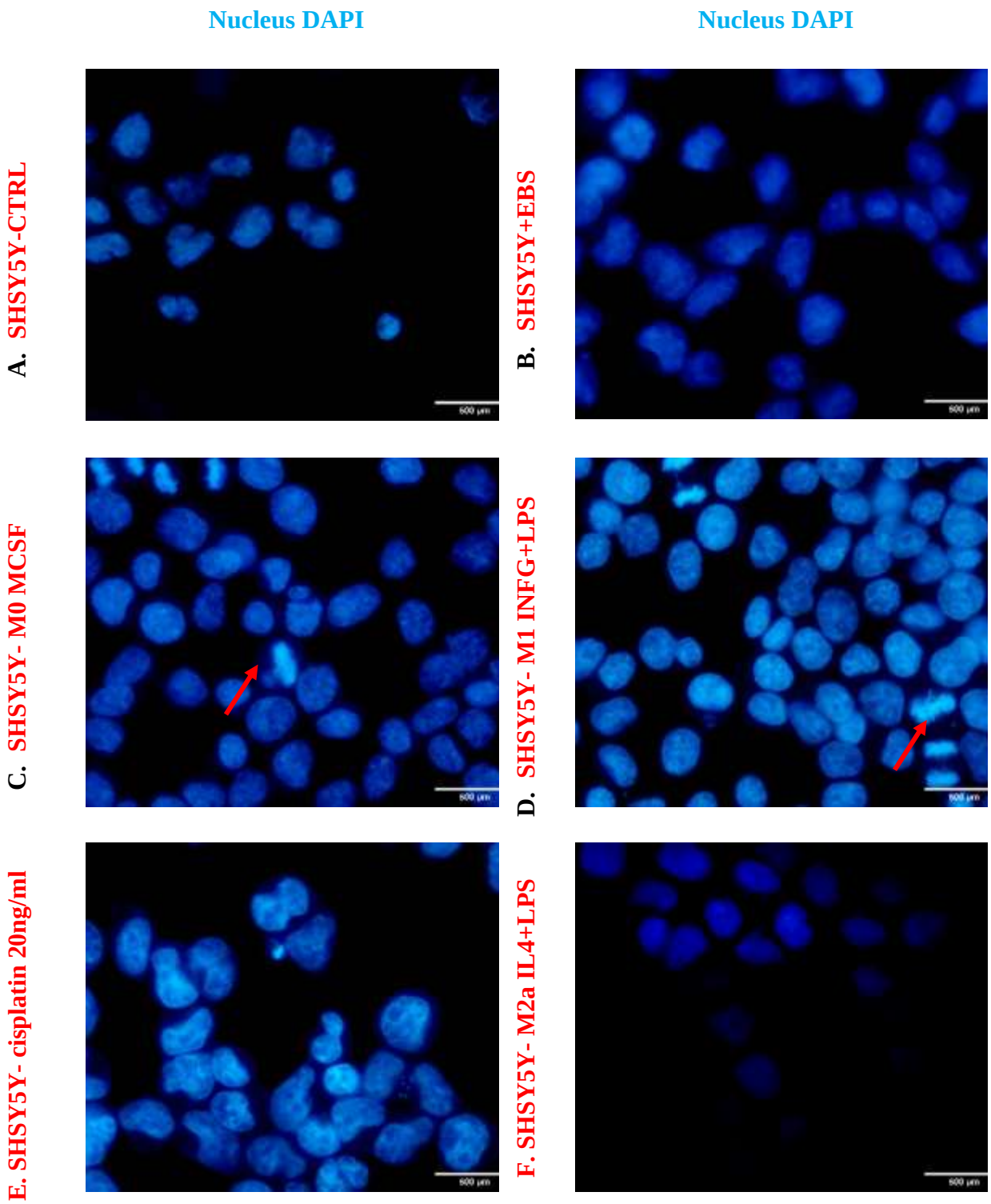


**Figure 31. Early Apoptosis Assay.**

This figure described the early apoptosis induction in SHSY5Y human neuroblastoma cells. Nuclei stained with DAPI. A & B show no evidence for damaged nuclei. Unlike E and F, which show apoptotic bodies and damaged nucleus. Surprisingly, C and D show increased mitosis activity (red arrow). These results indicate that the conditioned media of M1 cells had a proliferative effect on cancer cell line SHSY5Y. Also, the conditioned media of M0 control had the same proliferative effect on SHSY5Y. 2 um scale bar.

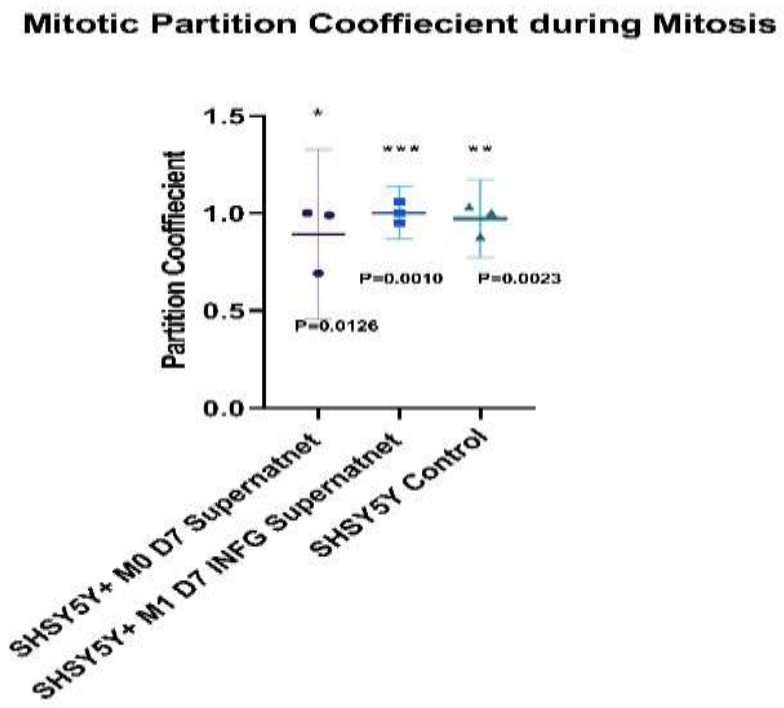


**Figure 31, G. Statistical analysis of Mitotic partition coefficient during Mitosis.**

The most significant or the highest proliferative activity was observed in SHSY5Y incubated in M1 INFG+LPS supernatant when compared to control.

**Increased Atg16L1 pre-autophagosomal expression in M1 and M2a lineage mRNA and protein**

Previously we mentioned that Atg16L1 is a pre-autophagosome marker. It mediates the pre-autophagosome formation through of N-terminal of the WD40 domain, which is important for interaction with Atg5-Atg12 complex that mediates the conjugation with PE (phosphatidyl-ethanolamine). Also, the Coiled-Coil domain CDD interacts with PE for LC3-1 lipidation and autophagosome formation **(Zhao and Zhang (2019).** It's noteworthy to mention that Atg16L1 was predicted as a hub protein**.** It was also a target for the predicted transcription factors Stat 4, Mlxpl, Gabpa, and Elk1 **(figures 18 & 19**). Moreover, Atg16L1 is a common target for the NOD2 receptor **(figures 20 & 22).**

Atg16L1 protein has 7 different isoforms. Here we predicted their tertiary structure from their amino acid sequences. Then we selected isoforms Atg16L1-1 and Atg16L1-3 for further studies, the reason behind this selection was the structure similarity between Atg16L1 -1 (Alpha) and Atg16L1-3 (Gamma) (**figure 33**). Therefore, it was important to investigate the gene expression of Atg16L1-1 and Atg16L1-3 on mRNA level at all BMDM φ lineages**.** Also, we examined their mRNA transcriptional level in M0, M1, and M2a lineages at day 7 and day 14 polarization. The Atg16L1-1 variant showed a significant fold change at day 7 and day 14 polarization. There was an expression variation between Atg16l1-1 and Atg16L1-3 gene variants in both M1 and M2a lineages at D7 and D14 polarization ***(figure 34)***.

Atg16L1 serves as a precursor for the homotypic fusion of lysosomal VAMP7 /SNARE proteins for the pre-autophagosome formation and LC3 autophagosome maturation. Therefore, we examined the expression of the VAMP7 gene at M0, M1, and M2a lineages at day 7 and day 14 polarization.

Finally, M2a lineage showed the highest and the most significant Atg16L1-1, Atg16L1-3, and Vamp7 fold change in both 7 days and 14 days' polarization. Interestingly, Atg16L1-1 alpha showed a 30-fold increase in M2a day 14 polarization than M2a D7 polarization. Also, the Atg16L1-3 Gamma variant showed an 18-fold increase in M2a d7 than M2a d14 polarization. The same as for vamp7 in M2a d7 showed a 10-fold increase than M2a day 14 polarization.

**A- Multisequence Alignment for Atg16L1 three isoforms**

**B- Structure of Atg16L1 three isoforms**

```
CLUSTAL O(1.2.4) multiple sequence alignment

Atg16L1-1       mssglraadfpnvkrhiaeelnrrdrlqrqafeeiilqytklleksdlhsvltqklqaek   60
Atg16L1-2       mssglraadfpnvkrhiaeelnrrdrlqrqafeeiilqytklleksdlhsvltqklqaek   60
Atg16L1-3       mssglraadfpnvkrhiaeelnrrdrlqrqafeeiilqytklleksdlhsvltqklqaek   60
                ************************************************************

Atg16L1-1       hdnpnrheispghdgawndsqlqemaqlrikhqeeltelhkkngelaqlvidlnnqnqqk   120
Atg16L1-2       hdnpnrheispghdgawndsqlqemaqlrikhqeeltelhkkngelaqlvidlnnqnqqk   120
Atg16L1-3       hdnpnrheispghdgawndsqlqemaqlrikhqeeltelhkkngelaqlvidlnnqnqqk   120
                ************************************************************

Atg16L1-1       dveiqmneakiseylqtisdletncldlrtklqdlevanqtlkdeydalqitftaleekl   180
Atg16L1-2       dveiqmneakiseylqtisdletncldlrtklqdlevanqtlkdeydalqitftaleekl   180
Atg16L1-3       dveiqmneakiseylqtisdletncldlrtklqdlevanqtlkdeydalqitftaleekl   180
                ************************************************************

Atg16L1-1       rktteenqelvtrwmaekaqeanrlnaenekdsrrrqarlqkelaeaakeplpveqdddi   240
Atg16L1-2       rktteenqelvtrwmaekaqeanrlnaenekdsrrrqarlqkelaeaakeplpveqdddi   240
Atg16L1-3       rktteenqelvtrwmaekaqeanrlnaenekdsrrrqarlqkelaeaakeplpveqdddi   240
                ************************************************************

Atg16L1-1       evivdetsdhteetspvravsraatkrlsqpagglldsitnifglsespllghhssdaar   300
Atg16L1-2       evivdetsdhteetspvravsraatkrlsqpagglldsitnifg----------------   284
Atg16L1-3       evivdetsdhteetspvravsraa------------------------------------t   265
                ************************

Atg16L1-1       rrsvssipvpqdindthpasgkdvrvpttasyvfdahdgevnavqfspgsrllatggmdr   360
Atg16L1-2       rrsvssipvpqdindthpasgkdvrvpttasyvfdahdgevnavqfspgsrllatggmdr   344
Atg16L1-3       rrsvssipvpqdindthpasgkdvrvpttasyvfdahdgevnavqfspgsrllatggmdr   325
                ************************************************************

Atg16L1-1       rvklweafgdkcefkgslsgsnagitsiefdsagayllaasndfasriwtvddyrlrhtl   420
Atg16L1-2       rvklweafgdkcefkgslsgsnagitsiefdsagayllaasndfasriwtvddyrlrhtl   404
Atg16L1-3       rvklweafgdkcefkgslsgsnagitsiefdsagayllaasndfasriwtvddyrlrhtl   385
                ************************************************************

Atg16L1-1       tghsgkvlsakflldnarivsgshdrtlklwdlrskvciktvfagsscndivcteqcvms   480
Atg16L1-2       tghsgkvlsakflldnarivsgshdrtlklwdlrskvciktvfagsscndivcteqcvms   464
Atg16L1-3       tghsgkvlsakflldnarivsgshdrtlklwdlrskvciktvfagsscndivcteqcvms   445
                ************************************************************

Atg16L1-1       ghfdkkirfwdirsesvvremellgkitaldlnpertellscsrddllkvidlrtnavkq   540
Atg16L1-2       ghfdkkirfwdirsesvvremellgkitaldlnpertellscsrddllkvidlrtnavkq   524
Atg16L1-3       ghfdkkirfwdirsesvvremellgkitaldlnpertellscsrddllkvidlrtnavkq   505
                ************************************************************

Atg16L1-1       tfsapgfkcgsdktmvvfspdgsyvaagsaegslyvwsvltgkvekvlskqhsssinava   600
Atg16L1-2       tfsapgfkcgsdktmvvfspdgsyvaagsaegslyvwsvltgkvekvlskqhsssinava   584
Atg16L1-3       tfsapgfkcgsdktmvvfspdgsyvaagsaegslyv-svltgkvekvlskqhsssinava   564
                ********************************** ***********************

Atg16L1-1       wapsglhvvsvdkgsravlwaqp  623
Atg16L1-2       wapsglhvvsvdkgsravlwaqp  607
Atg16L1-3       wapsglhvvsvdkgsravlwaqp  587
                ************************
```

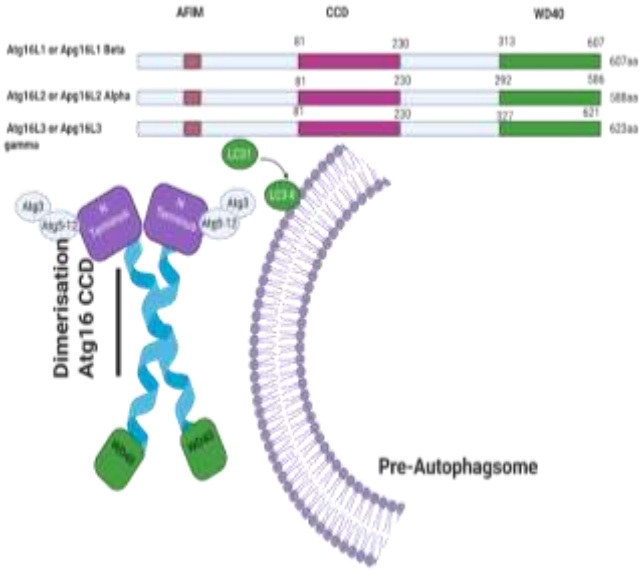


**C- Atg16l1 – lysosomal homotypic**

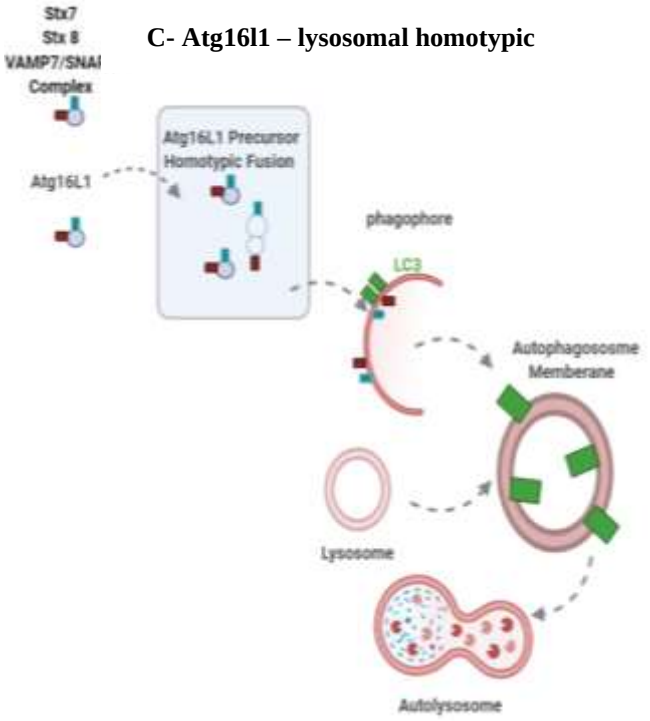

**Figure 32. The computational Multi-sequence Alligmenet of Atg16L1 -1, Atg16L1-2, and Atg16L-3.**

(A) Multi-sequence Alignment using Clustal software showed high amino acid sequence similarity among Atg16L1-1 or alpha and Atg16L1-3 or gamma, and the similarity in the N- terminal domain in both isoforms Atg16L1-1 and Atg16L1-3. B) diagram described the structure of Atg16L1 protein with its 3 isoforms and its N-terminal domain. N terminal domain is crucial for binding with lysosomal complex protein Vamp7 at (C).

**A-Atg16l1-5 isoform, WD40 domain 311 aa residues**

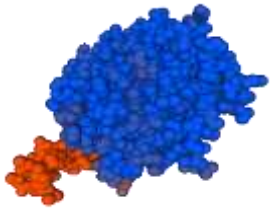

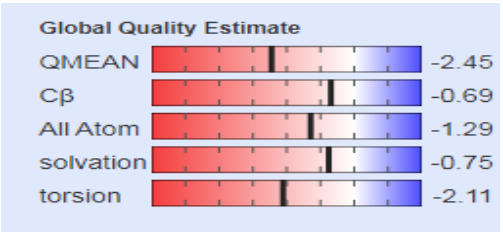


**B - Atg16l1-4 Isoform, WD40 domain 126 aa residue**

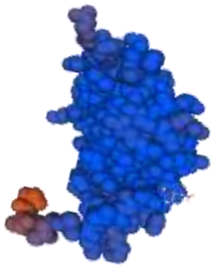

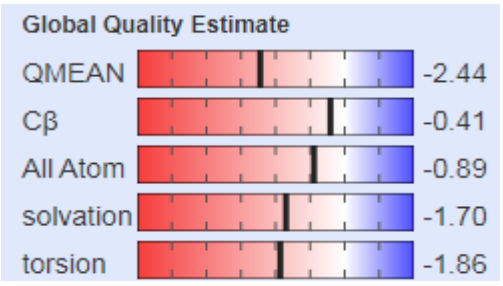


**C-Atg16l1-3 gamma isoform, 295 aa residues WD40**

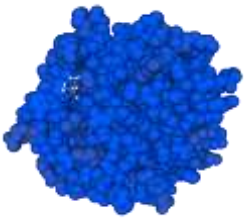

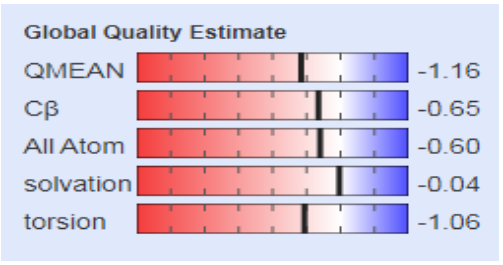


**D-Atg16L1-2 beta isoform, WD40 domain 296aa residue**

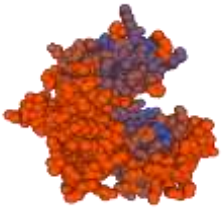

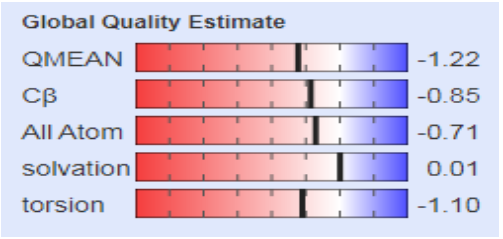


**E- Atg16L1-1-alpha isoform, WD40 domain 296aa residue**

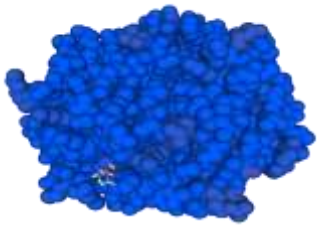

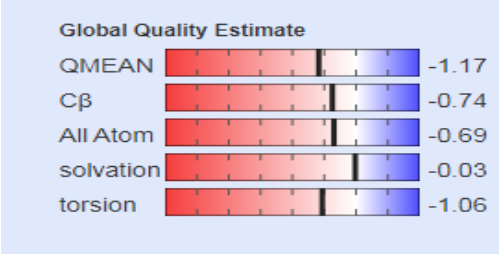

**Figure 33. The predicted tertiary structure of Atg16L1 isoforms**

The tertiary structure was predicted using the amino acid sequence of each isoform of Atg16L1 (5 isoforms) using the Swiss model plugin. The predicted models or structures were numbered according to their quality using a global quality estimate. QMEAN is one of the indicators of structural similarity and model quality. It is noteworthy to mention that structures C and E showed high 3D structure similarity (C, Atg16L1-3 with QMEAN value -1.16 and E Atg16L1-1 with QMEAN value -1.16).

**A- Atg16L1-1 Alpha variant Gene Expression at day 7 poalrization**

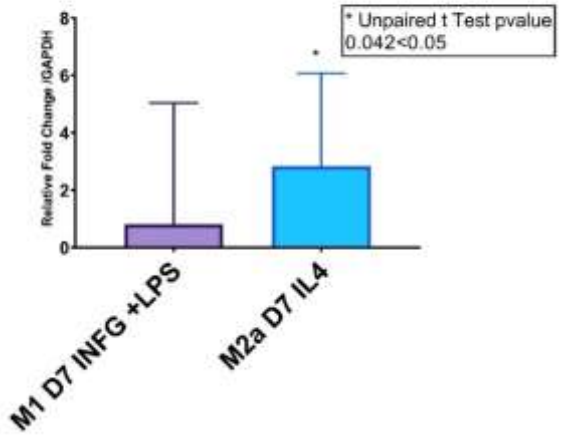


**B- Atg16L1-1 Alpha variant Gene Expression at day 14 poalrization**

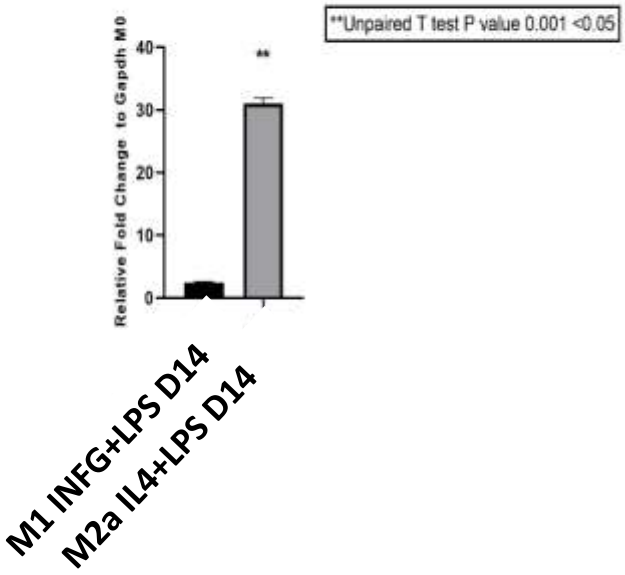


**C-Atg16L1-3 Gamma variant Gene Expression at day 7 polarization**

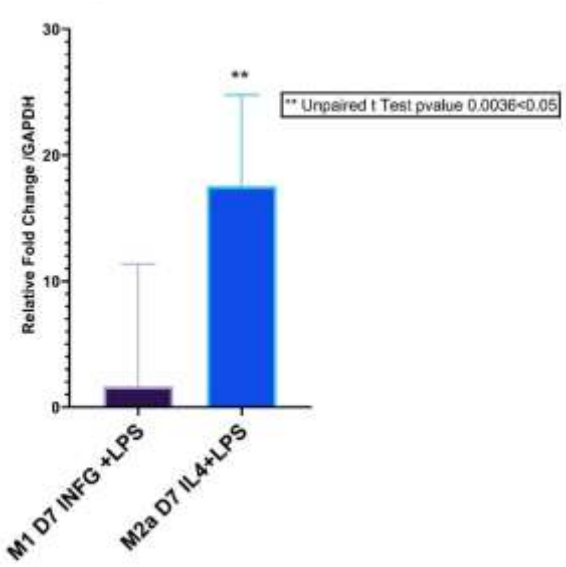


**D-Atg16L1-3 Gamma variant Gene Expression at day 14 poalrization**

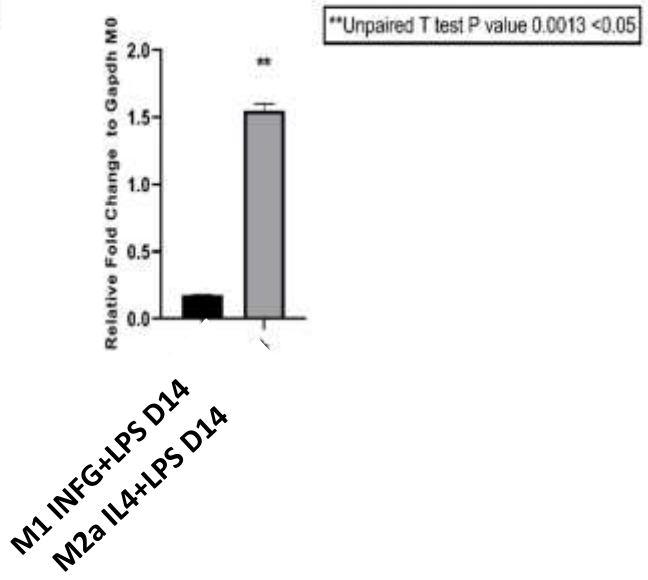

**Figure 34. ATG16L1-1, and Atg16L1-3 Gene Expression significance.**

Representation of the gene expression of Atg16L1-1, Atg16L1-3 at day 7 and day 14 polarization normalized to GAPDH. **A & B** bar plot showing the statistical significance of relative fold change of Atg16L1-1 alpha variant in M1 and M2a at D7 polarization (**A**) and D14 polarization **(B)**. Unpaired t-test was used to calculate the significance (n=4, p-value 0.042 < 0.05, and = 0.001 respectively). **C & D** bar plot shows the statistical significance of relative fold change of Atg16L1-3 Gamma variant in M1 and M2a at D7 (**C)** polarization and at D 14 polarization (**D**). Unpaired t-test was used to calculate the significance (n=4, and p-value < 0.05 and ).

**E. Vamp7 Gene Expression day 7 polarization**

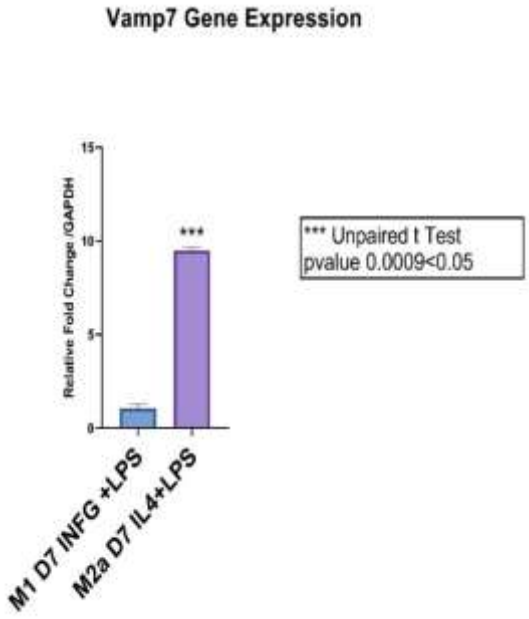


F. **Vamp7 Gene Expression day 14polarization**

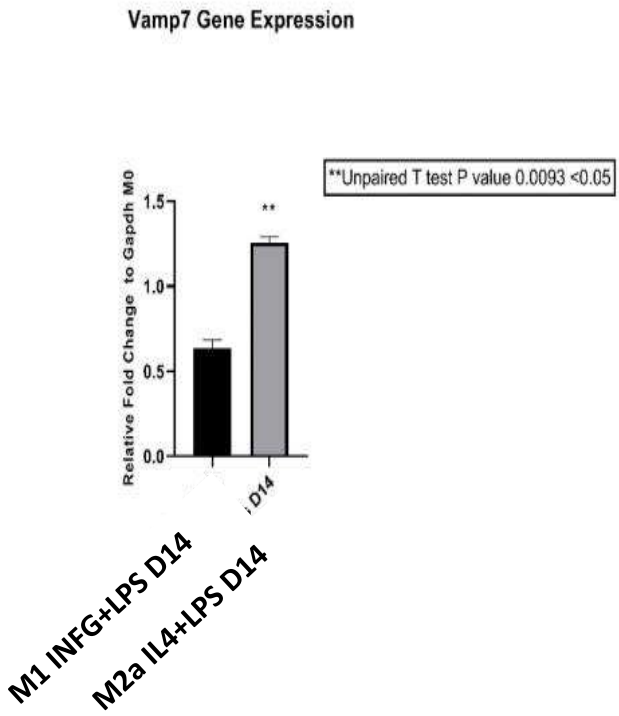


**Figure 34 (E & F). VAMP7 Gene Expression.**

The figure shows the expression Vamp 7 on day 7 and day14 polarization normalized to GAPDH. The bar plot shows the statistical significance of relative fold change of Vamp7 variant in M1 and M2a at D 7 **(E)** and D14 **(F)** polarization. Unpaired t-test was used to calculate the significance (n=4, and p-value < 0.05).

**Atg16L1-1 and Atg16L1-3 upregulated in M2a lineage**

M2a cell lineage showed upregulation for both Atg16L1-1 and Atg16L1-3 variants. One protein level, immune co-localization studies using fluorescence microscopy can give insights about the expression of pre-autophagosomal protein Atg16L1 in the cytoplasm and nuclear boundaries. Using an automated spot detection algorithm, we were able to detect the pre-autophagosome spots, also, their sizes in M0, M1, and M2a lineages (**Figure 35 & 36**).

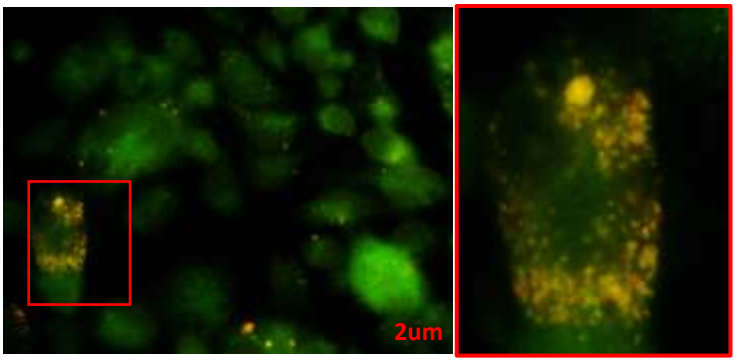


**A-Atg16L1 in M0 CTRL FITC**

**B- Cytoplasmic Atg16L1 Pre-auto phagosomes**

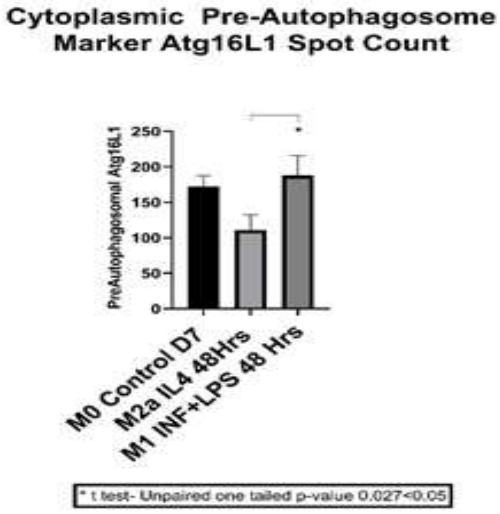


**C- Statistical Significance of Atg16L1 Pre-auto phagosome Count in Cytoplasm**

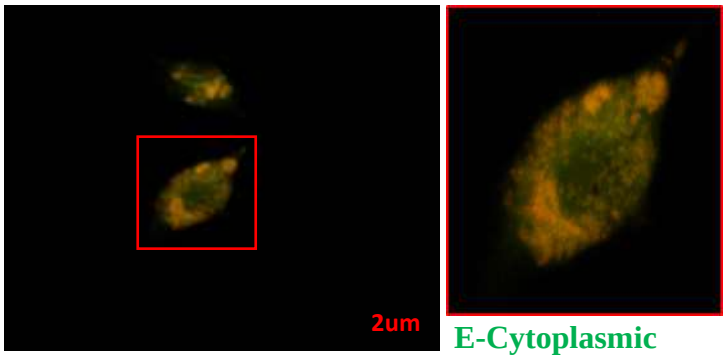


**D-Atg16L1 in M1 INFG+LPS FITC**



**E-Cytoplasmic Atg16L1 Pre-auto phagosomes**

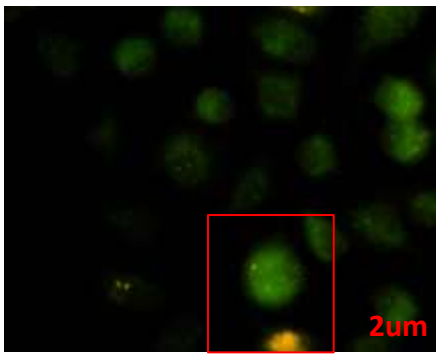


**G. Atg16L1 in M2a IL4 + LPS FITC**

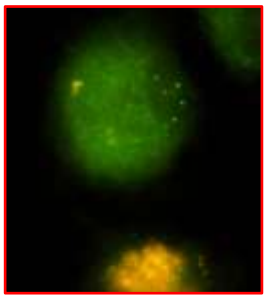

**H. Cytoplasmic Atg16L1 Pre-auto phagosome**

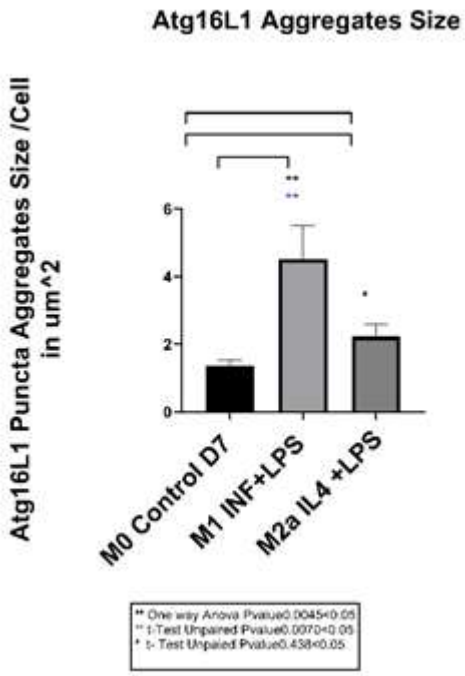


**F- Statistical Significance of Atg16L1 Pre-auto phagosome in Cytoplasm**

**Figure 35. Immune co-localization studies for cytoplasmic Pre- autophagosome Atg16L1.**

Cytoplasmic and nuclear pre-autophagosomes stained for Atg16L1. A, D and G are the M0, M1, and M2a lineages, respectively, showing cytoplasmic pre-auto phagosomes as yellow to green spots (red box). Pre-auto phagosomes appeared yellow to green spots in the cytoplasmic boundary (B, E, and H). C statistical representation of cytoplasmic pre-autophagosomes counting per cell. Unpaired t-test (n= 6 images, at least 5 cells /image, p-value $0.027 < 0.05$).

M1 lineage showed the highest number of pre-auto phagosomes in the cytoplasm. For statistical analysis of pre-autophagosome size per cell, we used one-way ANOVA to compare between the M0, M1, and M2a conditions (n= 6 images, at least 5 cells /image, p-value $0.0045 < 0.05$). Unpaired t-test was used to compare between M0 and M2a lineage M1 lineage (n= 6 images, at least 5 cells /image, p-value $0.043 < 0.05$). M1 showed the highest significance among the three conditions. However, M2a lineage showed a significant increase in cytoplasmic Atg16L1 spot size when compared to M0 lineage control. Interestingly, we noticed that the average spot size of Atg16L1 in M1 lineage is more than 4 um diameter, which is above normal value for pre-auto phagosome (from 500 to 1000 nm) or (0.5-1 um) diameter.

**A-Nuclear Atg16L1 Merge M0 CTRL**

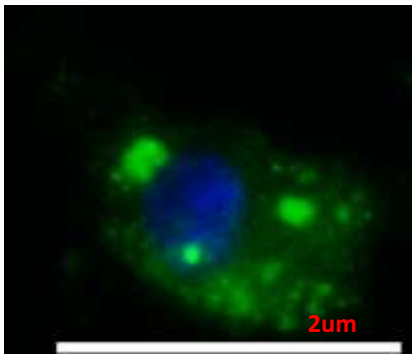


**B -Nuclear Atg16L1 Merge M1**

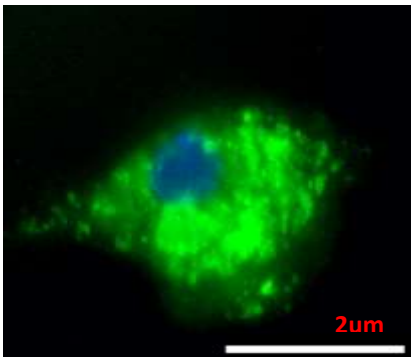


**C- Nuclear Atg16L1 Merge M2a**

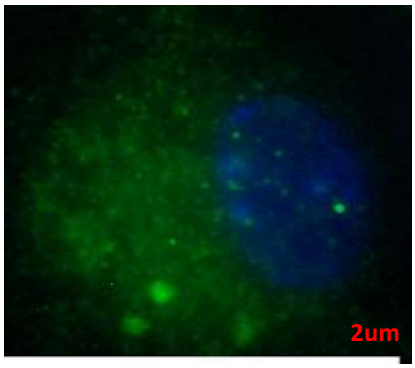


**D- Nuclear Atg16L1 Merge M0+EBS**

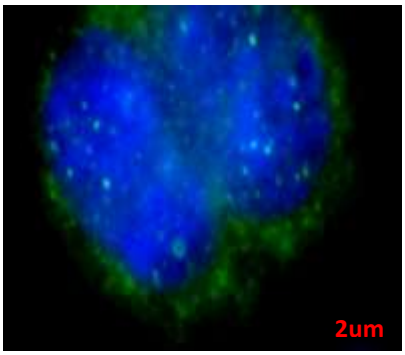


**Figure 36. Immune co-localization of nuclear Atg16L1 Pre-autophagosomes.**

This figure describes the immune co-localization studies of pre-autophagosomes in the nuclear compartment. A, B, C, and D show the nuclear Atg16L1 pre-autophagosomes as green to yellow dots in M0, M1, M2a, and M0 + Earle balanced salt, respectively. Green dots represent the auto phagosomes. No autophagosomes were observed in the M0 CTRL and in M1 macrophages. However, we observed these dots in M2a lineage (C) and positive autophagy M0+EBS cells (D).

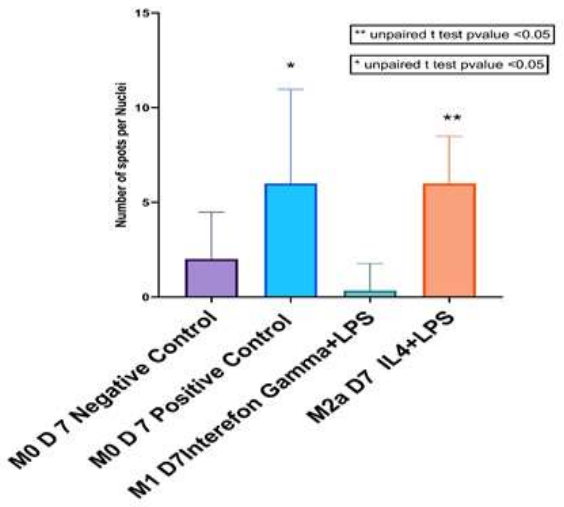


**A-Nuclear Atg16L1 Pre-auto phagosome Count**

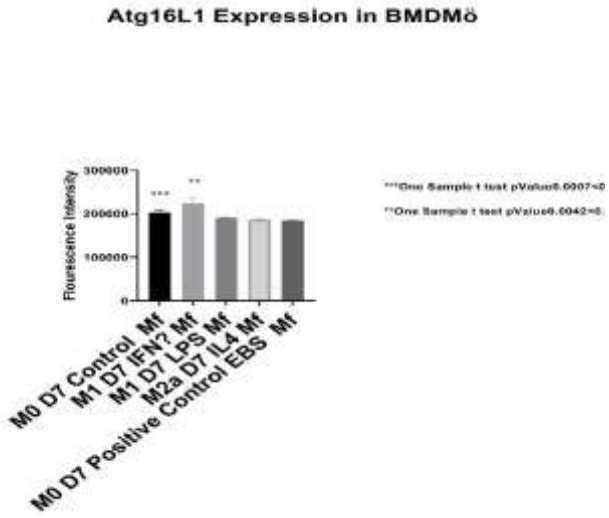


**B-Atg16L1 protein Relative Expression**

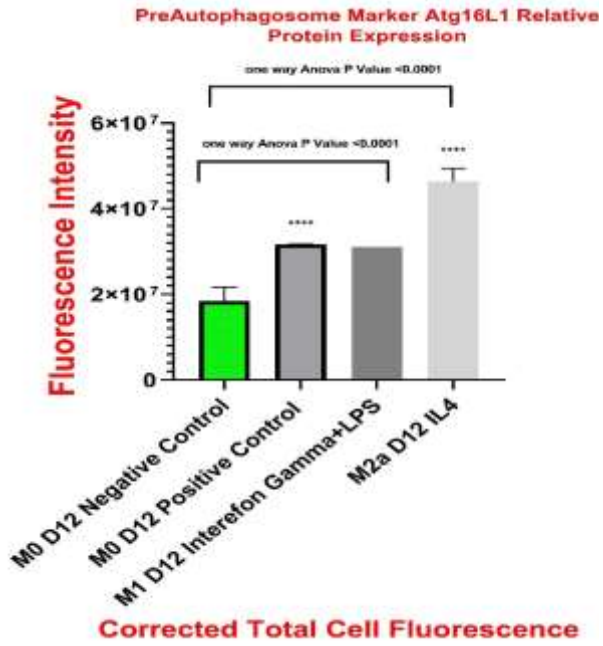


**C- Atg16L1 protein Relative Expression**

**Figure 37. statistical significance of Nuclear Atg16L1 and Relative Protein Expression:**

A) Unpaired t test was used to compare M0 negative control and M0+EBS as positive control (n= 3 images, at least 5 nuclei /image, p-value 0.036 < 0.05), and between M2a and M0 control (n= 3 images, at least 5 nuclei /image, p-value 0.008 < 0.05). B & C show relative fluorescence intensity. M2a showed the most significant increase (one-way ANOVA, n=3, p -value <0.0001).

M2a lineage showed a significant increase in both nuclear pre –autophagosome number and cytoplasmic Atg16L1 size. This supports the previous gene expression data that showed increased fold change of Atg16L1-1 gene variation M2a at day 7 polarization (**Figure 34**).

**INF gamma increased Atg7 expression in M1 cell lineage and caused increased pre-autophagosome size.**

This study's relevance is in finding significant target protein candidates for macrophage polarization and Macro-autophagy and understanding how macro-autophagy could impact macrophage polarization process, which affects the activation of either M1 (proinflammatory lineage) or M2a (anti-inflammatory and cytotoxic lineage). Based on our previous findings, Atg7 is an important protein target that links macro-autophagy and Macrophages polarization processes (Figure 23). Here we show immune co-localization studies for Pre-autophagosomes of Atg7 protein and gene expression data. (figure 40). Statistical significance of Atg7 pre-autophagosomes in terms of spot count and size is further explained (figure 40).

**A-Atg7 Pre- autophagosome in M0**

**CTRL FITC**

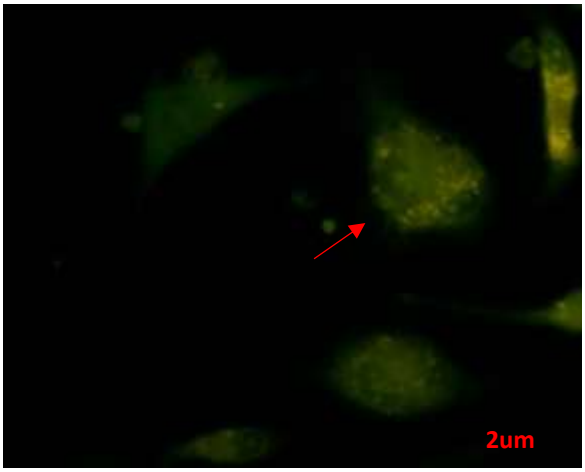


**B- Atg7 Pre- autophagosome in M1**

**INFG+LPS FITC**


**C- Atg7 Pre- autophagosome in M2a**

**IL4+LPS FITC**

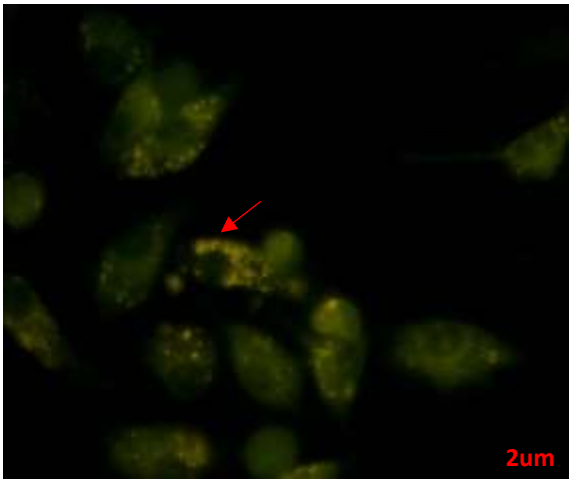


**Figure 38. Immune co-localization of Atg7 Pre-autophagosomes.**

Green or yellow dots (A) represent Atg7 expression as pre-auto phagosomes distributed in the cytoplasmic compartment (red arrow). B & C Show the Atg7 expression in M1 and M2a lineages, respectively. Red arrows (A, B, and C) refer to the cytoplasmic Atg7 protein expression.

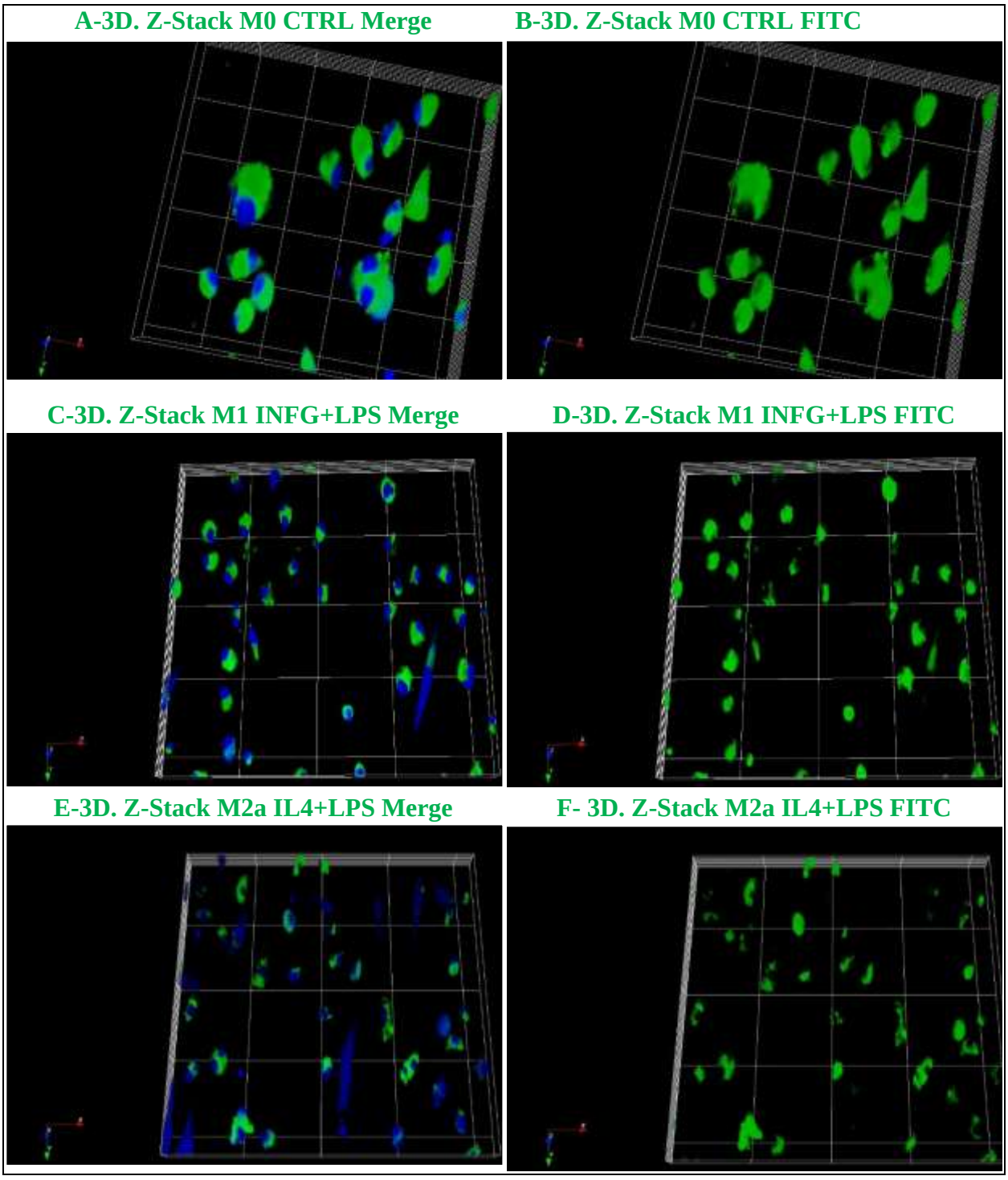


**Figure 39. Immune co-localization of Atg7 using Laser Confocal Microscopy.**

3D Reconstruction for Z – stack confocal images revealed a significant number of pre-autophagosomes formed at M1 and M2a lineages. However, M0 control showed the largest size of pre-autophagosomes **(B, D, and F)**.

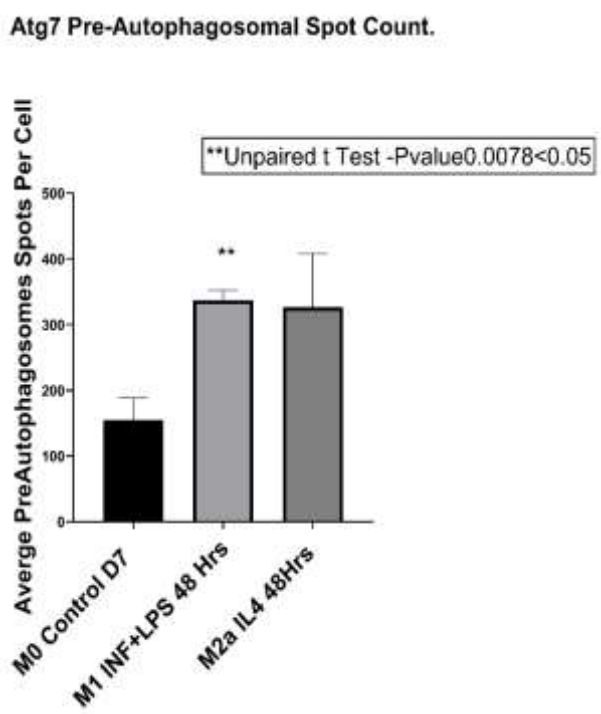


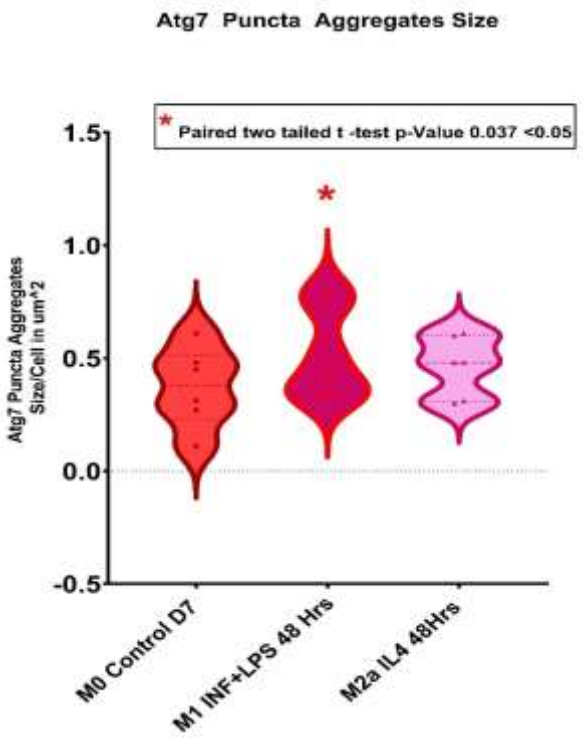


**A-Atg7 Pre-auto phagosome count** **B- Atg7 Pre-auto phagosome size**

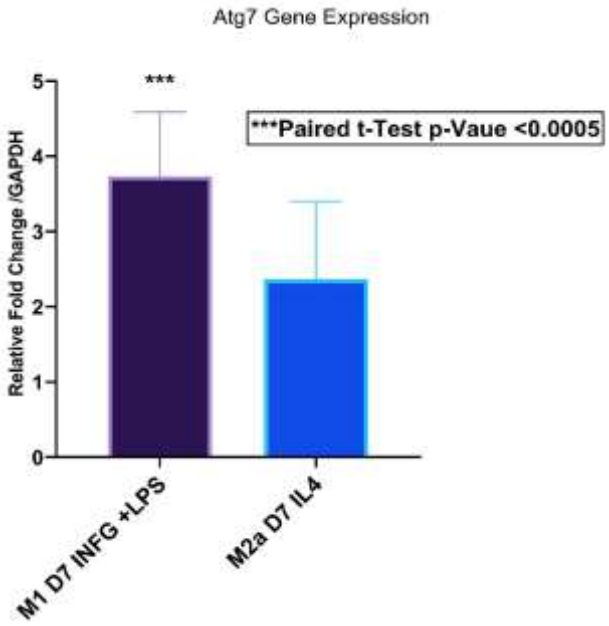


**C-Atg7 Gene Expression Data**

**Figure 40. Statistical analysis of Atg7 pre-autophagosomes and gene expression.**

Statistical analysis of Atg7 or pre-autophagosome number per cell. Unpaired t-test was used to calculate the significance between M0 CTRL and M1 lineage (A, n= 6 images, p-value 0.0078 < 0.05). There was no significant difference between M1 and M2a (300 spots/cell).

Figure 40, B shows the violin plot of Atg7 pre-autophagosome size, measured by automated spot detection plugin on ImageJ ® software. The paired two-tailed t-test (n= 6 images, p-value 0.027 < 0.05**)** showed that M1 showed an increased spot size of more than 1 um in diameter. These results support our findings (figure 39), which indicate Atg7 pre-autophagosome aggregated together.

Relative fold change of gene expression was normalized to GAPDH (C) gene as endogenous control, using paired t-test to calculate significance (n=4, and p-value 0.0002 < 0.05). Mean and standard deviation for fold change relative to Gapdh in M0 were: Mean=3.7, and 2.36 folds, Standard deviation ± 0.46 and ± 0.56 for M1 and M2a, respectively.

Therefore, INF gamma promoted the expression of Atg7 protein and mediated up-regulation of Atg7 gene expression in M1 and M2a cells. While Interferon-γ and lipopolysaccharide increased Atg7 protein and mRNA in M1 lineage.

**Increased Smad1 gene expression on day 14 polarization in M1 and M2a lineages.**

The protein encoded by this transcription factor has an important role in biological processes such as apoptosis, cell growth, and immune responses. We report Smad1 as one of our predicted transcription factors (**figure 18**) and its downstream targets IL6 and MAPLC3A genes. Smad1 was downregulated in M1 and M2a at day 7 polarization compared with 14 days' polarization results. Flow cytometry results showed a significant difference in Smad1 protein expression at day 7 polarization in M2a compared to M0 and M1 (**Figure 42**). Fold change in M2a cells at day 7 polarization was only 1.5 folds (**Figure 42**). However, there was significant overexpression of Smad1 in both M1 and M2a lineages at day 14 polarization (**Figure 42**).

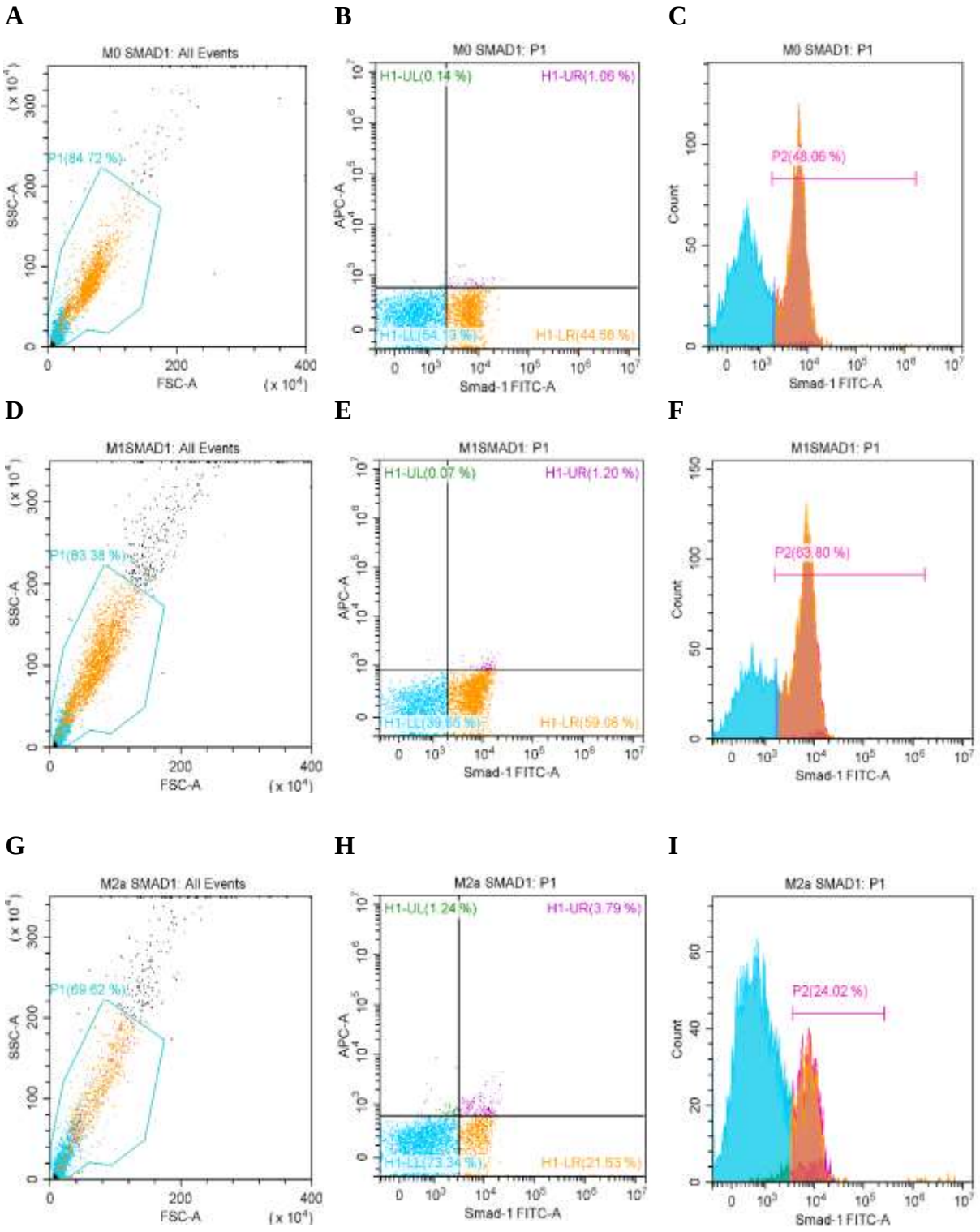


**Figure 41. Flow cytometry Analysis for Smad 1 Expression in Bone Marrow-Derived Macrophages.**

The figure represents Smad1 by flow cytometry analysis for M1 and M2a. M0 macrophages were used as control. Samples were gated on 81%, and Smad1 expression was read using FITC Filter. A, D and G represent the gating for 5000 events (event= single cell) inside scatter plots (SSC-A) on X-axis and forwarded scatter plots (FSC-A) on Y-axis. A, D, and G for M0, M1, and M2a lineages, respectively. On the other hand, B, E, and H are quadrant plots for M0, M1, and M2a, respectively. C, F, and I are fluorescence peak signal plots for Smad1 expression in M0, M1, and M2a cells, which indicates a higher expression of Smad1 at M2a. However, M0 and M1 lineages had the lower expression, (n=3).

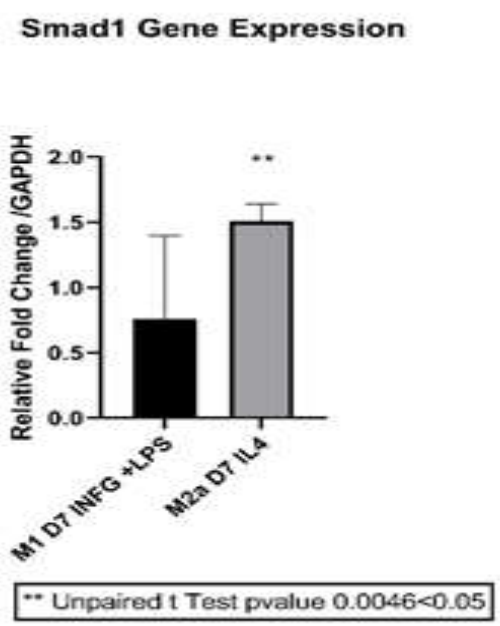


A

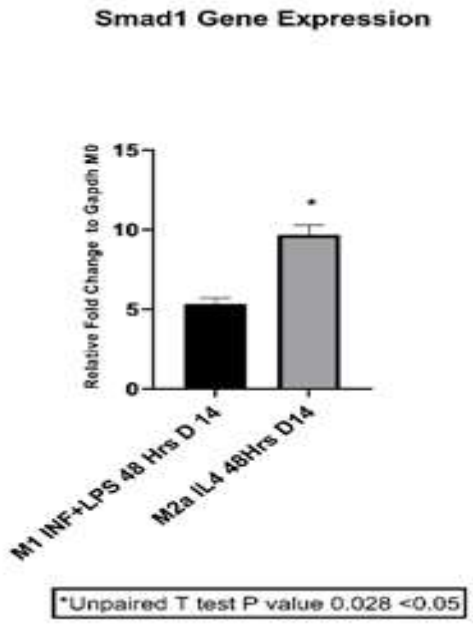


B

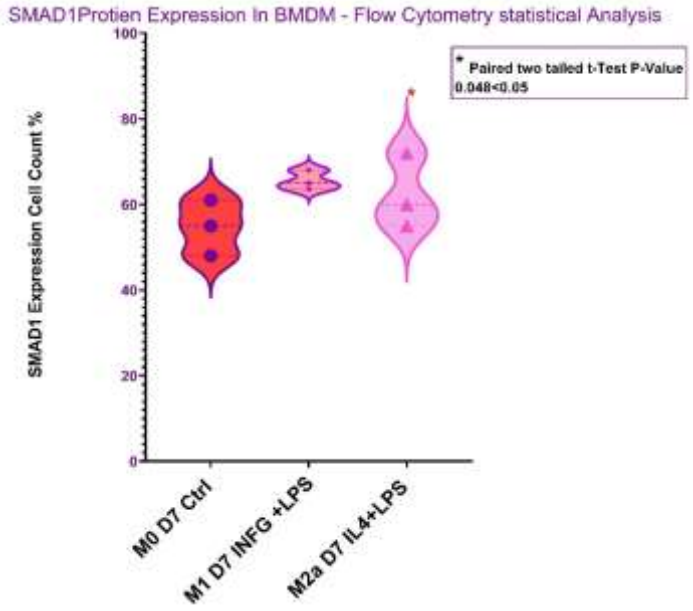


C

**Figure 42. Statistical analysis of flow cytometry data for the expression of Smad1.**

M1 and M2a at day 14 polarization showed a significant increase in Smad1 gene expression.

The bar plots show the statistical representation of Smad1 transcription factor fold change in both M 1 and M2a at days 7 and 14 polarization normalized to GAPDH, as endogenous control, and M0 lineage as control. Unpaired t-test was used to calculate the significance (n=4, and p-value 0.0064 < 0.05). Mean and standard deviation for fold change relative to Gapdh in M0 were: Mean=0.76 and 1.5 folds, Standard deviation ± 0.05 and ± 0.01 for M1 and M2a respectively). B) Bar plot shows the statistical representation of Smad1 transcription factor fold change in both M 1 and M2a at day 14 polarization normalized to GAPDH as endogenous control and M0 lineage as control. Unpaired t-test was used to calculate significance (replicates number, n=4) and (p-value -0.028 < 0.05). Mean and standard deviation for fold change relative to Gapdh in M0 were calculated using Excel (Mean= 6.1 and 8.6 folds, Standard deviation = 0.4 ± and 1.6 ± for, M1 and M2a respectively). (C) Violin plot is showing the statistical significance for Smad1 total expression ( n=3). Statistical significate was calculated using a paired two-tailed t-test (n=3, p-value 0.048 < 0.05). This showed an increase in M2a lineage; however, there was no significant difference in expression of Smad1 in M0 and M1 lineages. Mean and standard deviation were calculated using Excel (Mean=54.6 %, 65.5 % and 72.3% Standard deviation = ±5 .3 %, ±1,8 and ±f 7.1 for M0, M1, M2a respectively).

**Autophagy associated protein complex LC3 A&B expression increased in M1 and M2a macrophages.**

The MAP1-LC3s or LC3 A & B protein complex is responsible for autophagosome formation and lysosomal fusion. It is also considered an autophagosome marker as it appears on the surface of autophagosomes. Therefore LC3 A&B quantification can give insights about autophagy inside the cell lineages M0, M1, and M2a. We found that the distribution of autophagosomes inside the nuclear and cytoplasmic compartments is not uniformly distributed. Here we show (figure 43) nuclear autophagosomes formed in M2a cells and M0 positive autophagy. However, autophagosomes were not localized in the nucleus in M1 and M0 control. Counting using ImageJ ® showed that the average number of basal autophagosomes in M0 was 1800, in M1, it was 2436 spot and in M2a increased to 2471 (figure 46). Remarkably autophagosome aggregations were also observed. We use the term "aggregations" as the autophagy activity was remarkably increased. 3D reconstruction of Z-stack images, we observed the LC3 A&B autophagosomes formed aggregations, and it increased in M1 and M2a lineages compared to the M0 control (figure 44). Flow cytometry single-cell quantification showed a significant increase in M1 and M2a cells.

Finally, mRNA levels of LC3B but not LC3A increased in M1 to 4 folds and M2a 3 folds, respectively. These results support our systems biology approach that LC3 A&B is a hub protein in the interplay between autophagy and macrophage polarization. Collectively, (INFG +LPS) induced macroautophagy inside M1 and (IL4+LPS) induced macroautophagy in M2a cells (Figure 45 & 46).

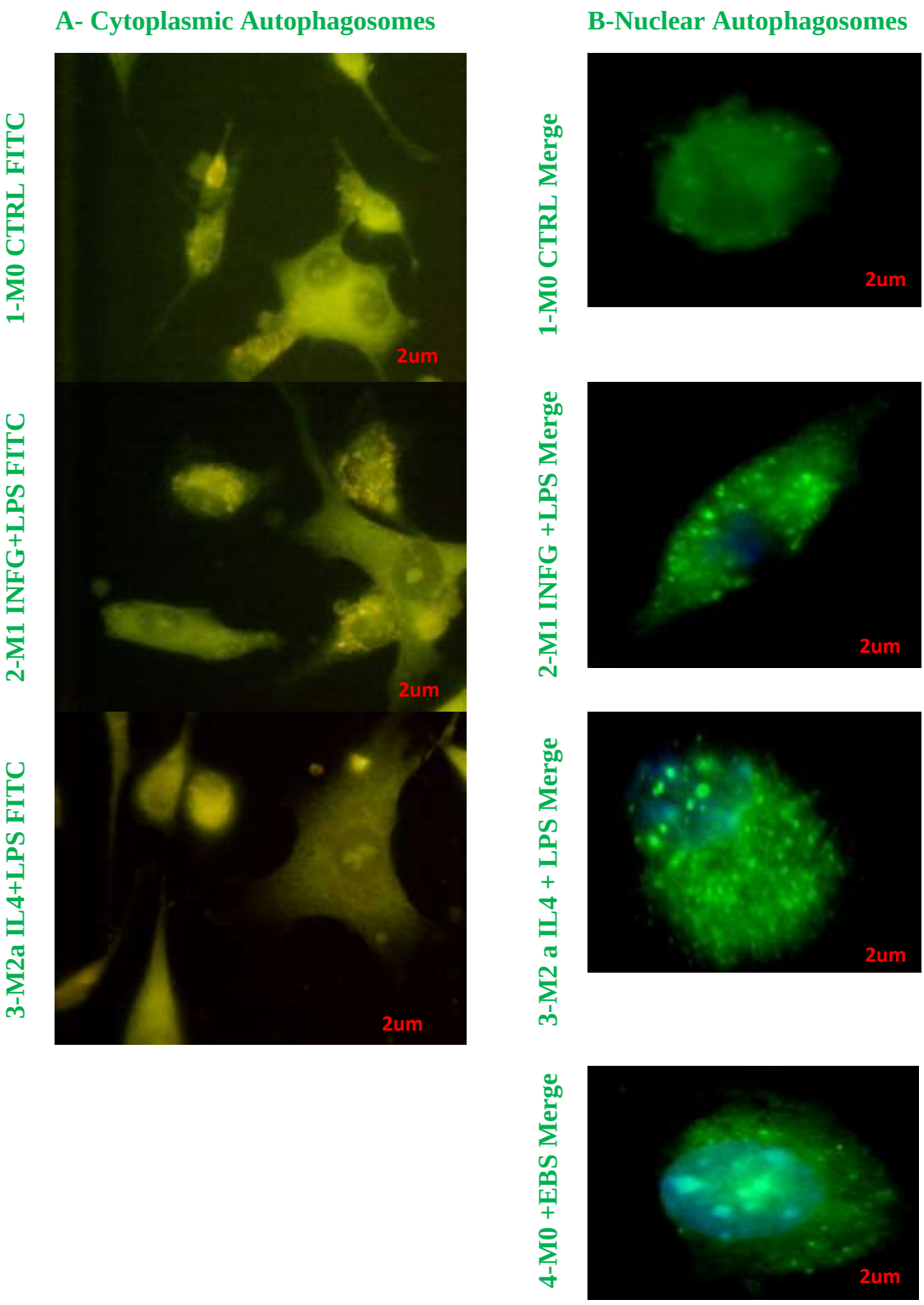


**Figure 43. Immune co-localization studies for LC3A&B protein complex.**

Panel A shows immune co-localization studies for cytoplasmic Autophagosomes (yellow to green spots) in M0, M1, and M2a lineages, respectively. On the other hand, Panel (B) describes the LC3 A&B staining showing nuclear Autophagosomes (yellow dots inside the nuclear compartment).

A high number of LC3 A&B protein localized in the nuclear compartment of M2a lineage and M0+EBS cells. The number of autophagosomes was counted inside the cytoplasm and in the nucleus using the automated ImageJ plugin.

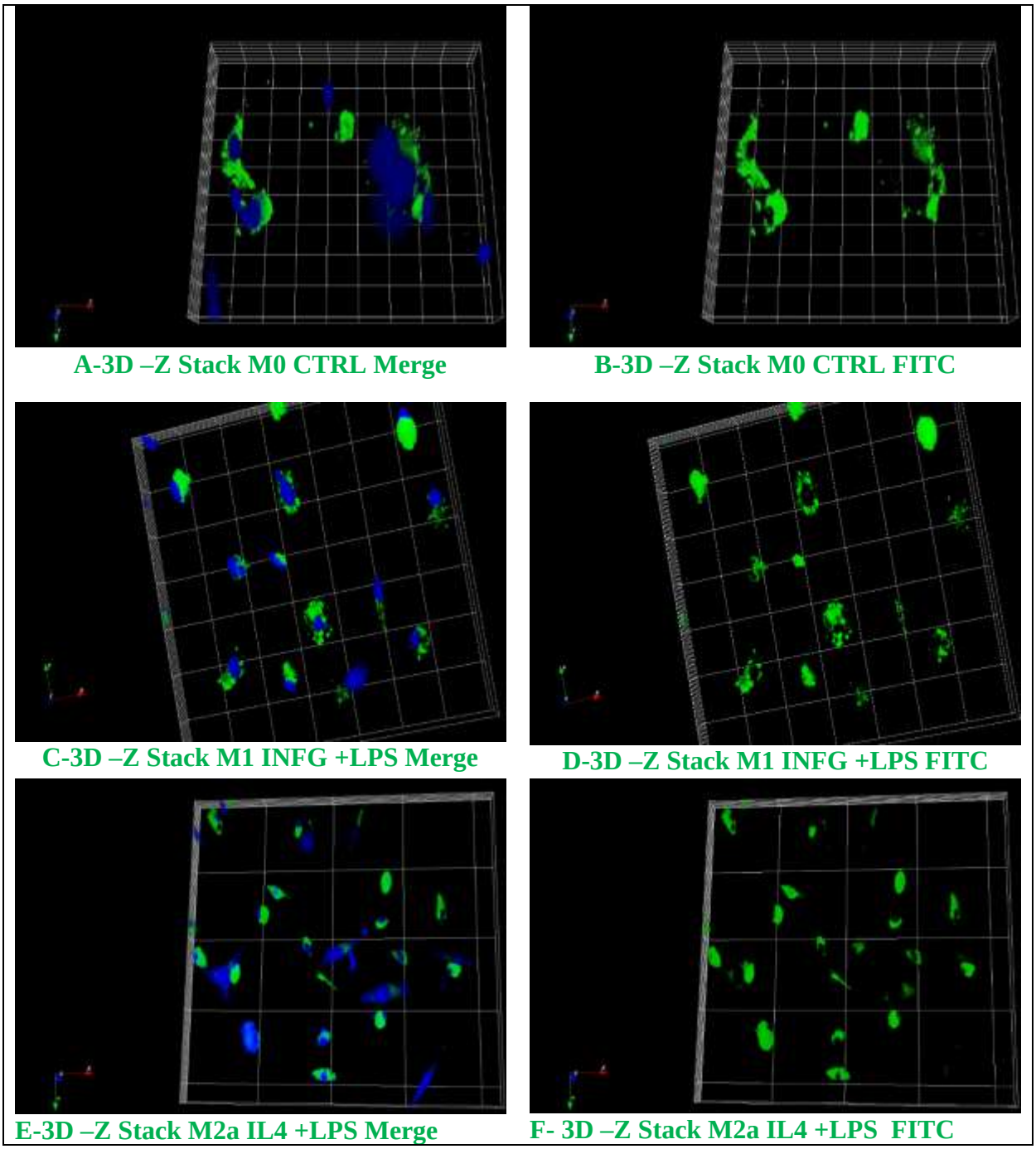


**Figure 44. Immune co-localization using Laser Confocal Microscopy for LC3 A&B Protein Complex.**

3D reconstruction of Z – stack laser confocal images revealed many autophagosomes formed in M10 and M1 lineages. M2a showed the largest size of pre-autophagosome (B, D, and F).

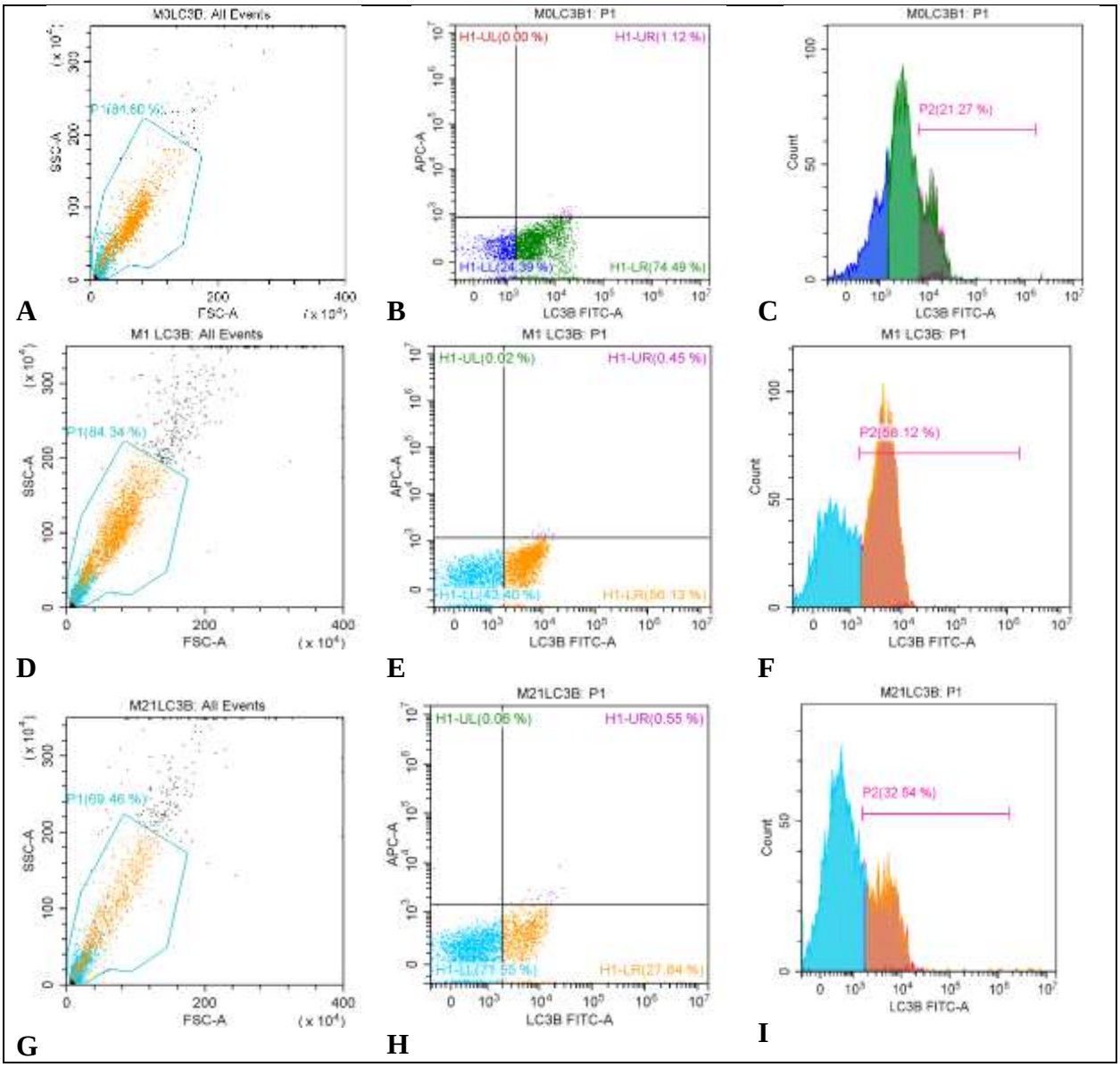


**Figure 45. Flow cytometry analysis for LC3 A&B protein complex expression in Bone Marrow-Derived Macrophages**

Flow cytometry analysis of LC3 A&B protein complex expression in M1 and M2a. M0 macrophages were used as control. Higher expression of LC3 A&B protein complex was found in M1 and M2a cells; however, M0 showed low expression. Samples were gated on 81%, and LC3 A&B protein complex expression was read using FITC Filter. A, D, and G represent the gating for 5000 events (event= single cell) inside scatter plots (SSC-A) on X-axis and forwarded scatter plots (FSC-A) on Y-axis. B, E, and H are quadrant plots for M0, M1, and M2a, respectively. C, F, and I are fluorescence Peak signal plots for LC3 A&B protein complex expression in M0, M1, and M2a cells. (n=3).

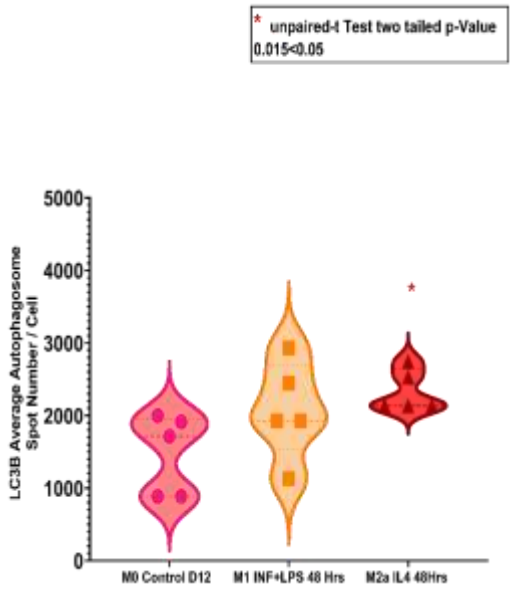


**A- LC3 A&B Autophagsosme count per Cell**

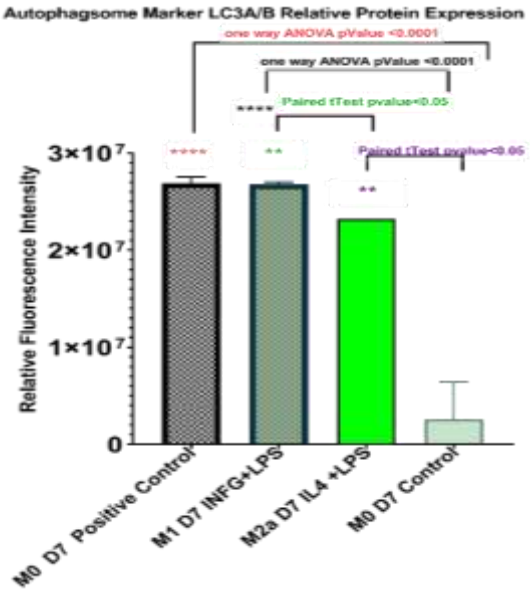


**B- LC3 A&B relative protein expression**

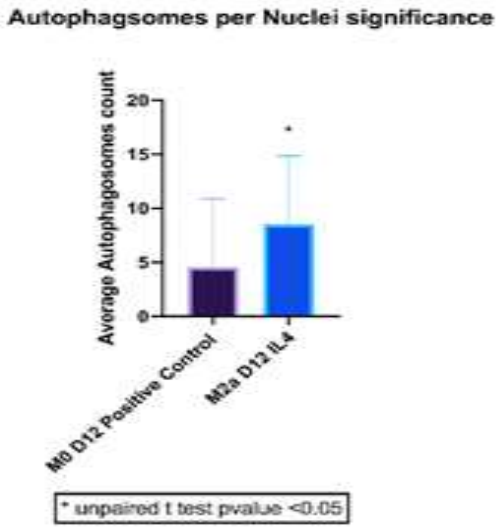


**C- LC3 A&B Autophagsosme Count Per Nuclei**

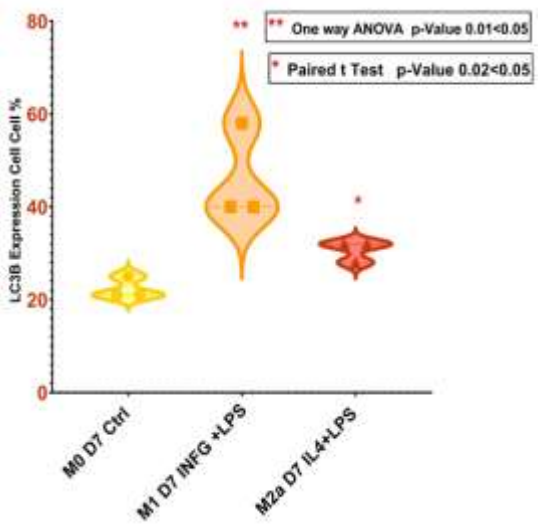


**D- Flow Cytometry Analysis of LC3 A&B**

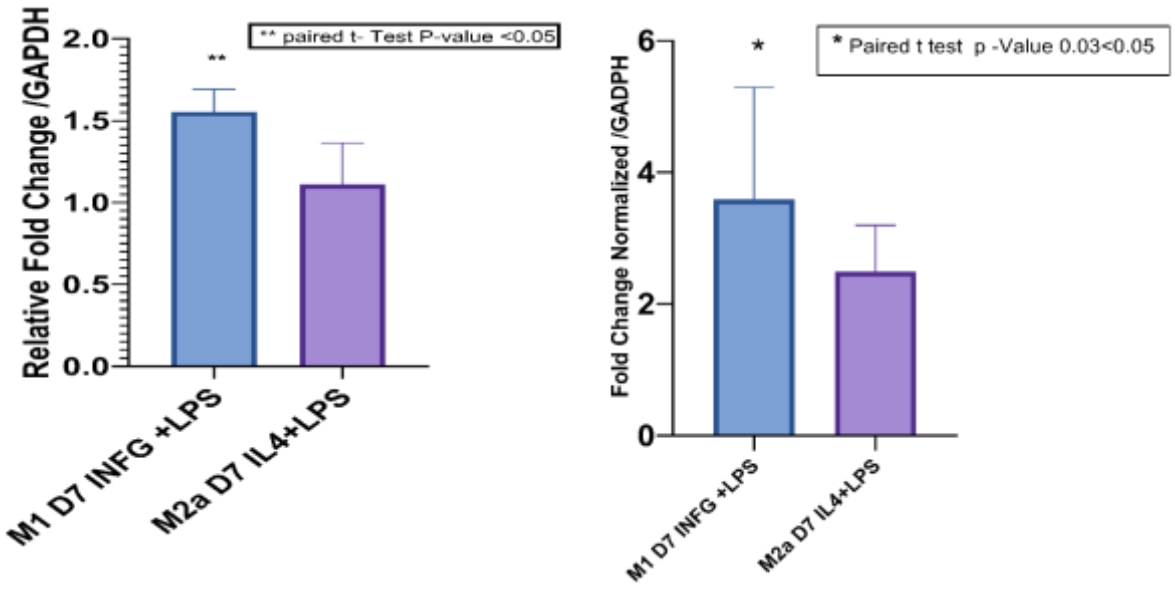


**E- LC3A Gene Expression Data at day 7 polarization**

**F- LC3B Gene Expression Data at day 7 polarization**

**Figure 46. Representation for LC3 A&B protein complex expression.**

LC3 A&B protein complex was quantified, unpaired t-test was used to compare between M0 and M2a lineage, 5 images with at least 5 cells/ image were counted using ImageJ (p-value 0.015 < 0.05). Mean and standard deviation were: Mean = 1857, 2436, and 2471 spot, STD ± 118, ± 409, and ± 253 for M0, M1, and M2a, respectively). Also, we manually counted the number of nuclear autophagosomes figure (C). the unpaired t-test was used to calculate the significant difference between M0 positive autophagy as positive control and M2a lineage (n= 5 images, at least 5 cells/ image were counted using ImageJ, p-value 0.029 < 0.05).

3D reconstruction of Z –stack images supported the results from figure A. High autophagosomal aggregates were formed in both M1 and M2a lineage compared to M0 control (figures 44 B, D, and F). Relative fluorescence intensity of LC3A&B showed a significant increase in M1 and M2a lineage compared to M0 control.

Single-cell flow cytometry analysis (figure 45) was used to investigate the total cell percentage of LC3 A&B complex protein in M0, M1, and M2a lineages. Mean, and standard deviation were (Mean = 22, 46, and 30 %, STD = ±1.8, ± 8.4, and ± 1.88 % for M0, M1, and M2a, respectively).

Statistical analysis using violin plot for flow cytometry (figure 46, D) data of cells that express LC3 A&B protein showed that highest expression of LC3A&B was in M1 lineage, and M2a shiwed higher expression of LC3A&B protein more than M0 control . One-way ANOVA was used to calculate the significance between all conditions M0, M1, and M2a, (n= 3, and p-value $0.01<0.05$). A paired t-test was used to calculate the significance between M0 and M2a ( n= 3, and p-value $0.02 < 0.05$).

Figure 46.E Statistical analysis of LC3A fold change in both M 1 and M2a at day 7 polarization normalized to Gapdh as endogenous control and M0 lineage as a control showed that , LC3A was up regulated in M1(1.5 folds) and showed a normal expression pattern in M2a (1 fold ) . Paired t-test used to calculate significance (n=4, and p-value - $0.0012 < 0.05$). Mean and standard deviation for fold change relative to Gapdh in M0 were: Mean=1.5 and 1.15 folds, Standard deviation ± 0.07 and ± 0.12 for M1 and M2a respectively. Figure 46, F shows a statistical representation of LC3B fold change in both M 1 and M2a at day 7 polarization normalized to Gapdh as endogenous control and M0 lineage as a control showed that , LC3B was up regulated in M1(more than 3 folds) and showed a up regulationM2a (1 fold ) . however , M1 expressed LC3B higher than M2a lineage.Paired t-test used to calculate significance (n=4, and p-value - $0.03 < 0.05$). Mean and standard deviation for fold change relative to Gapdh in M0 were: Mean=3.96 and 2.65 folds, Standard deviation ±1.27 and ±0.53 for, M1 and M2a respectively).

**Does increased Autophagy activity decrease the phagocytic activity of bone marrow-derived macrophages?**

Our systems biology approach predicted the candidate protein targets that mediate the interplay between autophagy and macrophage polarization. Atg16L1 was one of the important hub proteins; we found significant overexpression of Atg16L1-1 gene variant in M2a at day 14 polarization (30 folds' increase) (figure 34, B). We also found a 15 fold increase in Atg16L1-3 gene variant in M2a lineage at day 7 polarization (figure 34, C). These results indicate an increased autophagy activity in M2a than M1, specially Atg16L1 gene expression.

IL4 induced macroautophagy in M2a cell lineage at day 7 and day 14 polarization. We were curious about whether autophagy affects macrophage phagocytosis or not. Flow cytometry studies

revealed macrophages at day 14 polarization showed a decreased arginase expression figure (48, A) in M0, M1, and M2a lineage when compared at day 7 polarization (figure 27 A). Also, M1 and M2a showed a decreased CD68 expression when they compared to M0 ctrl at day 14 figure (48: A). previously, we reported Interleukin 4 and Lipopolysaccharide combination induced macroautophagy and increased the autophagy-related genes Atg16l1-1, Atg16L1-3, LC3A, and LC3B, Atg7, and VAMP7.

These results suggest that increasing the polarization time from 7 days to 14 days increased the autophagy activity and might decrease the phagocytosis markers like Arginase -1 and Cd68. However, to further confirm these results, we performed autophagy inhibition and investigation of phagocytosis marker expression.

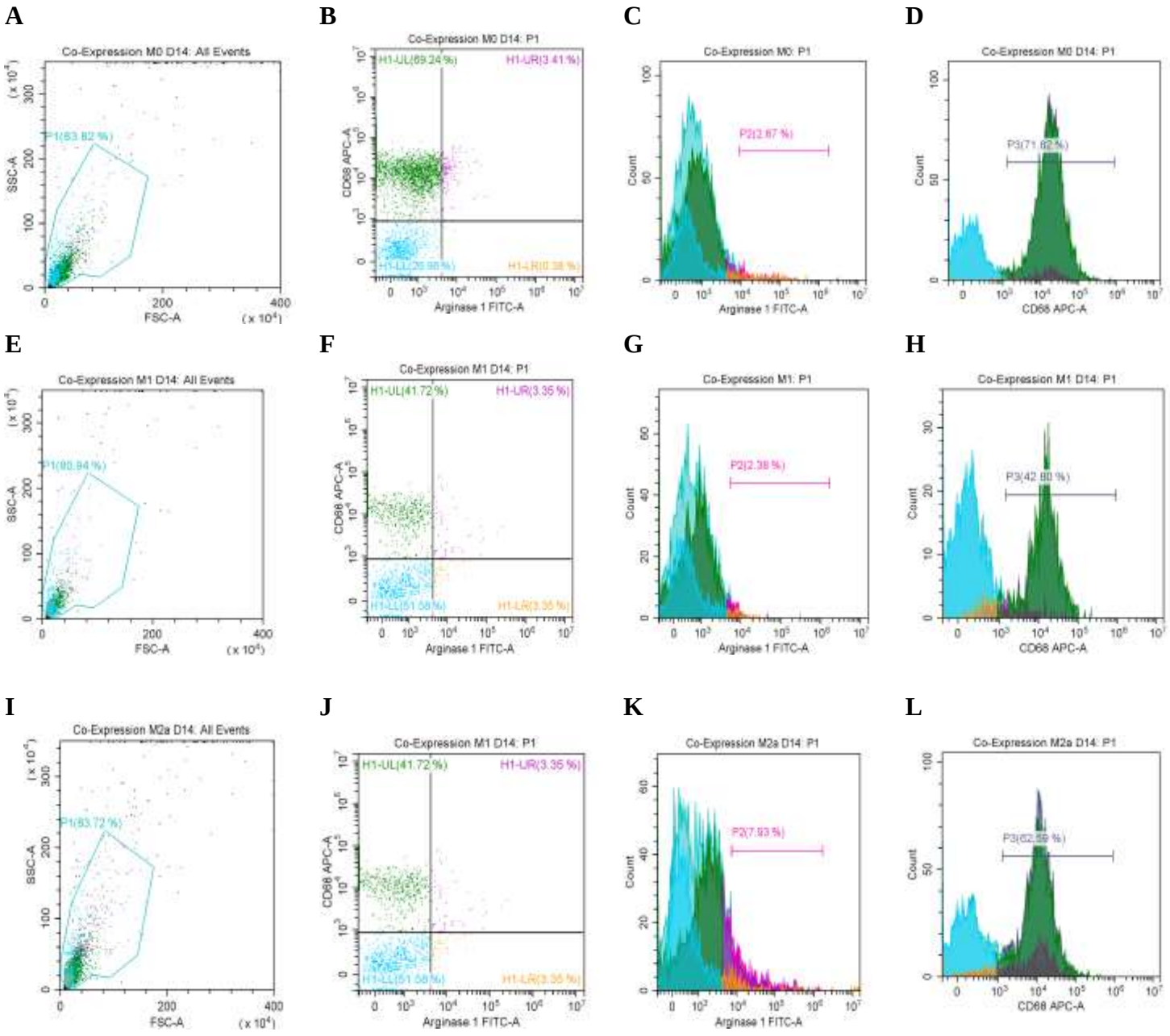


**Figure 47. Flow cytometry Analysis for Bone Marrow-Derived Macrophages at Day 14 Polarization**

Representation of phagocytosis markers Cd68 and Arginase 1 expression at day 14 polarization. Panel A shows the flow cytometry analysis for both Cd68 and Arginase 1 at M0, M1, and M2a day14 polarization.

Figure 47 represents the co-expression of both Cd-68 and arginase -1 by flow cytometry analysis for M1 and M2a, using M0 macrophages as a control. Samples were gated on 81%, and Cd-68 expression was assessed at APC - Filter, and Arginase-1 was read at FITC- Filter. Figure 48 A, E, and I represent the gating for 5000 events (event= single cell) inside scatter plots (SSC-A) on X-axis and forwarded scatter plots (FSC-A) on Y-axis. (A, E, and I) for M0, M1, and M2a lineages, respectively. On the other hand, (B, F, J) are quadrant plots for M0, M1, and M2a, respectively.

Figure 47 C, G, and K are fluorescence peak signal plots for Arginase -1 percentage expression in M0, M1, and M2a cells, which indicate lower expression of arginase-1 at M1 and M2a lineages compared to figure 25 H and L. Figure 48 D, H, and L represents the fluorescence signal peak for CD68 expression in M0, M1, and M2a respectively. Surprisingly at day 14 polarization M0 showed no expression for arginase -1 (figure 47C) compared to M0 lineage at Day 7 polarization (figure 25 D). M0 lineage should not express arginase -1, which means there were Arginase -1 induced phenotypic changes in M0 at day 14 polarization.

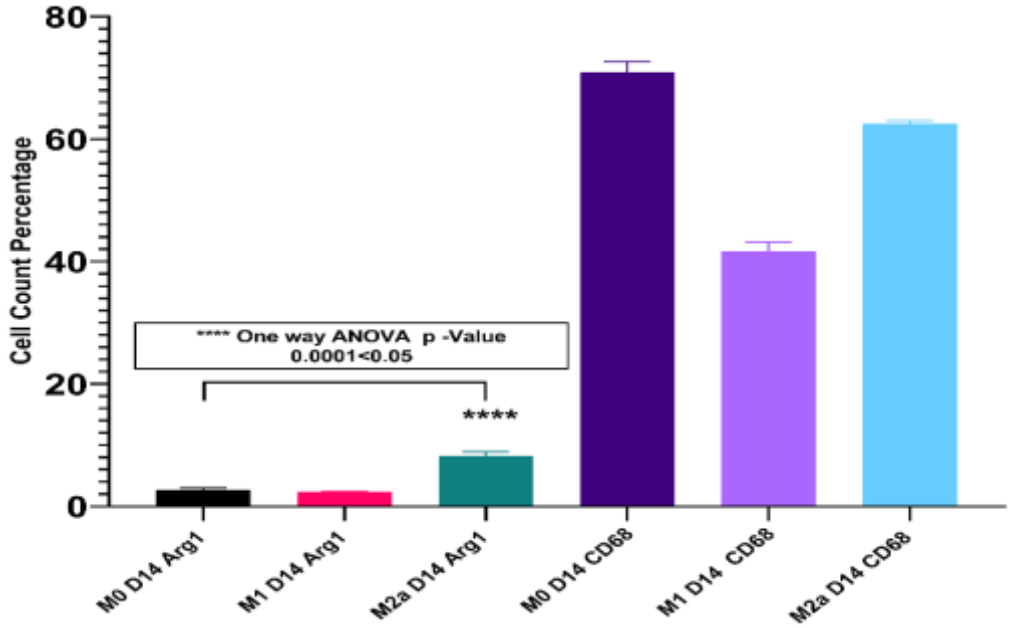


**Figure 48, A. Flow Cytometry Analysis of CD68 and Arginase -1 in BMDM at Day 14 Polarization.**

The figure shows the statistical analysis of Arginase 1 and CD68 expression flow cytometry data in terms of cell count. One way Anova was used to calculate the arginase -1 significance (number of samples n=3, p-value 0.0001<0.05). However, CD68 showed no significant difference between all samples, including M0, M1, and M2a lineages.

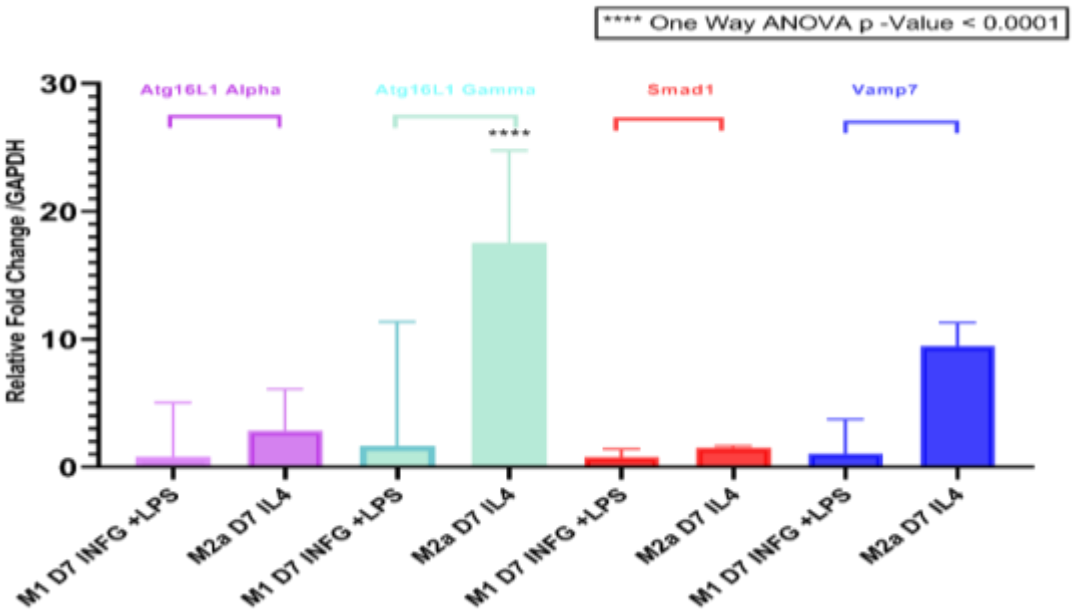


**Figure 48, B. Summary for Gene Expression Data in BMDM at Day 7 Polarization**

A summary of all gene expression studies performed on day 7, including: Smad1, Atg16L1-1, Atg16L1-3, and Vamp7. It shows the significance of fold increase in Atg16L1-3 by M2a more than (20 folds' increase) and in Vamp7 gene up-regulated more than 10 folds' increase in M2a lineage.

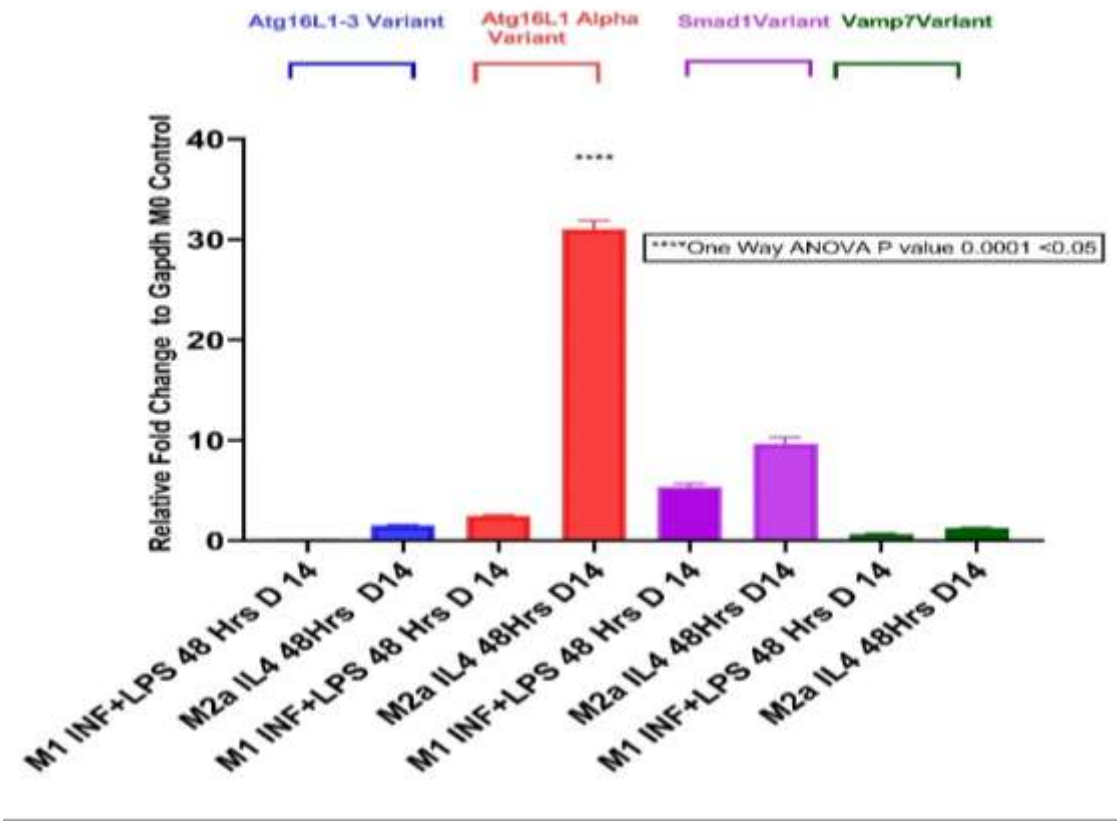


**Figure 48, C. Summary for Gene Expression Data in BMDM at Day 14 Polarization**

A summary of gene expression data at day 14 polarization. Interestingly, interleukin -4 activated macrophages M2a lineage expressed a 30 folds increase in Atg16L1-1 but not Atg16L1-3. Also, Smad1 was upregulated in M2a lineage with 10 folds increase. These results indicate a high autophagic activity in M2a lineage and lead us to investigate the impact of autophagy inhibition on Macrophages phenotypic characters.

**Autophagy Inhibitor Bafilomycin-A Significantly increased CD68 and Arginase 1 Expression in M0, M1, and M2a Lineages.**

Accumulation of autophagosomes LC3 A&B protein complex inside the cytoplasmic boundary of Interferon-γ activated M1 lineage, and Interleukin 4 activated M2a lineage gave us insight into the increased autophagy activity in both cell phenotypes from immune co-localization studies (Figure 43; 1B, 2B, and 3B & Figure 44; D and F). Both of Interferon-γ and Interleukin 4 induced macroautophagy M1 and M2a cell lineages. Also, based on the gene expression data at day 7 polarization of both Atg16L1-3 and Vamp7 upregulated in M2a lineage by 18 folds and 10 folds, respectively (figure 48 B). And Atg16L1-1 gene upregulated in M2a lineage at day 14 polarization by 30 folds' increase (figure 48 C).

Macrophages are highly dynamic immune cells, and phagocytosis is one of its important biological roles. Therefore, we tried to investigate the interplay between autophagy and macrophage polarization in the phagocytosis process. Autophagy was inhibited using autophagy inhibitor Bafilomycin-A (200 n M) in M0, M1 and M2a cell lineages, surprisingly we found high expression pattern for both phagocytosis markers Arginase -1 and CD 68 in M0, M1 and M2a cells when compared to previous flow cytometry results (figure 27, A, B , C, and D). Also, autophagy inhibitor Bafilomycin-A increased the percentage of double-positive (CD68/Arginase1) cells in both M1 and M2a.

**Autophagy induction decreased the phagocytosis activity of M2a but not M1**

We evaluated the impact of autophagy induction on phagocytosis activity. The average number of phagocytic events were counted manually. After autophagy induction with Earle balanced salt, M2a lineage showed decreased phagocytic activity. However, no significant effect on M0, and M1 lineage was observed.

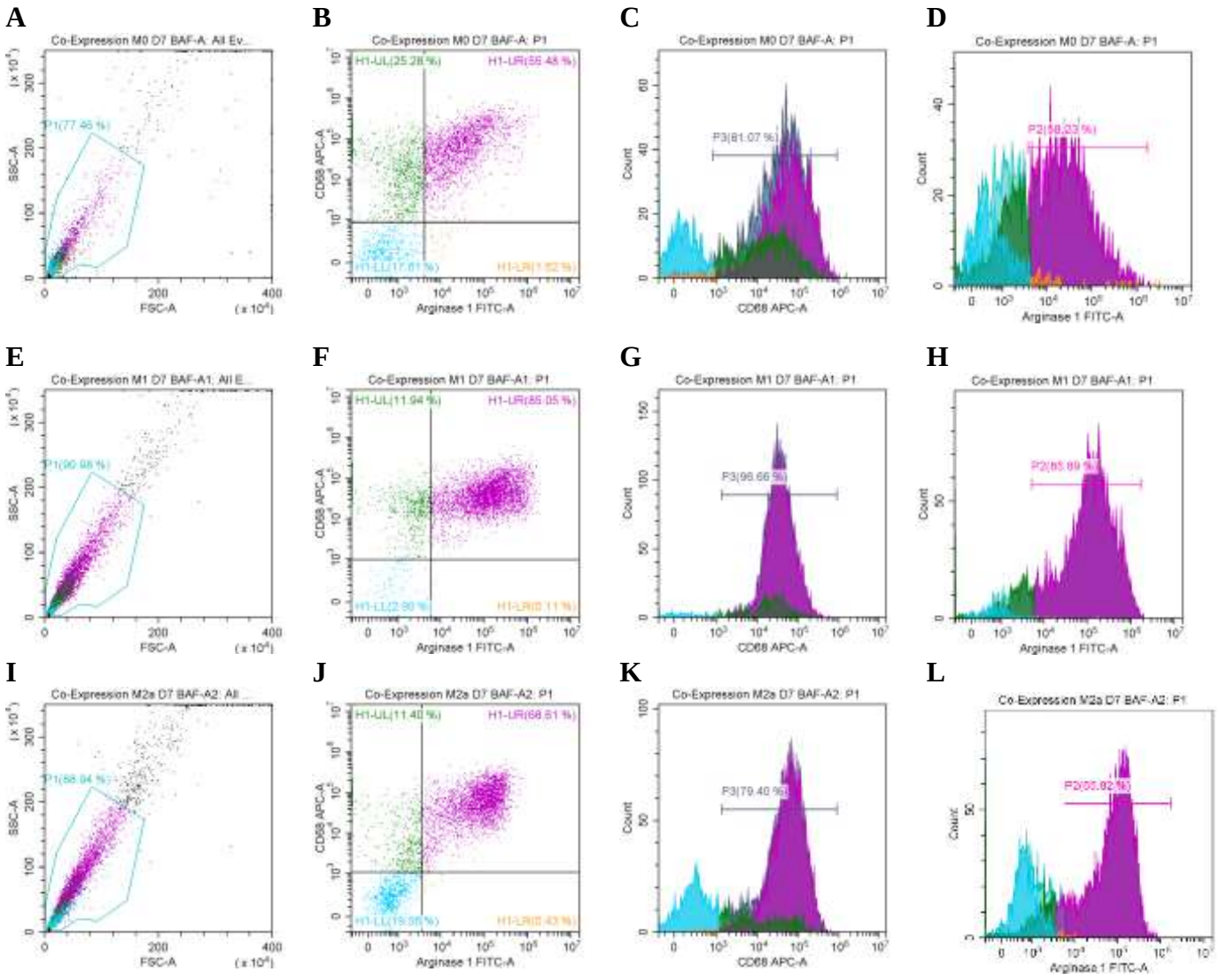


**Figure 49. Flow cytometry Analysis for Bafilomycin-A induced autophagy inhibition in Bone Marrow-Derived Macrophages**

Figures represent co-expression of both Cd-68 and arginase -1 by flow cytometry analysis for M1 and M2a. M0 macrophages were used as control. Panel A shows the flow cytometry analysis for both Cd68 and Arginase 1 in Bafilomycin-A treated M0, M1, and M2a at day 7 polarization. Samples were gated on 81%, and Cd-68 expression was assessed at APC - Filter, and Arginase-1 was read at FITC- Filter. A, E, and I represent the gating for 5000 events (event= single cell) inside scatter plots (SSC-A) on X-axis and forwarded scatter plots (FSC-A) on Y-axis. A, E, and I show M0, M1, and M2a lineages, respectively. On the other hand, B, F, and J are quadrant plots for M0, M1, and M2a, respectively. C, G, and K are fluorescence peak signal plots for CD68 expression

in M0, M1, and M2a cells, indicating an increased expression of CD68 in all cell lineages. D, H, and L represent the fluorescence signal peak for Arginase -1 expression in M0, M1, and M2a.

Surprisingly, autophagy inhibition in (D) showed a great increase in arginase -1 expression more than 50% in M0 lineage at day 7 polarization, when compared to M0 at day 7 polarization with the normal basal autophagy activity. Further statistical significance analysis is described in the upcoming figure (50).

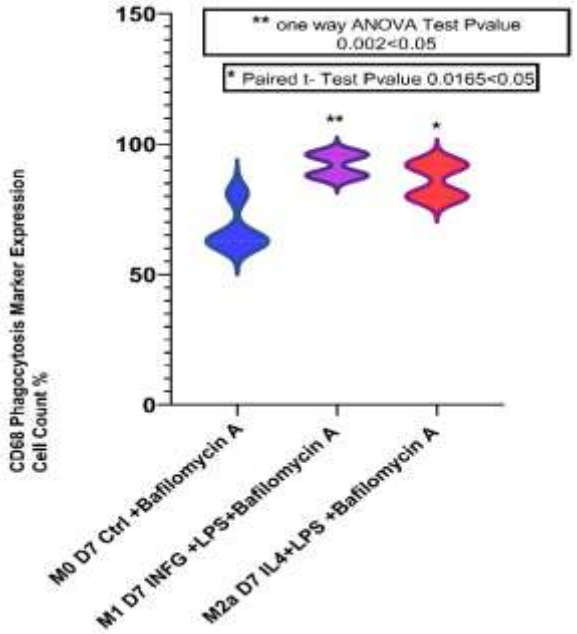


**A- CD68 Expression in Bafilomycin-A induced autophagy.**

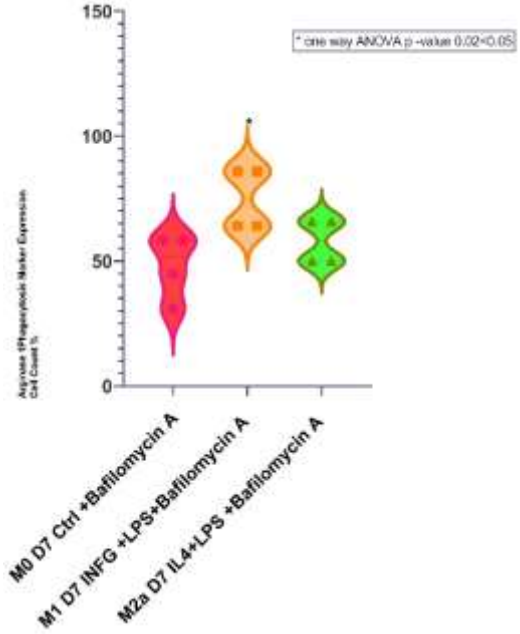


**B- Arg-1 Expression in Bafilomycin-A induced autophagy.**

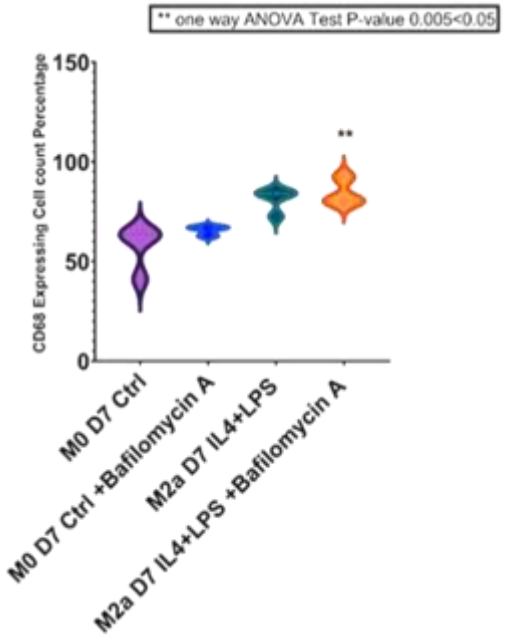


**C- Comparison of CD68 expression between M0, M1, & M2a macrophages and Bafilomycin-A induced autophagy.**

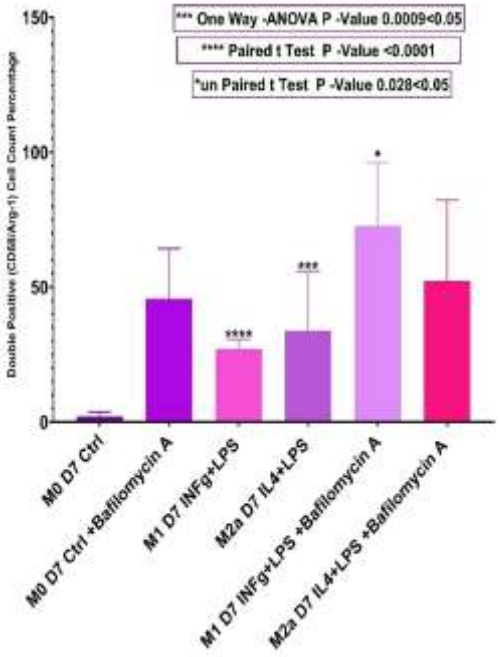


**D- Flow cytometry of CD68 and Arg-1 double-positive cells.**

**Figure 50. Analysis of flow cytometry studies for M0, M1, and M2a cells at day 7 polarization treated with Bafilomycin-A.**

Figure (A) violin plot to show the statistical significance of total cell expression of CD 68 protein in M0, M1, and M2a. One way ANOVA test was used to calculate the M1 significance (n=3, p-value 0.002<0.05). A paired t-test was used to calculate the significance in M2a (number of samples n=3, p-value 0.0165<0.05). Mean and standard deviation calculated using Excel software (Mean= 68.8, 93 and 88 %, STD = ± 8, ± 3.7, ± 5.6 for M0, M1, and M2a respectively). Figure (B) violin plot to show the statistical significance of total cell percentage expressing Arg-1 protein in M0, M1, and M2a. A one-way ANOVA test was used to calculate the M1 significance (n=3, p-value 0.02 < 0.05). Mean and standard deviation calculated using Excel software (Mean= 49, 71 and 55 %, STD = ± 6.33, ± 10.8 and ± 7.4 for M0, M1, and M2a, respectively).

Figure (C) violin plot to show the statistical significance of total cell percentage expressing CD68 protein in M0, M2a and M2a incubated with Bafilomycin A. One-way ANOVA test was used to calculate the M2a significance (n=3, p-value 0.0024 <0.05). M2a incubated with Bafilomycin-A showed the highest expression for CD68. Figure (D) Bar plot showing the statistical significance of double-positive cells that express both (CD68/Arg-1) in M0, M1, and M2a at day 7 polarization and M0, M1, and M2a incubated with Bafilomycin-A. A one-way ANOVA test was used to calculate the M1 significance (number of samples n=3, p-value 0.0009 < 0.05). Paired T-test was used to calculate the M2a significance (n=3, p-value <0.0001). Unpaired t-test was used to calculate the M1 incubated with Bafilomycin-A significance (n=3, p-value 0.028<0.05). Mean and standard deviation calculated using Excel software (Mean= 2.32, 27.44 and 29.5 &42.8, 68.5 and 46.8 %, STD = ± 0.93, ± 2.09 and ± 11.31 & ±9.5, ±12 and ± 15 for M0, M1 and M2a& M0, M1 and M2a incubated with Bafilomycin A).

**Immunostaining studies for Phagocytosis Assay**

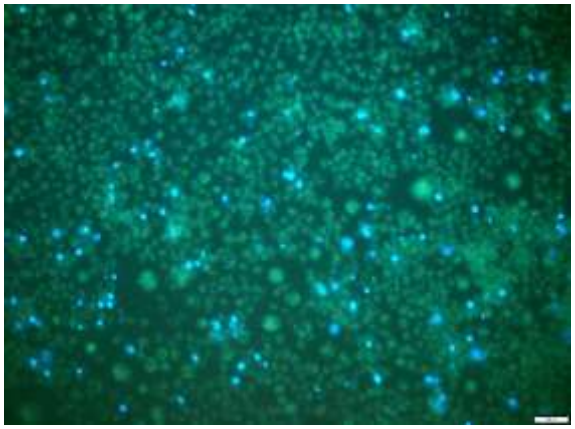

**A. M0 D7 EBS 16 Hrs. + E. coli**

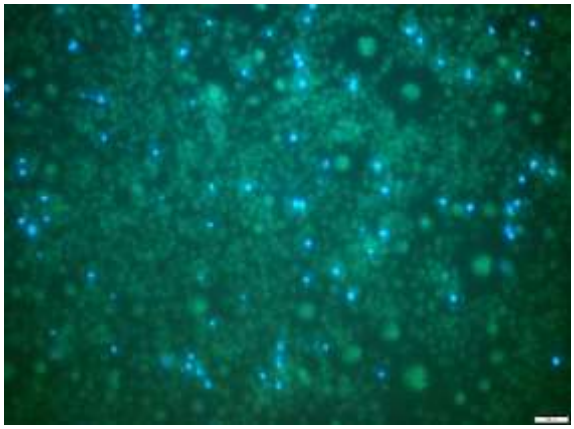

**B. M1 D7 EBS 16 Hrs. + E. coli**

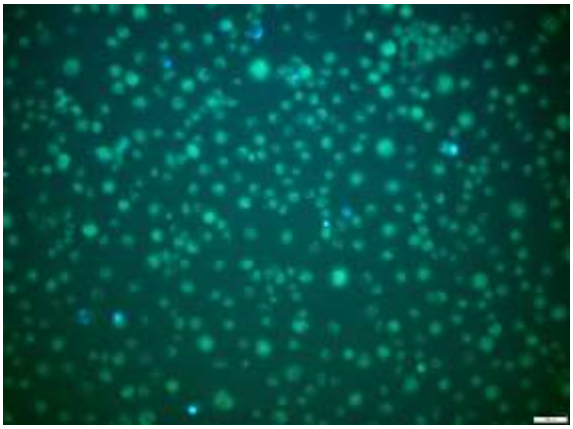

**C. M2a D7 EBS 16 Hrs. + E. coli**

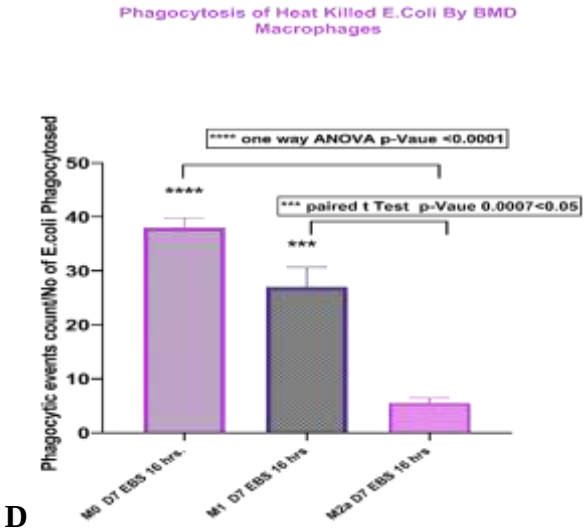


**D**

**Figure 51. Phagocytosis Assay**

Figures (A, B, and C) immune staining studies using mak38 autophagy detection kit. Cells stained in Cyan are M0, M1, and M2a at day 7 respectively incubated in Earle balanced salt for 16 hrs., Heat killed E. coli 10 ul suspension added in equal amount after stained with DAPI blue stain. Phagocytic events were captured using a fluorescence microscope. Figure (D) Bar plot showing the statistical significance of M0, M1, and M2a incubated with Earle Balanced salt for 16 hrs. A one-way ANOVA test was used to calculate the M0 significance ( n=5 images, p-value <0.0001). A paired T-test was used to calculate the M1 significance (n= 5 images, p-value 0.0007<0.05). Autophagy decreased the phagocytic activity of M2a compared to M1 and M0.

## SUMMARY


- Our systems biology approach revealed predicted target proteins that mediate the interplay between autophagy and macrophage activation Smad1, LC3A&B, Atg16L1, Atg7, IL6, CD68, Arg-1, and Vamp7.
- We succefuly isolated Bone marrow-derived monocytes were the femur and tibia of female mice. After differentiation of monocytes to M0, M1, and M2a, the lineage phenotypes were characterized using flow cytometry. Afterward, we validated the targets of Smad1, LC3A&B, Atg16L1, Atg7, IL6, CD68, Arg-1, and Vamp7. Finally, we investigated the impact of autophagy inhibition on all immune lineages using autophagy inhibitor Bafilomycin-A.

- Immune phenotyping by flow cytometry revealed three macrophage phenotypes: (IL6+/CD68+) M0 φ, (IL6+/CD68+/Arg-1 +) M1 φ and (CD68+/Arg-1) M2a φ lineages. And 3-D reconstruction of laser confocal microscopy Z-stalk images revealed an increase of autophagy activity in both M1 and M2a lineages.

- In addition, a significant increase was also observed in pre autophagosome size and number of Atg-7, Atg-16L1 in interleukin -4 activated M2a cells compared to control M 0 naïve cells. The size of LC 3 A& B auto phagosomal aggregates showed an increase in M2a cells. RT qPCR supported these findings and showed the high gene expression profile of Atg 16 L 1- 3, and Vamp 7 in M2a lineage at day 7 poalrization. Bafilomycin –A, an autophagy inhibitor, increased expression of CD68 and Arg-1 in all cell lineages at day 7 poalrization.

- Phagocytosis assay with Heat killed E Coli bacteria showed decreased phagocytosis activity in IL-4 activated M2a cells but not M1 cells at day 7 polarization.

- **In conclusion ,** This study suggests that autophagy reprograms macrophages through CD68 and Arginase-1 phagocytosis markers in Atg 16 L 1 -3 dependent manner.

## CHAPTER IV: DISCUSSION

Autophagy is a highly regulated process on transcriptional, post-transcriptional, translational, and post-translational levels. Autophagy-related genes, proteins, and mRNAs mediate this regulation. Activated macrophages are key players in the immune system. They exert immune quality control and pathogen -phagocytosis biological roles. Macrophages encode an array of pattern recognition receptors (PPRs) and sensors to identify pathogen-associated molecular patterns that mediate the innate immune response.

Autophagy depends on the formation of a double-membrane vesicle called autophagosome that fuses with the lysosome to degrade pathogens, proteins, and organelles. Both phagocytosis and autophagy are inter-dependent processes. The interplay between autophagy, macrophage activation, and phagocytosis is still poorly understood ***(Uribe-Querol and Rosales (2020) &*Duan, Chen et al. (2018).**

In this study, we dissected both the autophagy and macrophage activation process to better understand the nature of this interplay. We were able to identify a list of common pathways, transcription factors, and target proteins that mediate this interplay. We further validated these targets in an in vitro study.

### Systems Biology Approach and Predicted Targets:

Manually curated 249 autophagy associated genes (Atgs) and 250 differentially expressed genes (DEGs). We identified five significantly enriched pathways common between autophagy-associated genes, and Differentially expressed genes for macrophage polarization (figure7). These pathways are; NF kappa, FOXO, HIF1, NOD-like receptor, and IL17 signaling pathways.

The NF- κ pathway is well known to regulate the secretion of cytokines such as IL6 and TNF γ. These pathways also enhance cell survival, proliferation, inflammatory response, and angiogenesis ***(Newton and Dixit (2012)***. Autophagy controls the degradation of NF-κ-B-inducing kinase (NIK) and the essential activator of NF-κB, IκB kinase (IKK) under heat shock protein 90 (Hsp90) inhibition conditions ***(Qing, Yan et al. (2006), Qing, Yan et al. (2007).***

Other studies showed that the increased expression of autophagy-associated gene MAP1LC3B by rapamycin disrupted macrophage M2 polarization **(Wang, Li et al. (2017).** We found that MAP1LC3B serves as a common target for predicted transcription factors such as; CEBPG (figure 19 B--), MLXIPIL (figure 18 B).

The NOD-like receptor pathway showed high significance in this study. NOD1 receptor is a major regulator for IL6, Atg16L1, and IL17 (figure 20). NOD-like receptor pathway (NLR) mediates innate immune response and pathogen recognition. Also, it activates downstream molecules like NF-Kappa B to activate proinflammatory response cytokines such as IL-1B. NOD1 is a potential therapeutic target for infection and inflammatory-related diseases such as atherosclerosis **(Moreno and Gatheral (2013).** NOD1 recruits the Autophagy-associated gene Atg16L1 to the plasma membrane at the site of bacterial entry ***(Travassos, Carneiro et al. (2010))*.**

It's notable to mention that our analysis showed mmu-miR 362-P as a negative regulator for ATGs such as Atg10, DEGs such as CXCL5, and ELK 1 transcription factor (figure 20), proving that the NOD-like receptor pathway is a potential target for the interaction between ATGs and DEGs. In other words, a regulator for Atg16L1 and DEGs (such as IL6 and IL17A) in the innate immunity and inflammatory response regulation.

None of the predicted miRNAs were previously reported to be involved in macrophage polarization. Although we did not validate the predicted mi-RNAs experimentally in vitro, proof from the literature shows that these miRNAs regulate transcription factors and downstream target genes in angiogenesis and inflammation. For instance, mmu-mir 149 regulates transcription factor SMAD1 and attenuates scar formation in wound healing by downregulating the proinflammatory cytokine IL6 **(Lang, Zhao et al. (2017).** In other studies, the systemic injection of anti-mir 26-a5 in mice increased angiogenesis through SMAD1 expression (**Icli, Wara et al. (2013)&Icli, Nabzdyk et al. (2016).** The third miRNA, mmu-mir-17-5p, is also involved in angiogenesis (**Banerjee and Sen (2015)**

Our results showed that the predicted target proteins (figure 22), Atg7, and Atg16L1 serve as central proteins for several signaling pathways in autophagy, macrophage polarization, and phagocytosis. We also found that during the inflammatory response, NOD-like receptor NOD1 and NOD2 (figure 20) might be potential targets in macrophage polarization (figure 12).

Nevertheless, more experimental validation is needed for other predicted targets, such as Atg16L1, Atg7, MAP1LC3A, MAP1LC3B, IL6, ARG1, CD68, SMAD1and VAMP7 (figure 22).

In the current study, we identify a new correlation between macrophage polarization and autophagy. This correlation is through IL17, NOD1, NF-Kappa-B, FOXO 1 signaling pathways, and transcription factors such as SMAD1, foxo1, and NOD1. Further experimental validation for these targets is needed. Moreover, our results suggest new therapeutic targets for inflammatory conditions such as wound healing through autophagy associated genes, especially Atg16L1, MAP1LC3A, MAP1LC3B, Atg10. Therefore, we picked Atg16L1, Atg7, MAP1LC3A, MAP1LC3B, IL6, ARG1, CD68, SMAD1and VAMP7 predicted targets to validate and investigate their role in the interplay between autophagy and macrophage activation in vitro.

**Macrophage activation (polarization) and phenotypic characterization**

Bone marrow-derived macrophages are a heterogeneous population consisting of several phenotypes M0 or Naïve Macrophages, M1 or proinflammatory macrophages, and M2a subset Anti-inflammatory macrophages. Bacterial lipopolysaccharide (LPS) is a structural component of gram-negative bacteria that is used to activate macrophages(Zhang, Zhang et al. (2019). When used in combination with type II interferon-γ M0 macrophages are activated to M1. While, LPS in combination with IL-4 activates M0 lineage to M2a (Zhang, Zhang et al. (2019)

To characterize the phenotypes of the isolated bone marrow-derived macrophages and the activated macrophages in vitro, we investigated the expression of phagocytic markers CD68, IL6, and Arginase -1 among various macrophage populations (figure 7 &23).

CD68 is a cell surface heavily glycosylated glycoprotein localized near the endosomal / lysosomes Compartment. It is commonly used as a phagocytic marker in dendritic cells and strongly expressed in total macrophages, including M1 and M2 (Bisgaard, Mogensen et al. (2016)&( Chistiakov, Killingsworth et al. (2017). It is also a marker of tumor-associated macrophages Troiano, Caponio et al. (2019). M0 and M1 macrophages were confirmed by the high expression of CD 68 more than (60%) as seen by flow cytometry (figure 25 C, G, and K ) and with

immunostaining (figure 26 D, E, and F ). M 2a subset exhibited the highest significant expression for CD 68 (84%, p-value <0.05). (Figure 27 B)

Arginase -1 is a novel marker for activated M2a cells (Yang and Ming (2014). Arginase -1 expression was analyzed by flow cytometry in all cell lineages. In M1 cells, the Arg-1+ expression was 20%, and M2a Arg-1+ expression was 46 % (p-value <0.0001, figure 27 A). However, M0 showed a rare expression for Arg-1- less than 2%. Flow cytometry analysis showed Strong expression of Cd68 in both M1 and M2a, also the absence of Arginase -1 in M0 and its moderate expression M1 and high expression in M2a. Also, immunostaining studies for both CD68 and Arginase-1 supported the same results (figure 26 A, B, C, D, E and F). Altogether gives a positive characterization for all lineages, M0, M1, and M2a (Weischenfeldt and Porse (2008)& Huang, Li et al. (2018).

Interleukin 6 (IL6) is a proinflammatory cytokine that we predicted to mediate the interplay between autophagy and macrophage activation (figure 24). It was confirmed by flow cytometry to be positive in M0, M1, and very low expression in M2a less than 25% (figure23 A). Interferon-γ and lipopolysaccharide combination promoted the expression of IL6 in M1 lineage at day (55%, p-value < 0.0001, figure 23 A &B). Besides phagocytosis, cytotoxic activity is one of the characteristics of bone marrow-derived macrophages (Uribe-Querol and Rosales (2020)& Krahenbuhl, Remington et al. (1980). Therefore, we co-cultured the neuroblastoma cell line shsy5y for 24 hrs. in conditioned media of M0, M1, and M2a receptively. When human neuroblastoma cells SH-SY5Y were co-cultured in IL6 +/CD 68+ M1 macrophages, high cell viability (99%) was with MTT cytotoxicity cell assay (Figure 30 D). Also, IL6 +/CD 68+ M1 Lineage supernatant increased the proliferation of SH-SY5Y by increasing the mitotic partition coefficient (p-value = 0.001, figure 31 G). However, Arg-1+/CD68+ M2a macrophage supernatant showed cytotoxic effect on SH-SY5Y (figure 30 C, D) causing over 50% cell death (p-value < 0.05). previously, derived human macrophages were reported to have cytotoxic activity (Cameron and Churchill (1979). It was also reported that intro activated M2a lineage has a cytotoxic effect on tumor cells ( Xu, Shen et al. (2018). Long and Beatty (2013) reviewed the cytotoxic and anti-tumor properties of macrophages M2a through their ability to inhibit tumor angiogenesis, also reviewed it's promising potential to be used as immunotherapy depending on their in-vitro polarization with interleukin -4 .Our findings show the cytotoxic activity M2a (Arg-1+/CD68+)

and it might hold a therapeutic potential as anti-tumor immunotherapy, however more work is needed to validate this finding.

Although we were able to predict candidate targets; Atg16L1, Atg7, MAP1LC3A, MAP1LC3B, IL6, ARG1, CD68, SMAD1and VAMP7 (figure 22 ), the autophagy process is highly complex, and it is hard to identify the exact detailed machinery inside the activated macrophages. Flow cytometry studies on LC3A&B protein expression revealed that interferon-γ and lipopolysaccharide-induced macro-autophagy in IL6+/CD68+ M1. Also, Interleukin -4 and lipopolysaccharide combination induced macro-autophagy in Arg-1+/CD68+ M2a macrophages (figure 45 D, F and I &figure 46 A, B and D ).

The following genes' gene expression level increased; Atg7, LC3A, LC3B in M1 (IL6+/CD68+) compared to M2a. We performed a sequence alignment between the 3 isoforms of the pre-auto phagosome marker Atg16L protein. High similarity was found between Atg16L1-1 and Atg16L1-3 (figure 33 C &E). The expression of the Atg16L1-1 variant increased from 3 folds to 30 folds from day 7 to day 14 polarization. However, Atg16L1-3 variant expression decreased from 19 fold to 1.5 fold from day 7 to day 14 polarization in M2a macrophages (Arg-1+/CD68+ M2a) (p-value $< 0.05$, (figure 34 A, B , C and D ).

Confocal microscopy and Z-stack reconstruction for Atg7 and LC3A & B proteins (figure 44 B, D, and F ) were performed, followed by quantification of LC3A&B, Atg7, and Atg16L1 staining. M1 (IL6+/CD68+) and M2a (Arg-1+/CD68+) activated macrophages showed higher staining indicating increased autophagic activity when compared to the M0 (IL6+/CD68+) control macrophages. Putting these findings together, we can conclude that significantly INFγ and IL4 in combination LPS induced macro-autophagy in both M1 and M2a lineages at day 7 polarization.

Yang, Yang et al. (2019) reported that INFγ induced autophagy in hepatocellular carcinoma cells through increased LC3 A&B expression. Macro-autophagy increased in INF-γ + T cells. This was also correlated to the pathogenesis of systemic lupus nephritis (Luo, Yuan et al. (2018). Increased autophagy activity in macrophages was found to increase the phagocytosis of Mycobacterium tuberculosis by the INF-γ signaling pathway (Singh, Kansal et al. (2018). IL-4 induced macro-autophagy in antigen-presenting B cells and is linked to asthma's pathophysiology(Xia, Deng et al. (2018). Finally, it is noteworthy to mention that IL-4 boosted autophagy induction to form

LC3A&B aggregates (figure 44 B, D, and F). The average number of spots increased significantly per cell ( p-value < 0.05 ), indicating high autophagy activity (figure 46 A ).

**Macro-Autophagy interplays with Macrophages activation through CD68 and Arginase-1 in phagocytosis process:**

As mentioned previously, we verified the polarization of isolated bone marrow-derived macrophages to M0 (IL6+/CD68+), M1 (IL6+/CD68+), and M2a (Arg-1+/CD68+) lineage macrophages. We also concluded that INFγ and IL-4, combined with LPS induced macro-autophagy in M1 (IL6+/CD68+) and M2a (Arg-1+/CD68+) macrophages. Moreover, we reported the overexpression of Atg16l-3 (p-value < 0.05) and VAMP7 (p-value <0.05) in M2a (Arg-1+/CD68+) macrophages at day 7 polarization, and the overexpression of Atg16L1-1 variant in day 14 polarization in M2a (Arg-1+/CD68+) (p-value < 0.05). Flow cytometry studies revealed that macrophages at day 14 polarization showed a decreased arginase expression (figure 48 A, p-value < 0.05) in M0, M1, and M2a lineage when compared with day 7 polarization (figure 27 A ). Also, M1 and M2a showed a decreased CD68 expression when they compared to M0 ctrl at day 14 figure (48 A). so at day14 polarization, the characterized phenotypes are Arg-1-/CD68+ M0, Arg-1-/CD68+ M1, and Arg-1-/CD68+ M2a lineage. Interesting note that smad1 transcription factor overexpressed in Arg-1-/CD68+ M2a lineage 10 folds (** p-value <0.05) (figure 42 A&B). Also, flow cytometry analysis revealed that (* p-value <0.05) SMAD1 expression was high in Arg-1+/CD68+ M2a at day 14 polarization (figure 42 C). from these results, we can conclude 14-day polarization resulted in the loss of arginase expression and increased autophagy-related gene expression atg16l1-1. Since Arginase -1 is a phagocytic marker for M1 and M2a especially, loss of expression of Arg-1 indicates loss of activation in M1 and M2a lineages at day 14 polarization ( Rőszer (2015). Interestingly, Atg16L1-1 alpha showed a 30-fold increase in M2a day 14 polarization than M2a D7 polarization. Also, the Atg16L1-3 Gamma variant showed an 18-fold increase in M2a d7 than M2a d14 polarization. The same as for vamp7 in M2a d7 showed a 10-fold increase than M2a day 14 polarization (figure 34 A, B, C, D, E, and F). These studies refer to that high autophagy activity at day 14 polarization can attenuate arginase -1 expression. However, ***(Luo, He et al. 2020)*** reported autophagy is required for Arginase-1 expression in alternatively activated M2a at day 7 polarization.

For better understand the interplay between autophagy and phagocytosis, we blocked the autophagosome and lysosomal fusion with autophagy inhibitor Bafilomycin –A in a dose of 200 Nano Molar Conc. (200 n.M) for 18 hrs incubation ***Sotthibundhu, McDonagh et al. (2016).*** Flow cytometry studies showed increase of expression of CD68 and Arginase-1 in M1 (Arg-1+/CD68+) cells (p-value < 0.05, and < 0.05, respectively). These results indicate autophagy inhibition by Bafilomycin -A, increased CD68 and Arg-1 expression in all lineages M1 and M2a, including the control M0. ***(Lapaquette, Guzzo et al. (2015)*** Reported Bafilomycin- A induced autophagy inhibition and (knockdown of autophagy-related protein Atg5) promoted M2 polarization.

From systems biology approach and Pathway enrichment analysis revealed that autophagy-related proteins, Atg16L1, Lc3A&B, Atg7 were enriched in the NOD-like receptor pathway (figure 22, figure 12). It is well established that Nod-like receptor pathway has a critical role in the pathogen phagocytosis process. ***(Franchi, Warner et al. (2009) &Creagh and O'Neill (2006)*** . We examined phagocytosis markers Arginase -1, and Cd 68 in all cell lineages with flow cytometry revealed high expression of CD 68 in M0, M1, and M2a at day 7 polarization.

Our findings summarized that upon autophagy inhibition with Autophagy inhibitor Bafilomycin –A, CD68, and Arginase -1 expression strongly increased in all cell lineages at day 7 polarization. Necessarily, we performed phagocytosis assay in all cell lineages at day 7 polarization. Phagocytosis assay is one of the functional assays for immune cells such as macrophages and dendritic cells ***(Schulz, Severin et al. (2019).*** Phagocytosis assay was performed by testing the ability of M0, M1, and M2a cells to engulf heat-killed E. coli bacteria (figure 51). Finally, we induced autophagy using Earle Balanced salt (EBS ) induction medium in M0 (IL6+/CD68+), M1 (IL6+/CD68+), and M2a (Arg-1+/CD68+) cells to test their phagocytic activity on heat-killed E-Coli bacteria. Interestingly, M0 (IL6+/CD68+), and M1 (IL6+/CD68+) cells showed significant phagocytic activity (p-value <0.0001, and < 0.05, respectively figure 51- D). However, M2a (Arg-1+/CD68+) cells showed decreased phagocytic activity, however, we previously reported autophagy inhibition with bafilomycin –A in M2a (Arg-1+/CD68+) cells significantly increased the expression of CD68 (p-value<0.05, figure 50 -A). several studies reported autophagy induction altered macrophage polarization and altered M2a phagocytic function. ***Liu, Zhao et al. (2015).***

***Thomson, Turnquist et al. (2009)*** reported, autophagy induction via rapamycin drug an (m-TOR pathway inhibitor) induced autophagy and inhibited phagocytic activity in dendritic cells. In summary, Autophagy Inhibitor Bafilomycin Significantly increased CD68 Expression and Increased Arginase 1 Expression in M0, M1, and M2a Lineages & Autophagy induction decreased the phagocytosis activity of M2a but not M1.

**The potential therapeutic role for autophagy-related protein Atg16L1**

As mentioned earlier, Atg16L1 is the most important hub protein in macro-autophagy and macrophage polarization. Overexpression of Atg16L1-3 and VAMP7 in M2a at 7 days of polarization and the increased number of cytoplasmic pre-auto phagosomes suggests that Atg16L1 is essential for IL4 induced macro-autophagy in M2a (Arg-1+/CD68+) cells. Also, autophagy induction decreased the phagocytic ability of M2a (Arg-1+/CD68+) cells. (***Wolfkamp, Verseyden et al. (2014)*** reported, Atg16L1 mutation increased the phagocytosis ability of monocytes isolated from Crohn's disease patients. In another study***, Zhu, Li et al. (2018)*** reported autophagy inhibition by 3-MA (autophagy inhibitor) increased the phagocytic ability of macrophages and rescued mice from MRSA (Methicillin-Resistant staph aureus) bacterial infection. Therefore, we suggest that Atg16L1 might serve as t therapeutic target for the treatment of altered phagocytosis related diseases such as Bacterial Infection, inflammation, lupus nephritis, and cancer. Further studies for this target protein are needed.

## CONCLUSION

In conclusion , our systems biology approach enabled us to predict the protein targets that mediate interplay between autophagy and macrophages polarization . Through narrowing down a 249 autophagy related gene and 250 differentially expressed gene responsible for M1-M2 polarization. We concluded Atg16L1, Atg7, MAP1LC3A, MAP1LC3B, IL6, ARG1, CD68, SMAD1and VAMP7are the target protein . Afterwords we validated these targets after invitro generation of three activated bone derived macrophage lineages ; (IL6+/CD68+) M0 φ, (IL6+/CD68+/Arg-1 +) M1 φ and (CD68+/Arg-1) M2a φ lineages. We report Interleukin 4 induced macroautophagy in (CD68+/Arg-1) M2a φ . Z stack images for LC3A&B and Atg7 showed autophagic aggregates formation in both M1 and higher in M2a lineage . More over , Autophagy Inhibitor Bafilomycin Significantly increased CD68 Expression and Increased Arginase 1 Expression in M0, M1, and M2a Lineages. Autophagy induction decreased the phagocytosis activity of M2a but not M1. Our findings showed the cytotoxic activity M2a (Arg-1+/CD68+) and it might hold a therapeutic potential as anti-tumor immunotherapy, however more work is needed to validate this finding. putting all these findings together , we suggest autophagy repogramms macrophages M1 and M2a through decreasing the phagocytosis markers expression of CD68 and Arginase -1 in Atg16L1-3 dependent manner. Atg16L1-3 might be a therpautic target for increasing the macrophages activity through it's inhibition and more research is recommended.

## CHAPTER V: BIBLIOGRAPHY


Agarwal, V., G. W. Bell, J. W. Nam and D. P. Bartel (2015). "Predicting effective microRNA target sites in mammalian mRNAs." Elife **4**.

Arakawa, S., S. Honda, H. Yamaguchi and S. Shimizu (2017). "Molecular mechanisms and physiological roles of Atg5/Atg7-independent alternative autophagy." Proc Jpn Acad Ser B Phys Biol Sci **93**(6): 378-385.

Bader, G. D. and C. W. Hogue (2003). "An automated method for finding molecular complexes in large protein interaction networks." BMC Bioinformatics **4**: 2.

Banerjee, J. and C. K. Sen (2015). "microRNA and Wound Healing." Adv Exp Med Biol **888**: 291-305.

Bindea, G., B. Mlecnik, H. Hackl, P. Charoentong, M. Tosolini, A. Kirilovsky, W. H. Fridman, F. Pagès, Z. Trajanoski and J. Galon (2009). "ClueGO: a Cytoscape plug-in to decipher functionally grouped gene ontology and pathway annotation networks." Bioinformatics **25**(8): 1091-1093.

Biondillo, D. E., S. A. Konicek and G. K. Iwamoto (1994). "Interferon-gamma regulation of interleukin 6 in monocytic cells." Am J Physiol **267**(5 Pt 1): L564-568.

Bisgaard, L. S., C. K. Mogensen, A. Rosendahl, H. Cucak, L. B. Nielsen, S. E. Rasmussen and T. X. Pedersen (2016). "Bone marrow-derived and peritoneal macrophages have different inflammatory response to oxLDL and M1/M2 marker expression - implications for atherosclerosis research." Sci Rep **6**: 35234.

Bogdan, C. (2015). "Nitric oxide synthase in innate and adaptive immunity: an update." Trends Immunol **36**(3): 161-178.

Bonilla, D. L., A. Bhattacharya, Y. Sha, Y. Xu, Q. Xiang, A. Kan, C. Jagannath, M. Komatsu and N. T. Eissa (2013). "Autophagy regulates phagocytosis by modulating the expression of scavenger receptors." Immunity **39**(3): 537-547.

Boulakirba, S., A. Pfeifer, R. Mhaidly, S. Obba, M. Goulard, T. Schmitt, P. Chaintreuil, A. Calleja, N. Furstoss, F. Orange, S. Lacas-Gervais, L. Boyer, S. Marchetti, E. Verhoeyen, F. Luciano, G. Robert, P. Auberger and A. Jacquel (2018). "IL-34 and CSF-1 display an equivalent macrophage differentiation ability but a different polarization potential." Sci Rep **8**(1): 256.

Braun, V., V. Fraisier, G. Raposo, I. Hurbain, J. B. Sibarita, P. Chavrier, T. Galli and F. Niedergang (2004). "TI-VAMP/VAMP7 is required for optimal phagocytosis of opsonised particles in macrophages." Embo j **23**(21): 4166-4176.

Briken, V. and D. M. Mosser (2011). "Editorial: switching on arginase in M2 macrophages." J Leukoc Biol **90**(5): 839-841.

Cameron, D. J. and W. H. Churchill (1979). "Cytotoxicity of human macrophages for tumor cells. Enhancement by human lymphocyte mediators." J Clin Invest **63**(5): 977-984.

Cassetta, L., E. Cassol and G. Poli (2011). "Macrophage polarization in health and disease." ScientificWorldJournal **11**: 2391-2402.

Chistiakov, D. A., M. C. Killingsworth, V. A. Myasoedova, A. N. Orekhov and Y. V. Bobryshev (2017). "CD68/macrosialin: not just a histochemical marker." Lab Invest **97**(1): 4-13.

Chitirala, P., K. Ravichandran, D. Galgano, M. Sleiman, E. Krause, Y. T. Bryceson and J. Rettig (2019). "Cytotoxic Granule Exocytosis From Human Cytotoxic T Lymphocytes Is Mediated by VAMP7." Front Immunol **10**: 1855.

Choi, J. S., I. S. Jeong, J. H. Han, S. H. Cheon and S. W. Kim (2019). "IL-10-secreting human MSCs generated by TALEN gene editing ameliorate liver fibrosis through enhanced anti-fibrotic activity." Biomater Sci **7**(3): 1078-1087.

Creagh, E. M. and L. A. O'Neill (2006). "TLRs, NLRs and RLRs: a trinity of pathogen sensors that co-operate in innate immunity." Trends Immunol **27**(8): 352-357.

de Chaumont, F., S. Dallongeville, N. Chenouard, N. Hervé, S. Pop, T. Provoost, V. Meas-Yedid, P. Pankajakshan, T. Lecomte, Y. Le Montagner, T. Lagache, A. Dufour and J. C. Olivo-Marin (2012). "Icy: an open bioimage informatics platform for extended reproducible research." Nat Methods **9**(7): 690-696.

Del Giudice, M. and S. W. Gangestad (2018). "Rethinking IL-6 and CRP: Why they are more than inflammatory biomarkers, and why it matters." Brain Behav Immun **70**: 61-75.

Deretic, V. (2008). "Autophagosome and phagosome." Methods Mol Biol **445**: 1-10.

Dikic, I. and Z. Elazar (2018). "Mechanism and medical implications of mammalian autophagy." Nat Rev Mol Cell Biol **19**(6): 349-364.

Doncheva, N. T., J. H. Morris, J. Gorodkin and L. J. Jensen (2019). "Cytoscape StringApp: Network Analysis and Visualization of Proteomics Data." J Proteome Res **18**(2): 623-632.

du Toit, A., J. S. Hofmeyr, T. J. Gniadek and B. Loos (2018). "Measuring autophagosome flux." Autophagy **14**(6): 1060-1071.

Duan, Z., Q. Chen, L. Du, J. Tong, S. Xu, R. Zeng, Y. Ma, X. Chen and M. Li (2018). "Phagocytosis of Candida albicans Inhibits Autophagic Flux in Macrophages." Oxid Med Cell Longev **2018**: 4938649.

Franchi, L., N. Warner, K. Viani and G. Nuñez (2009). "Function of Nod-like receptors in microbial recognition and host defense." Immunol Rev **227**(1): 106-128.
Gammoh, N. (2020). "The multifaceted functions of ATG16L1 in autophagy and related processes." J Cell Sci **133**(20).
Gammoh, N., O. Florey, M. Overholtzer and X. Jiang (2013). "Interaction between FIP200 and ATG16L1 distinguishes ULK1 complex-dependent and -independent autophagy." Nat Struct Mol Biol **20**(2): 144-149.
Geng, J. and D. J. Klionsky (2008). "The Atg8 and Atg12 ubiquitin-like conjugation systems in macroautophagy. 'Protein modifications: beyond the usual suspects' review series." EMBO Rep **9**(9): 859-864.
Glickman, M. E., S. R. Rao and M. R. Schultz (2014). "False discovery rate control is a recommended alternative to Bonferroni-type adjustments in health studies." J Clin Epidemiol **67**(8): 850-857.
Goeritzer, M., N. Vujic, S. Schlager, P. G. Chandak, M. Korbelius, B. Gottschalk, C. Leopold, S. Obrowsky, S. Rainer, P. Doddapattar, E. Aflaki, M. Wegscheider, V. Sachdev, W. F. Graier, D. Kolb, B. Radovic and D. Kratky (2015). "Active autophagy but not lipophagy in macrophages with defective lipolysis." Biochim Biophys Acta **1851**(10): 1304-1316.
Gordon, S. and F. O. Martinez (2010). "Alternative activation of macrophages: mechanism and functions." Immunity **32**(5): 593-604.
Harris, J. (2013). "Autophagy and IL-1 Family Cytokines." Front Immunol **4**: 83.
Huang, X., Y. Li, M. Fu and H. B. Xin (2018). "Polarizing Macrophages In Vitro." Methods Mol Biol **1784**: 119-126.
Huynh, K. K., J. G. Kay, J. L. Stow and S. Grinstein (2007). "Fusion, fission, and secretion during phagocytosis." Physiology (Bethesda) **22**: 366-372.
Icli, B., C. S. Nabzdyk, J. Lujan-Hernandez, M. Cahill, M. E. Auster, A. K. Wara, X. Sun, D. Ozdemir, G. Giatsidis, D. P. Orgill and M. W. Feinberg (2016). "Regulation of impaired angiogenesis in diabetic dermal wound healing by microRNA-26a." J Mol Cell Cardiol **91**: 151-159.
Icli, B., A. K. Wara, J. Moslehi, X. Sun, E. Plovie, M. Cahill, J. F. Marchini, A. Schissler, R. F. Padera, J. Shi, H. W. Cheng, S. Raghuram, Z. Arany, R. Liao, K. Croce, C. MacRae and M. W. Feinberg (2013). "MicroRNA-26a regulates pathological and physiological angiogenesis by targeting BMP/SMAD1 signaling." Circ Res **113**(11): 1231-1241.
Italiani, P. and D. Boraschi (2014). "From Monocytes to M1/M2 Macrophages: Phenotypical vs. Functional Differentiation." Front Immunol **5**: 514.
Iula, L., I. A. Keitelman, F. Sabbione, F. Fuentes, M. Guzman, J. G. Galletti, P. P. Gerber, M. Ostrowski, J. R. Geffner, C. C. Jancic and A. S. Trevani (2018). "Autophagy Mediates Interleukin-1β Secretion in Human Neutrophils." Front Immunol **9**: 269.
Jablonski, K. A., S. A. Amici, L. M. Webb, D. Ruiz-Rosado Jde, P. G. Popovich, S. Partida-Sanchez and M. Guerau-de-Arellano (2015). "Novel Markers to Delineate Murine M1 and M2 Macrophages." PLoS One **10**(12): e0145342.
Jacquel, A., S. Obba, L. Boyer, M. Dufies, G. Robert, P. Gounon, E. Lemichez, F. Luciano, E. Solary and P. Auberger (2012). "Autophagy is required for CSF-1-induced macrophagic differentiation and acquisition of phagocytic functions." Blood **119**(19): 4527-4531.
Janky, R., A. Verfaillie, H. Imrichová, B. Van de Sande, L. Standaert, V. Christiaens, G. Hulselmans, K. Herten, M. Naval Sanchez, D. Potier, D. Svetlichnyy, Z. Kalender Atak, M. Fiers, J. C. Marine and S. Aerts (2014). "iRegulon: from a gene list to a gene regulatory network using large motif and track collections." PLoS Comput Biol **10**(7): e1003731.
Jiang, L., X. Li, Y. Zhang, M. Zhang, Z. Tang and K. Lv (2017). "Microarray and bioinformatics analyses of gene expression profiles in BALB/c murine macrophage polarization." Mol Med Rep **16**(5): 7382-7390.
Jiang, T., B. Qin, J. He, S. Lin and S. Ding (2013). "Three isoforms of the Atg16L1 protein contribute different autophagic properties." Mol Cell Biochem **378**(1-2): 257-266.
Kaiser, S. E., Y. Qiu, J. E. Coats, K. Mao, D. J. Klionsky and B. A. Schulman (2013). "Structures of Atg7-Atg3 and Atg7-Atg10 reveal noncanonical mechanisms of E2 recruitment by the autophagy E1." Autophagy **9**(5): 778-780.
Kim, H. Y., J. Y. Jhun, M. L. Cho, J. Y. Choi, J. K. Byun, E. K. Kim, S. K. Yoon, S. H. Bae, B. H. Chung and C. W. Yang (2014). "Interleukin-6 upregulates Th17 response via mTOR/STAT3 pathway in acute-on-chronic hepatitis B liver failure." J Gastroenterol **49**(8): 1264-1273.
Kimura, S., T. Noda and T. Yoshimori (2008). "Dynein-dependent movement of autophagosomes mediates efficient encounters with lysosomes." Cell Struct Funct **33**(1): 109-122.
King, J. S. (2012). "Autophagy across the eukaryotes: is S. cerevisiae the odd one out?" Autophagy **8**(7): 1159-1162.
Klionsky, D. J., J. M. Cregg, W. A. Dunn, Jr., S. D. Emr, Y. Sakai, I. V. Sandoval, A. Sibirny, S. Subramani, M. Thumm, M. Veenhuis and Y. Ohsumi (2003). "A unified nomenclature for yeast autophagy-related genes." Dev Cell **5**(4): 539-545.

Krahenbuhl, J. L., J. S. Remington, R. McLeod and R. Keller (1980). Cytotoxic and Microbicidal Properties of Macrophages. Mononuclear Phagocytes: Functional Aspects. R. van Furth. Dordrecht, Springer Netherlands**:** 1631-1653.
Kuma, A., M. Komatsu and N. Mizushima (2017). "Autophagy-monitoring and autophagy-deficient mice." Autophagy **13**(10): 1619-1628.
Kumar, P., A. Nagarajan and P. D. Uchil (2018). "Analysis of Cell Viability by the MTT Assay." Cold Spring Harb Protoc **2018**(6).
Lang, H., F. Zhao, T. Zhang, X. Liu, Z. Wang, R. Wang, P. Shi and X. Pang (2017). "MicroRNA-149 contributes to scarless wound healing by attenuating inflammatory response." Mol Med Rep **16**(2): 2156-2162.
Lapaquette, P., J. Guzzo, L. Bretillon and M.-A. Bringer (2015). "Cellular and Molecular Connections between Autophagy and Inflammation." Mediators of Inflammation **2015**: 398483.
Lehtonen, A., S. Matikainen and I. Julkunen (1997). "Interferons up-regulate STAT1, STAT2, and IRF family transcription factor gene expression in human peripheral blood mononuclear cells and macrophages." J Immunol **159**(2): 794-803.
Levine, B. and G. Kroemer (2008). "Autophagy in the pathogenesis of disease." Cell **132**(1): 27-42.
Lewis, B. P., I. H. Shih, M. W. Jones-Rhoades, D. P. Bartel and C. B. Burge (2003). "Prediction of mammalian microRNA targets." Cell **115**(7): 787-798.
Li, P., Q. Du, Z. Cao, Z. Guo, J. Evankovich, W. Yan, Y. Chang, L. Shao, D. B. Stolz, A. Tsung and D. A. Geller (2012). "Interferon-γ induces autophagy with growth inhibition and cell death in human hepatocellular carcinoma (HCC) cells through interferon-regulatory factor-1 (IRF-1)." Cancer Lett **314**(2): 213-222.
Li, Y., D. Zhou, Y. Ren, Z. Zhang, X. Guo, M. Ma, Z. Xue, J. Lv, H. Liu, Q. Xi, L. Jia, L. Zhang, Y. Liu, Q. Zhang, J. Yan, Y. Da, F. Gao, J. Yue, Z. Yao and R. Zhang (2019). "Mir223 restrains autophagy and promotes CNS inflammation by targeting ATG16L1." Autophagy **15**(3): 478-492.
Liu, K., E. Zhao, G. Ilyas, G. Lalazar, Y. Lin, M. Haseeb, K. E. Tanaka and M. J. Czaja (2015). "Impaired macrophage autophagy increases the immune response in obese mice by promoting proinflammatory macrophage polarization." Autophagy **11**(2): 271-284.
Long, K. B. and G. L. Beatty (2013). "Harnessing the antitumor potential of macrophages for cancer immunotherapy." Oncoimmunology **2**(12): e26860.
Luo, J., Y. He, F. Meng, N. Yan, Y. Zhang and W. Song (2020) "The Role of Autophagy in M2 Polarization of Macrophages Induced by Micro/Nano Topography." International journal of nanomedicine **15**, 7763-7774 DOI: 10.2147/ijn.s270100.
Luo, X. Y., J. L. Yuan, J. Liu, C. N. Luo, M. H. Yang, Q. Wei, M. Yang, Y. Chen, Y. Liu and G. H. Yuan (2018). "Increased Macroautophagy in Interferon-Gamma-Producing T Cells from Patients with Newly Diagnosed Systemic Lupus Erythematosus." Chin Med J (Engl) **131**(13): 1527-1532.
Mancino, A. and T. Lawrence (2010). "Nuclear factor-kappaB and tumor-associated macrophages." Clin Cancer Res **16**(3): 784-789.
Marks-Bluth, J., A. Khanna, V. Chandrakanthan, J. Thoms, T. Bee, C. Eich, Y. C. Kang, K. Knezevic, Q. Qiao, S. Fitch, L. Oxburgh, K. Ottersbach, E. Dzierzak, M. F. de Bruijn and J. E. Pimanda (2015). "SMAD1 and SMAD5 Expression Is Coordinately Regulated by FLI1 and GATA2 during Endothelial Development." Mol Cell Biol **35**(12): 2165-2172.
Martinez, F. O. and S. Gordon (2014). "The M1 and M2 paradigm of macrophage activation: time for reassessment." F1000Prime Rep **6**: 13.
Matsushita, M., N. N. Suzuki, Y. Fujioka, Y. Ohsumi and F. Inagaki (2006). "Expression, purification and crystallization of the Atg5-Atg16 complex essential for autophagy." Acta Crystallogr Sect F Struct Biol Cryst Commun **62**(Pt 10): 1021-1023.
Mercer, T. J., A. Gubas and S. A. Tooze (2018). "A molecular perspective of mammalian autophagosome biogenesis." J Biol Chem **293**(15): 5386-5395.
Min, Y., W. Xu, D. Liu, H. Shen, Y. Xu, S. Zhang, L. Zhang and H. Wang (2013). "Earle's balanced salts solution and rapamycin differentially regulate the Bacillus Calmette-Guerin-induced maturation of human dendritic cells." Acta Biochim Biophys Sin (Shanghai) **45**(3): 162-169.
Mizushima, N. and B. Levine (2010). "Autophagy in mammalian development and differentiation." Nat Cell Biol **12**(9): 823-830.
Moreno, L. and T. Gatheral (2013). "Therapeutic targeting of NOD1 receptors." Br J Pharmacol **170**(3): 475-485.
Mühl, H. and J. Pfeilschifter (2003). "Anti-inflammatory properties of pro-inflammatory interferon-gamma." Int Immunopharmacol **3**(9): 1247-1255.

Newton, K. and V. M. Dixit (2012). "Signaling in innate immunity and inflammation." Cold Spring Harb Perspect Biol **4**(3).
Nixon, R. A. (2013). "The role of autophagy in neurodegenerative disease." Nat Med **19**(8): 983-997.
Pan, H., L. Chen, Y. Xu, W. Han, F. Lou, W. Fei, S. Liu, Z. Jing and X. Sui (2016). "Autophagy-associated immune responses and cancer immunotherapy." Oncotarget **7**(16): 21235-21246.
Park, S. M., J. Ou, L. Chamberlain, T. M. Simone, H. Yang, C. M. Virbasius, A. M. Ali, L. J. Zhu, S. Mukherjee, A. Raza and M. R. Green (2016). "U2AF35(S34F) Promotes Transformation by Directing Aberrant ATG7 Pre-mRNA 3' End Formation." Mol Cell **62**(4): 479-490.
Parkhitko, A. A., O. O. Favorova and E. P. Henske (2013). "Autophagy: mechanisms, regulation, and its role in tumorigenesis." Biochemistry (Mosc) **78**(4): 355-367.
Parzych, K. R. and D. J. Klionsky (2014). "An overview of autophagy: morphology, mechanism, and regulation." Antioxid Redox Signal **20**(3): 460-473.
Peral de Castro, C., S. A. Jones, N. C. C, C. A. Hearnden, L. Williams, J. Winter, E. C. Lavelle, K. H. Mills and J. Harris (2012). "Autophagy regulates IL-23 secretion and innate T cell responses through effects on IL-1 secretion." J Immunol **189**(8): 4144-4153.
Perdiguero, E. G. and F. Geissmann (2016). "The development and maintenance of resident macrophages." Nat Immunol **17**(1): 2-8.
Pinno, J., H. Bongartz, O. Klepsch, N. Wundrack, V. Poli, F. Schaper and A. Dittrich (2016). "Interleukin-6 influences stress-signalling by reducing the expression of the mTOR-inhibitor REDD1 in a STAT3-dependent manner." Cell Signal **28**(8): 907-916.
Qing, G., P. Yan, Z. Qu, H. Liu and G. Xiao (2007). "Hsp90 regulates processing of NF-kappa B2 p100 involving protection of NF-kappa B-inducing kinase (NIK) from autophagy-mediated degradation." Cell Res **17**(6): 520-530.
Qing, G., P. Yan and G. Xiao (2006). "Hsp90 inhibition results in autophagy-mediated proteasome-independent degradation of IkappaB kinase (IKK)." Cell Res **16**(11): 895-901.
Quan, W., Y. M. Lim and M. S. Lee (2012). "Role of autophagy in diabetes and endoplasmic reticulum stress of pancreatic β-cells." Exp Mol Med **44**(2): 81-88.
Richards, D. M. and R. G. Endres (2014). "The mechanism of phagocytosis: two stages of engulfment." Biophys J **107**(7): 1542-1553.
Ritchie, M. E., B. Phipson, D. Wu, Y. Hu, C. W. Law, W. Shi and G. K. Smyth (2015). "limma powers differential expression analyses for RNA-sequencing and microarray studies." Nucleic Acids Res **43**(7): e47.
Rivals, I., L. Personnaz, L. Taing and M. C. Potier (2007). "Enrichment or depletion of a GO category within a class of genes: which test?" Bioinformatics **23**(4): 401-407.
Rőszer, T. (2015). "Understanding the Mysterious M2 Macrophage through Activation Markers and Effector Mechanisms." Mediators Inflamm **2015**: 816460.
Scherz-Shouval, R., H. Weidberg, C. Gonen, S. Wilder, Z. Elazar and M. Oren (2010). "p53-dependent regulation of autophagy protein LC3 supports cancer cell survival under prolonged starvation." Proc Natl Acad Sci U S A **107**(43): 18511-18516.
Schulz, D., Y. Severin, V. R. T. Zanotelli and B. Bodenmiller (2019). "In-Depth Characterization of Monocyte-Derived Macrophages using a Mass Cytometry-Based Phagocytosis Assay." Sci Rep **9**(1): 1925.
Shang, L. and X. Wang (2011). "AMPK and mTOR coordinate the regulation of Ulk1 and mammalian autophagy initiation." Autophagy **7**(8): 924-926.
Shannon, P., A. Markiel, O. Ozier, N. S. Baliga, J. T. Wang, D. Ramage, N. Amin, B. Schwikowski and T. Ideker (2003). "Cytoscape: a software environment for integrated models of biomolecular interaction networks." Genome Res **13**(11): 2498-2504.
Shapouri-Moghaddam, A., S. Mohammadian, H. Vazini, M. Taghadosi, S. A. Esmaeili, F. Mardani, B. Seifi, A. Mohammadi, J. T. Afshari and A. Sahebkar (2018). "Macrophage plasticity, polarization, and function in health and disease." J Cell Physiol **233**(9): 6425-6440.
Sharma, V., S. Verma, E. Seranova, S. Sarkar and D. Kumar (2018). "Selective Autophagy and Xenophagy in Infection and Disease." Front Cell Dev Biol **6**: 147.
Shen, M. and L. Lin (2019). "Functional variants of autophagy-related genes are associated with the development of hepatocellular carcinoma." Life Sci **235**: 116675.
Shibutani, S. T., T. Saitoh, H. Nowag, C. Münz and T. Yoshimori (2015). "Autophagy and autophagy-related proteins in the immune system." Nat Immunol **16**(10): 1014-1024.
Silva, M. T. (2011). "Macrophage phagocytosis of neutrophils at inflammatory/infectious foci: a cooperative mechanism in the control of infection and infectious inflammation." J Leukoc Biol **89**(5): 675-683.

Singh, N., P. Kansal, Z. Ahmad, N. Baid, H. Kushwaha, N. Khatri and A. Kumar (2018). "Antimycobacterial effect of IFNG (interferon gamma)-induced autophagy depends on HMOX1 (heme oxygenase 1)-mediated increase in intracellular calcium levels and modulation of PPP3/calcineurin-TFEB (transcription factor EB) axis." Autophagy **14**(6): 972-991.
Sotthibundhu, A., K. McDonagh, A. von Kriegsheim, A. Garcia-Munoz, A. Klawiter, K. Thompson, K. D. Chauhan, J. Krawczyk, V. McInerney, P. Dockery, M. J. Devine, T. Kunath, F. Barry, T. O'Brien and S. Shen (2016). "Rapamycin regulates autophagy and cell adhesion in induced pluripotent stem cells." Stem Cell Res Ther **7**(1): 166.
Szklarczyk, D., A. L. Gable, D. Lyon, A. Junge, S. Wyder, J. Huerta-Cepas, M. Simonovic, N. T. Doncheva, J. H. Morris, P. Bork, L. J. Jensen and C. V. Mering (2019). "STRING v11: protein-protein association networks with increased coverage, supporting functional discovery in genome-wide experimental datasets." Nucleic Acids Res **47**(D1): D607-d613.
Thomson, A. W., H. R. Turnquist and G. Raimondi (2009). "Immunoregulatory functions of mTOR inhibition." Nat Rev Immunol **9**(5): 324-337.
Travassos, L. H., L. A. Carneiro, M. Ramjeet, S. Hussey, Y. G. Kim, J. G. Magalhães, L. Yuan, F. Soares, E. Chea, L. Le Bourhis, I. G. Boneca, A. Allaoui, N. L. Jones, G. Nuñez, S. E. Girardin and D. J. Philpott (2010). "Nod1 and Nod2 direct autophagy by recruiting ATG16L1 to the plasma membrane at the site of bacterial entry." Nat Immunol **11**(1): 55-62.
Troiano, G., V. C. A. Caponio, I. Adipietro, M. Tepedino, R. Santoro, L. Laino, L. Lo Russo, N. Cirillo and L. Lo Muzio (2019). "Prognostic significance of CD68(+) and CD163(+) tumor associated macrophages in head and neck squamous cell carcinoma: A systematic review and meta-analysis." Oral Oncol **93**: 66-75.
Uribe-Querol, E. and C. Rosales (2020). "Phagocytosis: Our Current Understanding of a Universal Biological Process." Frontiers in Immunology **11**(1066).
Uribe-Querol, E. and C. Rosales (2020). "Phagocytosis: Our Current Understanding of a Universal Biological Process." Front Immunol **11**: 1066.
Velazquez-Salinas, L., A. Verdugo-Rodriguez, L. L. Rodriguez and M. V. Borca (2019). "The Role of Interleukin 6 During Viral Infections." Front Microbiol **10**: 1057.
Wang, Y., Y. Li, H. Li, H. Song, N. Zhai, L. Lou, F. Wang, K. Zhang, W. Bao, X. Jin, L. Su and Z. Tu (2017). "Brucella Dysregulates Monocytes and Inhibits Macrophage Polarization through LC3-Dependent Autophagy." Front Immunol **8**: 691.
Weischenfeldt, J. and B. Porse (2008). "Bone Marrow-Derived Macrophages (BMM): Isolation and Applications." CSH Protoc **2008**: pdb.prot5080.
Wolfkamp, S. C., C. Verseyden, E. W. Vogels, S. Meisner, K. Boonstra, C. P. Peters, P. C. Stokkers and A. A. te Velde (2014). "ATG16L1 and NOD2 polymorphisms enhance phagocytosis in monocytes of Crohn's disease patients." World J Gastroenterol **20**(10): 2664-2672.
Xia, F., C. Deng, Y. Jiang, Y. Qu, J. Deng, Z. Cai, Y. Ding, Z. Guo and J. Wang (2018). "IL4 (interleukin 4) induces autophagy in B cells leading to exacerbated asthma." Autophagy **14**(3): 450-464.
Xie, Y., R. Kang, X. Sun, M. Zhong, J. Huang, D. J. Klionsky and D. Tang (2015). "Posttranslational modification of autophagy-related proteins in macroautophagy." Autophagy **11**(1): 28-45.
Xu, L., M. Shen, X. Chen, D. R. Yang, Y. Tsai, P. C. Keng, S. O. Lee and Y. Chen (2018). "In vitro-induced M2 type macrophages induces the resistance of prostate cancer cells to cytotoxic action of NK cells." Exp Cell Res **364**(1): 113-123.
Yang, S., L. Yang, X. Li, B. Li, Y. Li, X. Zhang, Y. Ma, X. Peng, H. Jin and H. Li (2019). "New insights into autophagy in hepatocellular carcinoma: mechanisms and therapeutic strategies." Am J Cancer Res **9**(7): 1329-1353.
Yang, Z. and X. F. Ming (2014). "Functions of arginase isoforms in macrophage inflammatory responses: impact on cardiovascular diseases and metabolic disorders." Front Immunol **5**: 533.
Yin, Z., T. Ma, Y. Lin, X. Lu, C. Zhang, S. Chen and Z. Jian (2018). "IL-6/STAT3 pathway intermediates M1/M2 macrophage polarization during the development of hepatocellular carcinoma." J Cell Biochem **119**(11): 9419-9432.
Yoshii, S. R. and N. Mizushima (2017). "Monitoring and Measuring Autophagy." Int J Mol Sci **18**(9).
Zachari, M. and I. G. Ganley (2017). "The mammalian ULK1 complex and autophagy initiation." Essays Biochem **61**(6): 585-596.
Zavodszky, E., M. Vicinanza and D. C. Rubinsztein (2013). "Biology and trafficking of ATG9 and ATG16L1, two proteins that regulate autophagosome formation." FEBS Lett **587**(13): 1988-1996.
Zhang, W., Y. Zhang, Y. He, X. Wang and Q. Fang (2019). "Lipopolysaccharide mediates time-dependent macrophage M1/M2 polarization through the Tim-3/Galectin-9 signalling pathway." Exp Cell Res **376**(2): 124-132.
Zhang, X., R. Goncalves and D. M. Mosser (2008). "The isolation and characterization of murine macrophages." Curr Protoc Immunol **Chapter 14**: Unit 14.11.

Zhao, Y. G. and H. Zhang (2019). "Autophagosome maturation: An epic journey from the ER to lysosomes." J Cell Biol **218**(3): 757-770.
Zhou, G., O. Soufan, J. Ewald, R. E. W. Hancock, N. Basu and J. Xia (2019). "NetworkAnalyst 3.0: a visual analytics platform for comprehensive gene expression profiling and meta-analysis." Nucleic Acids Res **47**(W1): W234-w241.
Zhu, J., Y. Li, Z. Tian, X. Hua, J. Gu, J. Li, C. Liu, H. Jin, Y. Wang, G. Jiang, H. Huang and C. Huang (2017). "ATG7 Overexpression Is Crucial for Tumorigenic Growth of Bladder Cancer In Vitro and In Vivo by Targeting the ETS2/miRNA196b/FOXO1/p27 Axis." Mol Ther Nucleic Acids **7**: 299-313.
Zhu, Y., H. Li, S. Ding and Y. Wang (2018). "Autophagy inhibition promotes phagocytosis of macrophage and protects mice from methicillin-resistant staphylococcus aureus pneumonia." J Cell Biochem **119**(6): 4808-4814.
Zhuang, S. F., D. X. Liu, H. J. Wang, S. H. Zhang, J. Y. Wei, W. G. Fang, K. Zhang, L. Cao, W. D. Zhao and Y. H. Chen (2017). "Atg7 Regulates Brain Angiogenesis via NF-κB-Dependent IL-6 Production." Int J Mol Sci **18**(5).